Technische Universität München
TUM School of Engineering and Design

Characterizing water flow in vegetated lysimeters using lumped-parameter approaches and numerical modeling linked with stable water isotopes

Fatemeh Shajari

Vollständiger Abdruck von der TUM School of Engineering and Design der Technischen Universität München zur Erlangung des akademischen Grades einer

Doktorin der Naturwissenschaften (Dr. rer. nat.)
genehmigten Dissertation.

Vorsitz: Priv.-Doz. Dr. Arno Rein

Prüfer der Dissertation:

1. Prof. Dr. Florian Einsiedl
2. Prof. Dr. Massimo Rolle

Diese Dissertation wurde am 16.05.2022 bei der Technischen Universität München eingereicht und durch TUM School of Engineering and Design am 23.08.2022 angenommen.

ABSTRACT

Characterizing unsaturated water flow in the subsurface is a requirement for understanding the effects of droughts on agricultural production or the impacts of climate change on groundwater recharge. In this study, we have used stable water isotopes ($\delta^{18}O$ and $\delta^{2}H$) in combination with lumped-parameter modeling LPM for characterizing unsaturated flow in two lysimeters vegetated with maize. The lysimeters contained undisturbed soil cores dominated by sandy gravel (Ly1) and clayey sandy silt (Ly2). Stable water isotopes were measured and analyzed in precipitation and seepage water over about three years.

The flow and transport parameters (mean transit time of water T and dispersion parameter P_D) and contribution of preferential flow were determined by three different approaches; a "traditional" LPM approach where parameters were considered as a mean value for the whole observation period -three years- (constant values), an extended LPM approach where parameters were specifically determined for each sub-period -6 month- (variable values, which represent variation seasonally), and a numerical modeling approach using HYDRUS-1D. Moreover, stable water isotope transport modeling was performed with consideration of the matrix flow only (i) and of the matrix plus preferential flow (ii). Findings revealed that the consideration of preferential flow paths could substantially improve the model curve fits.

In the "traditional" LPM approach, different assumptions were compared to estimate the input function, i.e., stable water isotope content in the recharging water. Using the isotopic composition of precipitation as input (no modification) resulted in reasonable model estimations. However, the best model fits for the entire observation were obtained by weighting the recharging isotopes according to average precipitation within periods of 3 and 6 months, in correspondence to changing vegetation phases and seasonal influences. Input functions that consider actual evapotranspiration improved modeling at some periods, significantly; however, this led to deviations between modeled and observed $\delta^{18}O$ at other periods. This indicates the influence of variable flow, for which the extended LPM approach is recommended. A comparison of simulation results, obtained from each approach, showed that extended LPM curves are closer to the observations. Therefore, the division of the whole observation period

into hydraulically characteristic sub-periods for lumped-parameter modeling (where each sub-period implements steady-state flow) showed further improvement in the modeling procedure. In general, findings obtained from the extended LPM were in good agreement to numerical modeling results. However, observations were more difficult to describe mathematically for Ly2, where the periodicity of seasonal stable water isotope fluctuation in seepage water (lysimeter outflow) was not fully met by numerical modeling. Furthermore, an extra isotopic upshift of 1 ‰ for $\delta^{18}O$ improved simulations for Ly2, probably controlled by exchange processes between mobile soil water and immobile water within stagnant zones of Ly2. Finally, although LPM requires less input data compared to numerical models, both approaches achieve comparable decision-support integrity. The extended LPM approach can thus be a powerful tool for groundwater management approaches.

KURZFASSUNG

Die Charakterisierung der ungesättigten Strömung im Untergrund ist eine Voraussetzung für das Verständnis der Auswirkungen von Dürren auf die landwirtschaftliche Produktion oder der Auswirkungen des Klimawandels auf die Grundwasserneubildung. In dieser Studie haben wir stabile Wasserisotope ($\delta^{18}O$ und $\delta^{2}H$) in Kombination mit Lumped-Parameter-Modellen LPM verwendet, um ungesättigte Strömungen in zwei mit Mais bewachsenen Lysimetern zu charakterisieren. Die Lysimeter enthielten ungestörte Bodenkerne, die von sandigem Kies (Ly1) und tonigem Sandschluff (Ly2) dominiert waren. In Niederschlags- und Sickerwasser wurden über etwa drei Jahre stabile Wasserisotope gemessen und analysiert.

Die Strömungs- und Transportparameter (mittlere Verweilzeit des Wassers T und Dispersionsparameter P_D) sowie der Beitrag der präferenziellen Bypass-Flüsse wurden durch drei verschiedene Ansätze bestimmt; einem „traditionellen“ LPM-Ansatz, bei dem Parameter als Mittelwert für den gesamten Beobachtungszeitraum -drei Jahre- betrachtet wurden (konstante Werte), einem erweiterter LPM-Ansatz, bei dem Parameter für jeden Teilzeitraum spezifisch bestimmt wurden -6 Monate- (variable Werte) und der numerischen Modellierung mit HYDRUS-1D. Darüber hinaus wurde eine Transportmodellierung stabiler Wasserisotope durchgeführt, unter Berücksichtigung von Strömung und Transport durch die Untergrundmatrix (i) und der Matrix plus entlang präferenzieller Fließpfade (ii). Die Ergebnisse zeigten, dass die Berücksichtigung präferenzieller Fließpfade die Modellkurvenanpassungen erheblich verbessern konnte.

Beim „traditionellen“ LPM-Ansatz wurden verschiedene Annahmen verglichen, um die Eingabefunktion abzuschätzen, d. h. den Gehalt stabiler Wasserisotope im Sickerwasser. Die Verwendung der Isotopenzusammensetzung des Niederschlags als Eingabe (keine Modifikation) führte bereits zu plausiblen Abschätzungen. Jedoch wurden die besten Modellanpassungen für die Gesamtbeobachtung durch die Gewichtung der infiltrierenden Wasserisotope mit mittleren Niederschlagsraten in Zeiträumen von 3 und 6 Monaten erzielt, entsprechend wechselnder Vegetationsphasen und jahreszeitlichen Einflüssen. Eingabefunktionen, die die

aktuelle Evapotranspiration berücksichtigen, verbesserten die Modellierung in einigen Zeiträumen erheblich; in anderen Zeiträumen führte dies jedoch zu Abweichungen zwischen modellierten und beobachteten $\delta^{18}O$-Werten. Dies weist auf den Einfluss der variablen Strömung hin, für dessen Berücksichtigung der erweiterte LPM-Ansatz empfohlen wird. Ein Vergleich der Simulationsergebnisse, die bei den jeweiligen Ansätzen erzielt wurden, zeigt, dass die Modellkurven aus dem erweiterten LPM-Ansatz näher an den Beobachtungen liegen. Daher ergibt die Aufteilung des gesamten Beobachtungszeitraums in hydraulisch charakteristische Teilzeiträume (mit jeweils stationärer Strömung) eine weitere Verbesserung des Modellierungsverfahrens. Im Allgemeinen stimmten die Ergebnisse des erweiterten LPM-Ansatzes gut mit den Ergebnissen der numerischen Modellierung überein. Allerdings waren die Beobachtungen für Ly2 schwieriger mathematisch zu beschreiben, wo die Periodizität der saisonalen Schwankungen stabiler Wasserisotope im Sickerwasser (Lysimeterabfluss) durch die numerische Modellierung nicht vollständig erfasst wurde. Darüber hinaus verbesserte eine zusätzliche Isotopenerhöhung von 1 ‰, für $\delta^{18}O$, die Simulationen für Ly2, was möglicherweise mit Austauschprozessen erklärt werden kann, die zwischen mobilem Bodenwasser und immobilem Wasser (in stagnierenden Zonen) stattfinden. Obwohl LPM-Ansätze im Vergleich zu numerischen Modellen weniger Eingabedaten erfordern, erreichen beide Ansätze eine vergleichbare Integrität für die Entscheidungsunterstützung. Der erweiterte LPM-Ansatz stellt somit ein leistungsfähiges Werkzeug für das Grundwassermanagement dar.

PUBLICATIONS

Some text, figures and tables have appeared previously in the following publication:

- **Characterizing water flow in vegetated lysimeters with stable water isotopes and modeling**

  Fatemeh Shajari, Florian Einsiedl, Arno Rein,
  Groundwater (2020), 58, no. 5: 759-770.
  DOI: 10.1111/gwat.12970

- **Improved lumped-parameter and numerical modeling of unsaturated water flow and stable water isotopes**

  Anne Imig, Fatemeh Shajari, Lea Augustin, Florian Einsiedl, Arno Rein
  (Submitted to Groundwater 2022)

  Anne Imig and Fatemeh Shajari share first authorship for this publication, where Anne Imig carried out numerical modelling (HYDRUS-1D) and Fatemeh Shajari conducted lumped-parameter modelling. The review of this publication was mostly edited by Anne Imig.

ACKNOWLEDGEMENTS

A journey from Tehran to Munich (München) will have many people to thank. I consider myself fortunate indeed to have had the opportunity to pursue research work toward the Ph.D. with Professor Dr. Florian Einsiedl at the chair of Hydrogeology at the Technical University of Munich, Germany.

It is a pleasure to express my deep sense of Thanks to Prof. Dr. Florian Einsiedl, not only for giving me the opportunity to conduct this research, but also for his scholarly advice and thoughtful comments. Thank you for checking up on my progress and for your valuable support in finishing and completing my work.

I would like to thank Dr. Arno Rein for all the guidance, insightful input and scientific approach I received since I started my research. Thank you for your support and encouragement. Furthermore, I would like to thank my mentor Prof. Dr. Massimo Rolle for the nice cooperation and contribution. I am also very thankful to Susanne Thiemann for her great support in the laboratory. A big Thanks goes out to my colleagues and co-authors, those who invest much time and energy to greatly improve the paper and manuscripts for our publications.

I acknowledge the Bavarian Environment Agency (Bayerisches Landesamt für Umwelt, LfU) for collecting water samples, providing field data and site-related support, as well as for partially financing this study.

I especially would like to thank my family and friends, Parvin Mehzad (my lovely strong mother), Mohammadali Shajari (my kind, wise brother), Pari Sharifi, Shahla Baniadam, Mahdiye Karimi, Hediyeh Govahi, Immanuel Paul von Woyna, Dr. Sardar Ateeq, Lingfeng Jiang, Faride Nuraddini, Talaat Sabbagh, Frank Herrmann, Thomas Hahn, Sibylle Höffner, Dr. Seyed Majid Azimi and Dr. Thomas Svec, who always encouraged me to follow my dreams and pursue my career path.

CONTENTS

LIST OF FIGURES

LIST OF TABLES

LIST OF ABBREVIATIONS AND SYMBOLS

Abbreviations/ Acronyms	**Description**
^{16}O, Oxygen-16	stable isotopes of oxygen with eight neutrons in its nucleus
^{18}O, Oxygen-18	stable isotopes of oxygen with ten neutrons in its nucleus
^{1}H	stable isotopes of hydrogen without neutron in its nucleus
^{2}H	stable isotopes of hydrogen with one neutron in its nucleus (deuterium)
CLARA-A2	name of the product, in which meteorological parameters are represented
CM SAF	satellite application facility on climate monitoring
D	stable isotopes of hydrogen with one neutron in its nucleus (deuterium)
DWD	(Deutscher Wetterdienst) German meteorological service
GMWL	global meteoric water line
GNIP	the global network of isotopes in precipitation
HYDRUS-1D	software package for simulating the movement of water, one Dimension; numerical modeling
IF	tracer input function
IF0	input function 0, using isotopic composition of precipitation
IF1	input function 1, weighting isotopic composition of precipitation
IF2	input function 2, consideration of actual ET (measured)
IF3	input function 3, with estimated ET based on Haude approach
IF4	input function 4, with estimated ET based on Penman Monteith approach
IF5	input function 5, with estimated ET based on Penman Monteith plus simulated maize transpiration

LfU	Bavarian Environment Agency (Bayerisches Landesamt für Umwelt)
LMWL	local meteoric water line
LPM	lumped-parameter model
Ly1	lysimeter 1
Ly2	lysimeter 2
ME	mean error
mod.	modeled
Par.	parameter
PEST	parameter estimation for optimization of parameters
PF	preferential flow
PM	Penman Monteith approach
R^2	coefficient of determination
RMSE	root mean square error
SHP	soil hydraulic parameters
T-LWIA	triple-Liquid Water Isotope Analyzer
V-SMOW	Vienna-standard mean ocean water

Parameter symbols	Unit symbol/ Quantity	Description
A	[m^2]	lysimeter surface area
C_{out}	[‰]	calculated tracer output concentration (here simulated stable water isotopes, i.e., delta-values [‰], in lysimeter seepage
C_{in}	[‰]	tracer input concentration (delta-values of infiltrating water) as a function of time (the input function).
$C_{in}(t-\tau)$	[‰]	input function
C	[M/L^3]	tracer concentration
c_p	[J/kg/°C]	specific heat of air
D	[L^2/T]	dispersion coefficient
D_L	[m^2/d]	longitudinal dispersion coefficient
$d\tau$	[-]	to the chosen temporal resolution
e_a	[kPa]	actual vapor pressure
e_s	[kPa]	saturation vapor pressure
ET	[L/d]	evapotranspiration
ET_{act}	[L/d]	actual evapotranspiration
$ET_{actual,weight}$	[L/d]	actual evapotranspiration estimated by water balance equation, considering weight of Lysimeter
$ET_{act,PM}$	[L/d]	actual evapotranspiration determined from the Penman-Monteith approach as a function of time
$ET_{act,PM\ and\ Q,maize}$	[L/d]	actual evapotranspiration determined from Penman-Monteith plus estimated transpiration for the maize plants
ET_i	[L/d]	actual evapotranspiration
$ET_{i,PM}$	[L/d]	actual evapotranspiration based upon the Penman-Monteith approach

ET_{pot}	[L/d]	potential evapotranspiration
ET_{pot}^{Haude}	[L/d]	potential evapotranspiration estimated by the Haude approach
ET_{pot}^{PM}	[L/d]	potential evapotranspiration estimated by the Penman-Monteith approach
f_{Haude}	[mm/(hPa d)]	Haude coefficient
F_{14}	[%]	relative air humidity
G	[J/(m²s)]	soil heat flux
$g(\tau)$	[-]	continuous transit-time distribution function (weighting function or system response function); it considers a Dirac pulse for tracer input into inflowing water
$g_M(\tau)$	[-]	continuous transit-time distribution function (weighting function or system response function, through the matrix)
$g_{PF}(\tau)$	[-]	continuous transit-time distribution function (weighting function or system response function, through the preferential flow)
h	[L]	hydraulic potential, hydraulic pressure head
h_{CritA}	[cm]	minimum allowed pressure head
k	[d^{-1}]	first-order rate constant for exponential plant growth
K_C	[-]	crop coefficient
$K_{C,ini}$	[-]	initial crop growth stage
$K_{C,mid}$	[-]	mid-season crop growth stage
$K_{C,end}$	[-]	late-season crop growth stage
K(h)	[L/T]	soil hydraulic functions, hydraulic conductivity as a function of hydraulic potential
K	[L/T]	hydraulic conductivity
K_s	[cm/s]	saturated hydraulic conductivity

l	[-]	pore connectivity factor
LAI	[-]	leaf area index
m	[kg]	lysimeter weight
m	[-]	empirical water retention curve shape parameters
M_{max}	[kg]	maximum plant mass
M_0	[kg]	initial plant mass
MTT	[d]	median transit time
n	[-]	empirical water retention curve shape parameters in van Genuchten-Mualem model
N	[-]	number of events during the weighting period.
P	[L/d]	precipitation
P_D	[-]	dispersion parameter
Pe	[-]	Peclet number
$P_{eff,i}$,	[L/d]	effective precipitation
P_i	[L/d]	precipitation rate
p_{PF}	[-]	the portion of preferential flow
P_{14}	[hPa]	saturation vapor pressure measured at 2 p.m.
Q	[L/T]	lysimeter outflow rate
Q_{PF}	[L/d]	simulated lysimeter outflow resulting from water flow along preferential flow paths
Q_{Maize}	[L/d]	calculated transpiration rate of maize
q	[L/T]	volumetric fluid flux
Q_M	[L/d]	simulated lysimeter outflow within the subsurface matrix
r_a	[s/m]	aerodynamic resistance
RH	[-]	relative air humidity
r_l	[s/m]	stomatal resistance

$R_{l,in}$	[µm]	incoming long-wave radiation
$R_{l,out}$	[µm]	outgoing long-wave radiation.
R_n	[J/(m²s)]	net solar radiation
RR	[-]	relative recovery
r_s	[s/m]	surface bulk resistance
$R_{s,in}$	[µm]	incoming short-wave radiation
$R_{s,out}$	[µm]	outgoing short-wave radiation.
R_{sample}	[-]	isotopic ratio ($^{18}O/^{16}O$ and $^{2}H/^{1}H$) of the sample
$R_{standard}$	[-]	isotopic ratio ($^{18}O/^{16}O$ and $^{2}H/^{1}H$) ratio of the standard or reference
S_e	[-]	effective saturation
T	[d]	mean transit time (or mean travel time) of water
T_a	[°C]	air temperature
T_C	[L/kg]	transpiration coefficient
T_{PF}	[d]	mean transit time of water within preferential flow paths.
TT	[d]	median travel time
v	[m/s]	mean water flow velocity
W	[m/s]	wind speed
x	[m]	flow length, lysimeter length
α	[L^{-1}]	water retention curve shape parameters in van Genuchten-Mualem model; related to the inverse air-entry suction
α_{albedo}	[-]	albedo or canopy reflection coefficient
$\alpha_i \cdot P_i$	[L/d]	recharge (infiltration) or effective precipitation
α_i	[-]	recharge factor

α_L	[m]	longitudinal dispersivity
γ	[kPa/°C]	psychrometic constant
$\delta(\tau - T_{PF})$	[‰]	dirac delta function
δD	[‰]	the relative difference of deuterium ratios between a sample and standard V-SMOW
δ^2H	[‰]	the relative difference of hydrogen ratios between a sample and standard V-SMOW
$\delta^{18}O$	[‰]	the relative difference of oxygen ratios between a sample and standard V-SMOW
δ_i	[‰]	delta-values measured in precipitation (input); isotopic composition of precipitation
$\overline{\delta_{out}}$	[‰]	average isotopic composition of lysimeter outflow within the observation period
Δ	[kPa/°C]	the slope of the vapor pressure curve
Δm	[kg]	change of lysimeter weight
ΔS	[L/d]	changes in soil water storage
θ	[L^3/L^3]	water content
θ_{av}	[L^3/L^3]	average pore water content, taking part in flow through the soil matrix
$\theta(h)$	[L^3/L^3]	soil hydraulic function, water content as a function of hydraulic potential
θ_r	[L^3/L^3]	residual water content
θ_s	[L^3/L^3]	saturated soil water content
λ	[J/kg]	latent heat flux
ρ_a	[kg/m^3]	density of air
ρ_w	[kg/m^3]	density of water
τ	[d]	transit time
Ψ_m	[kPa]	matric potential

quantity: (T: Time, L: Length, M: Mass), unit: (d:day, s: second, m: meter, µm: micrometer, kg: kilogram, kPa: kilopascal, J: joule, °C: degree Celsius, ‰: per mill)

1. INTRODUCTION

Knowledge of water flow in soil and the unsaturated zone is an important prerequisite for many environmental questions, e.g., related to agronomics and environmental issues such as soil water scarcity or the fate of agrochemicals like nitrate and pesticides and related impacts. An adequate understanding and quantification of unsaturated flow is also required with respect to subsurface contamination, such as for assessing the transport and fate of pollutants in the unsaturated zone and their impact to groundwater (e.g., Bradford et al. 2003; Dann et al. 2009; Hsieh et al. 2001; Stumpp et al. 2012b). This implies evaluating the effects of droughts on agricultural production, ecosystems and groundwater recharge, which is an issue of increasing importance for many regions due to climate change (e.g., Blanchoud et al. 2007; Vrba and Richts 2015; Kundzewicz and Döll 2009; Varis 2018; Woldeamlak et al. 2007).

Characterization of water flow includes laboratory and field investigations, as well as lysimeter studies (e.g., Maloszewski et al. 2006; Stumpp et al. 2009a-c; Mali et al. 2007; Koeniger et al. 2010; Stumpp et al. 2012b; Groh et al. 2018). For analyzing water flow in the unsaturated zone, stable water isotopes have been used as tracers for a long time (Barnes and Allison 1983; Fontes et al. 1986; Walker and Richardson 1991; Komor and Emerson 1994; Abbott et al. 2000; McGuire et al. 2002; Gazis and Feng 2004; O'Driscoll et al. 2005; Sprenger et al. 2015; Hale et al. 2016). Moreover, in the last decades, different approaches have been applied for isotope transport modeling in the unsaturated zone. Difficulties about isotope transport modeling are connected, among other, to the subsurface heterogeneity and the contribution of preferential flow and mobile water, as well as to an adequate representation of the tracer (stable water isotope) input function.

1.1. THE UNSATURATED ZONE

The unsaturated zone, often known as the vadose zone, is the portion of the subsurface which is located above the groundwater level. It contains solids, air and water, where a portion of soil-water (such as in small pores and around grains) is strongly bound in some pores due to the adhesion and capillary action. The unsaturated zone is of high

importance also for the management of groundwater resources because it affects recharge and can influence the quality of groundwater. The shape, size and arrangement of soil grain, which leads to a characteristic structure of soil pores, controls the water movement, water flow rate and transport of the contaminants in the unsaturated zone (Tindall et al. 1999).

Two important parameters related to the property of a porous medium (the unsaturated zone) are porosity and permeability which are affecting the water flow processes. The pore volume to total volume ratio is known as porosity. It shows the ability of soil materials for holding a fluid. If the soil materials in the unsaturated zone are having different grain sizes, i.e., are poorly sorted, the porosity will not be very high, because the smaller particles fill the gaps between larger particles. Permeability is an inherent property of a porous medium, which expresses how fast a fluid can flow through a porous solid. It depends on the pore size, tortuosity, surface area and connectivity of the pores, e.g., if the soil pores are not connected, the permeability of the subsurface is poor (Earle 2019 and Jain 2014). Hydraulic conductivity is also an important parameter, which describes how easily a fluid (usually water) can transmit through pore spaces or fractures of a soil. However, it depends also on the properties of the fluid such as viscosity, temperature, and density (Freeze and Cherry 1979), as explained in more detail in chapter 1.3., Investigation of water flow and stable water isotope transport in the unsaturated zone.

The number, size, and connections of pores in the subsurface (unsaturated zone) play a decisive role for water isotope transport. When water is trapped in a pore and has no connection to mobile water, it is considered as immobile water. The immobile water (second porosity system) can naturally be re-mobilized.

Water can flow through different paths in the unsaturated zone: through (i) the subsurface matrix and (ii) the preferential flow paths. Preferential flow (PF) paths can be induced by connected macro-pores in the subsurface, allowing for accelerated water transport (e.g., Van Ommen et al. 1989). Such macro-pores may include networks of connected soil pores, channels and fractures resulting from geological/geochemical processes (such as weathering, freeze/thaw cycles, shrinking/swelling of clay minerals, desiccation), biological activity (root channels, burrowing soil organisms like earthworms), and agricultural activity such as ploughing (Beven and Germann 1982;

Gazis and Feng 2004; Van Ommen et al. 1989). Matrix flow usually shows low flow velocities, while PF comparatively presents rapid flow velocities.

1.2. ENVIRONMENTAL ISOTOPES

Isotopes are atoms of an element that have the same number of protons but differ in the number of neutrons and, therefore, have different masses. Stable isotopes are referred to those isotopes that do not decay radioactively; thus, they are stable. Environmental isotopes are dissolved, suspended or floating substances/isotopes (Koeniger et al. 2010), which are often used as a marker for investigations in hydrogeology to determine groundwater quality, origin, recharge mechanism, and they aim at understanding the water flow processes (Barnes and Allison 1983; Fontes et al. 1986; Walker and Richardson 1991; Komor and Emerson 1994; Abbott et al. 2000; McGuire et al. 2002; Gazis and Feng 2004; O'Driscoll et al. 2005; Sprenger et al. 2015; Hale et al. 2016; Adelana 2005). The most common environmental isotopes are the naturally occurring water stable isotopes: deuterium, i.e., hydrogen-2 (stable isotope of hydrogen with two neutrons) and oxygen-18 (stable isotope of oxygen with ten neutrons).

To enhance measurement quality and interlaboratory results, the measured ratios of heavy (^{18}O) to light (^{16}O) isotopes in samples are compared to a standard (Vienna Standard Mean Ocean Water (VSMOW)) as shown in Equation 1 Kendall and Caldwell (1998b).

$$\delta\,[‰] = \frac{R_{sample} - R_{standard}}{R_{standard}} \cdot 1000 \qquad \text{Equation (1)}$$

where R_{sample} is the ratio of water isotopes of the water sample, which is obtained from Laboratory analysis and $R_{standard}$ stands for the ratio of reference (V-SMOW). The δ notation in ‰ (per mil) was introduced to compare the standardized ratios of isotopes. Comparing the isotopic abundance of a water sample with the standard enables tracking changes of the isotope signature and thus allows to analyze flow and stable water isotope transport processes in the subsurface.

Craig (1961) described a correlation between $\delta^{18}O$ and $\delta^{2}H$ isotopes in all meteoric water, which is derived from precipitation in the form of snow and rain, as:

$$\delta\ ^{2}H\ [‰] = 8 * \delta^{18}O + 10 \qquad \text{Equation (2)}$$

This relationship (Equation 2), called the global meteoric water line (GMWL), is often compared to an observed local meteoric water line (LMWL) to find out the similarity of the isotopic composition of the samples. The local relationship between $\delta^{18}O$ and $\delta^{2}H$, i.e., the LMWL, can deviate from the GMWL.

The isotopic composition of water could change due to several factors such as temperature, humidity, continental, seasonal, altitude, latitude and amount effects (Clark and Fritz 2013; Criss 1991; Bottinga 1969; Friedman 1953; Urey 1947). These factors can cause stable isotope fractionation. If the LMWL shows a deviation from the GMWL, this may indicate stable isotopic fractionation during evaporation (Clark and Fritz 2013). Due to the different masses between ^{18}O and ^{16}O as well as ^{2}H and ^{1}H, isotopes behave differently in a phase transition. The heavier water isotopes (^{18}O and ^{2}H) become enriched in the liquid phase, i.e., rain, while the lighter isotopes (^{16}O and ^{1}H) tend to increase in the vapor phase, such as in clouds (Kendall et al. 1995; Kendall et al. 1998b).

1.3. INVESTIGATION OF WATER FLOW AND STABLE WATER ISOTOPE TRANSPORT IN THE UNSATURATED ZONE

Investigations of subsurface water flow usually include studies about soil types and textures, water content, water potential and soil hydraulic parameters, which affect the water movement, water balance and stable water isotope transport in the unsaturated zone.

The residual water content θ_r is the amount of water trapped within small soil pores. It does not contribute to active flow either due to the blockage in dead-end pores or due to strong adsorption onto the solid phase (Luckner et al. 1989). The saturated water content θ_s is the maximum amount of water a soil can store. The concept of water potential is useful for understanding water movement. Matric potential Ψ_m is a

negative potential pressure due to the soil-water attraction and matrix effects (e.g., capillary and adhesive intermolecular forces, fluid cohesion and surface tension) (Fetter 2001). The relationship between the water content θ and water matric potential Ψ_m is described by the water retention curve. Soil water retention curves are characteristic for different types of soil. When the water content decreases, first the larger pores lose the water; therefore, the water retention curve of a medium with many large pores will rapidly drop to lower water content at high matric potential. Conversely, a medium with fine pores shows a flatter retention curve (Nimmo 2006). The shape of water retention curves can, e.g., be described by van Genuchten model. Two important parameters of the van Genuchten are the scaling parameter α and the curve shape factor n, which can be determined by field or laboratory testing (e.g., Srivastava et al. 2021).

How easily a fluid (usually water) can transmit through pore spaces or fractures of soil is described by hydraulic conductivity K. It depends not only on fluid (density and viscosity) but also on medium (permeability and water content). Saturated hydraulic conductivity K_S is the hydraulic conductivity in a saturated medium (soil) (Freeze and Cherry 1979). Residual and saturated soil water content (θ_r and θ_s), the water retention curve shape parameters (α and n), as well as the saturated hydraulic conductivity (K_S) are soil hydraulic parameters SHP, which determine soil water flow.

In our study case, the water balance equation described inputs and outputs for the lysimeters as Precipitation (P) = outflow (Q) + evapotranspiration (ET) +/- changes in storage (ΔS). In this equation, the principle of mass conservation was considered, which means any water entering the system (via precipitation) has to be transferred into evapotranspiration, outflow or stored in the soil water storage.

1.3.1. MODELING OF STABLE WATER ISOTOPE TRANSPORT

As mentioned above, stable water isotopes are used for characterizing water flow in the unsaturated zone. For the modeling of isotope transport in the unsaturated zone, different approaches including numerical and analytical modeling, have been developed.

Numerical modeling of stable water isotope transfer requires information about soil hydraulic properties. In this method, laboratory experiments or (inverse) modeling approaches are applied to determine soil hydraulic properties. Both have possible shortcomings; laboratory results may largely differ from those found at a field site, and additional uncertainties might occur from upscaling (e.g., Schwärzel et al. 2006; Dinelli et al. 2000; Winton and Weber 2018). On the modeling side, detailed site data are required that often are not available under reasonable efforts, such as for the initial and boundary conditions (e.g., Asadollahi et al. 2020). Simplifying assumptions have to be selected, accordingly, which may bear considerable uncertainty.

Analytical modeling of stable water isotope transport has often been applied as an alternative approach, e.g., if field monitoring of flow-related parameters such as soil moisture or hydraulic potentials is not feasible. Implementing analytical solutions, lumped-parameter models (LPM) can be coupled with the measurement of environmental isotopes, in order to obtain information on subsurface flow and relevant flow processes on the field scale (e.g., Leibundgut et al. 2009). LMPs require information on tracer input and output, and a reduced number of (lumped) fitting parameters (P_D dispersion parameter and T mean transit time of water) for the transfer function (weighting function) that describes the tracer transport within the system. As an advantage of LPMs, compared to numerical models, a limited number of input data (tracer input and output) and fitting parameters ("lumped" parameters) are required. P_D provides information on subsurface heterogeneity, which relates to the matrix that is affected by the tracer (e.g., Leibundgut et al. 2009). Depending on the hydrological conditions, different tracer transport models can be combined, such as advection-dispersion (for tracer transport within the subsurface matrix), piston-flow (e.g., for preferential flow or Karst conduits) or exponential models, as well as gamma distribution assumption (e.g., Maloszewski and Zuber 1982; Leibundgut et al. 2009; Maloszewski et al. 2002; Einsiedl et al. 2009; Maloszewski et al. 2006; Stumpp et al. 2009a, 2009b, 2009c; Hrachowitz et al. 2009; Tetzlaff et al. 2014; Stockinger et al. 2019). Maloszewski and Zuber (1982) developed LPM approaches for the interpretation of environmental tracers in groundwater systems, including analytical advection-dispersion and piston flow models for tracer transport. In long-term studies, Maloszewski et al. (2006) and Stump et al. (2009a-c) used similar approaches to describe stable water isotope transport (δ^2H and $\delta^{18}O$, referred to as delta-values) in

the unsaturated zone of lysimeters. Accordingly, when implementing the advection-dispersion model within the LPM, simulation gives the mean transit time of water T (as one of the fitting parameters) and thus information on the average residence time of water in the matrix of the unsaturated zone.

Inherent to the LPM concept, steady-state flow is considered as a prerequisite of the implemented analytical solutions, which requires constant coefficients and thus one set of parameters. Whereas this assumption can be adequate for long-term conditions of groundwater flow, it can be problematic for the unsaturated zone where pronounced temporal variations of flow often prevail. To this respect, Maloszewski et al. (2006) have considered a yearly changing mean transit time for simulating tracer transport, including stable water isotopes, in different lysimeters. Stumpp et al. (2007, 2009a and 2009b) have optimized this approach by variation of the dispersion parameter, in addition to mean transit time (yearly and 6-monthly variation), suggesting an improved model prediction. The aforementioned long-term studies showed that LPM approaches can also be applied successfully for transient flow, which is usually prevailing under field conditions. In case of strongly variable flow, it was revealed to be adequate for LPM application to separate the whole observation period into sub-periods, such as those related to seasonal influences or vegetation periods (Maloszewski et al. 2006; Stump et al. 2009a and b). Such sub-periods, characterized by specific mean transit times, could allow the hydraulic system to get closer to quasi steady-state flow conditions.

An important task related to LPM application is the determination of the tracer input function, in our case, the influx of stable water isotopes into the unsaturated zone with recharging water. Usually, this is not directly measured but needs to be estimated from available data such as stable water isotope content (delta-values) measured in precipitation. Infiltrating isotope concentrations also depend on the amount of infiltrating water, which varies, e.g., along with fluctuating precipitation and evapotranspiration. Accordingly, delta-values of precipitation can be weighted by the amount of recharging water, taking into account average recharge within characteristic periods. In this way, e.g., seasonal influences can be considered (Maloszewski and Zuber 1982; Grabczak et al. 1984).

Estimating an adequate input function is often challenging, not only with respect to the determination of infiltration (recharge) but also, in particular, on the catchment scale,

due to complex interactions between different components of the hydrological system. Thus, simple hydrological models are often implemented to derive the input function. Applying such a technique, Maloszewski et al. (1992) determined mean transit times for the groundwater runoff component and several karst springs in an Alpine catchment characterized by three different aquifer types. For a small catchment in the Vosges massif, France, Viville et al. (2006) were able to substantially improve the estimation of the input function by implementing a water balance model to describe the flow system, which was conceptualized by two coupled reservoirs (the unsaturated and saturated zone).

For lysimeters planted with different crops, Stumpp et al. (2009a and b) revealed the importance of considering actual evapotranspiration for the input function, in particular, for variable flow. The accuracy of predictions was also improved by considering specific vegetation periods for LPM application due to changing flow conditions (as mentioned above). Open questions remained, among others, on possible model improvements to describe the transitions between the different vegetation phases in more detail, so that abrupt changes in modeled output tracer concentration are avoided (Stumpp et al. 2009b).

Authors pointed towards preferential flow as an additional important contribution, requiring further investigation. E.g., for lysimeter studies carried out by Maloszewski et al. (2006), significant contributions of direct flow, acting as preferential flow, were calculated with a two-component mixing approach, assuming that direct flow is smaller than the sampling interval. The importance of preferential flow on adequately characterizing unsaturated zone flow and transport processes has been studied intensively, e.g., by Stumpp et al. (2009c), Isch et al. (2019), Benettin et al. (2019) and Radolinksi et al. (2021). The consideration of LPM in combination with preferential flow consideration has successfully been applied, e.g., by Stumpp et al. (2007).

1.4. OBJECTIVES OF THIS THESIS

The aim of this research is to improve the understanding of water flow characteristics in two different soils (sandy gravel and clayey sandy silt) planted with the same vegetation (maize) based on stable water isotope observations and modeling. This

includes investigating the influence of different soil textures on flow dynamics. To the best knowledge of the authors, to date, only a few lysimeter studies with stable water isotopes are available which consider the same vegetation but different soil types.

Determination of flow and transport parameters, i.e., the mean transit time of water T, dispersion parameter P_D and the portion of preferential flow p_{PF}, is an important goal for this study. Isotope transport was modeled with help of LPM approaches that consider (i) the soil matrix only, and (ii) the soil matrix and preferential flow paths.

Another goal is to find out how and to which extent, the vegetation and evapotranspiration could affect water flow in the subsurface (infiltration) and input of stable water isotopes (input function). To achieve this goal, different assumptions for evapotranspiration and input functions were compared.

Furthermore, we intend to optimize "traditional" LPM approaches by subdividing the whole simulation time into several sub-periods in order to mimic transient flow (extended LPM). In this way, one set of parameters (mean transit time and dispersion parameter) is fitted for each sub-period, instead of one parameter set, only, for the whole simulation period ("traditional" LPM). We want to show if the "traditional" LPM, which was originally developed for steady-state flow conditions, can produce a valid model for a variable flow. Further, we describe short-time fluctuation and measured peaks more accurately in the extended LPM. To do this, a dual-permeability system is implemented (separation of transport through the subsurface matrix and along preferential flow paths). Furthermore, we consider the influence of immobile water as a second porosity system on stable water isotopes by a constant isotopic upshift, as a simplification.

The extended LPM approach was compared with numerical simulations of water flow and stable water isotope transport, using HYDRUS-1D. We evaluate both methods for describing observations and to verify, by comparison to numerical (mechanistic) model results, that the extended LPM approach is not only related to mere fitting success.

2. MATERIAL AND METHODS

2.1. SITE AND CONSIDERED VEGETATION AND SOIL CORES OF LYSIMETER 1 AND LYSIMETER 2

Field investigations were done at a lysimeter site run by the Bavarian Environment Agency (Bayerisches Landesamt für Umwelt, LfU). This site is located near Wielenbach, Germany, about 48 km Southwest of Munich and at an elevation of 549 m asl (meter above sea level). The lysimeters are weighable, consisting of stainless steel cylinders filled with undisturbed cores from different soils. Each lysimeter has a surface area of 1 m^2 area (0.56 m radius) and a length of 2 m. Lysimeter weight and the weight of lysimeter seepage water were measured automatically at a temporal resolution of 0.5 hours. For our study, two lysimeters were considered: Lysimeter 1 (Ly1) is filled with sandy gravel taken from a former target shooting area near Garching, Germany, and Lysimeter 2 (Ly2) contains clayey sandy silt from an agricultural site at Hutthurm-Auberg near Passau, Germany. The soil of Ly1 can be characterized as a calcaric Regosol developed above sandy to silty calcareous gravels. It consists of a humic A-horizon extending until a depth of 50 cm, followed by a C-horizon continuing until 2 m depth. The latter is characterized by (silty-) sandy gravels (details see Table 1). Table 1 contains information on soil horizons and measured grain size distributions (only limited data available for Ly1). The soil of Ly2 corresponds to a Cambisol (Stagnosol) developed above gneiss, consisting of five horizons. Silt is predominant in most horizons, followed by the contribution of clay and sand at different percentages (Table 2).

Tables 1 and 2 summarize the characteristics of the soils within Ly1 and 2, respectively. In Ly1, the A-horizon consists of grain sizes >2mm at portions between 33 and 66%. It is followed by a C-horizon (50 cm depth and below), where grain sizes >2 mm contribute to around 80%. In Ly2, silt is predominant in most horizons, followed by the contribution of clay and sand at different percentage. An exception is the Bv-horizon in 40-90 cm depth, where clay is dominating. Contributions of clay and sand are similar except for the Bv-horizon (high portion of clay) and the BvCv-horizon in 90-130 cm depth (low portion of sand, high portion of clay).

Table 1. Soil characteristics, Ly1.

Depth [cm]	Horizon	Characteristics	Components <2 mm (%)	Components >2 mm (%)
0-20	Ah	Humic upper soil	51	49
20-30	Ah	Humic upper soil	49	51
30-40	Ah	Humic upper soil	67	33
40-50	Ah	Humic upper soil	34	66
50-100	C	C-horizon, Sandy gravel	19	81
100-200	C	C-horizon, Sandy gravel	21	79

Table 2. Soil characteristics, Ly2.

Depth [cm]	Horizon	Characteristics	Gravel (wt. %)	Sand (wt. %)	Silt (wt. %)	Clay (wt. %)
0-40	Ap	A-horizon, ploughed soil	4	23	49	23
40-90	Bv	B-horizon, loamy, brown	2	20	35	43
90-130	BvCv	Transition Bv to Cv	<1	5	55	39
130-180	Cv	C-horizon, loamy, brown	2	25	45	27
180-200	C	C-horizon, gneiss debris	3	21	55	20

Between April 2013 and October 2017, the lysimeters were planted with maize (upper boundary). The maize plantation covered an area of 30 m^2 in total. The lower boundary of each lysimeter was seepage face controlled (allowing drainage if the soil is saturated; no upward inflow).

2.2. FIELD MEASUREMENTS, SAMPLING AND MONITORED PARAMETERS

At the lysimeter site, precipitation and seepage water (lysimeter outflow water) have continuously been collected (July 1st 2013 to April 29th 2016) in one-week intervals (longer intervals in case of dry conditions and water scarcity, shorter intervals in case of high water availability) for subsequent analysis of stable water isotopes. Precipitation was collected with a heatable all-weather precipitation gauge (Pluvio, OTT Hydromet), using an automatic weight-based recording of precipitation amount (temporal resolution of 0.5 h). A meteorological weather station is present at the lysimeter site, run by the German Meteorological Service (Deutscher Wetterdienst DWD), from which data on precipitation (prior to 2013), air temperature and air humidity were taken (daily averages). Data on wind velocity and incoming short-wave solar radiation (daily averages) were taken from the DWD weather station near Hohenpeißenberg, Germany, located about 15 km Southwest of the lysimeter site (these data were not available at Wielenbach for the studied time period). Satellite observations for longwave radiation and other meteorological parameters (monthly

averages) were obtained from the Satellite Application Facility on Climate Monitoring (CM SAF, product CLARA-A2), which is representative of the wider (about 25 km x 25 km) area around the lysimeter site.
Measurements or sampling within the soil cores, such as of water content or hydraulic potential, were not possible due to experimental restrictions.

2.3. STABLE WATER ISOTOPE ANALYSIS

Precipitation and lysimeter seepage water samples were analyzed for stable water isotopes by laser spectroscopy, using the Triple-Liquid Water Isotope Analyzer (T-LWIA), Model 912-0050 (Los Gatos, Inc.). Measurements covered a time period of close to 3 years (July 1st 2013 to April 29th 2016). Prior to analysis, water samples (20 mL) were filtered (0.45 µm) and triplicates were prepared for stable isotope measurement (2 mL vials) using a syringe. The vials were sealed immediately with caps containing a silicon septum. Measurement of each sample involved eight replicates repeated four times. Hydrogen and oxygen isotope ratios were expressed in the internationally accepted delta-notation in respect to the Vienna Standard Mean Ocean Water (V-SMOW), with δ [‰] = (R_{sample} – $R_{standard}$) / $R_{standard}$ x 1000, where R stands for the $^{18}O/^{16}O$ and $^{2}H/^{1}H$ ratio of the sample and standard, respectively.

2.4. DETERMINATION OF EVAPOTRANSPIRATION

2.4.1. EVALUATION OF THE WATER BALANCE

If precipitation (P), lysimeter outflow (Q) and lysimeter weight (m) are measured and no surface runoff is expected (flat area), evapotranspiration can be estimated as ET = $\Delta m + P - Q$. In the latter water balance equation, $\Delta m = m_{i-1} - m_i$ is the change of lysimeter weight between the previous (i-1) and the actual (i) measurement, so that positive Δm indicates weight loss (e.g., Hirschi et al. 2017). In this study, P, Q and m were measured every 30 minutes. Weight changes due to on-site activities (such as seeding or harvest of maize plants) were corrected, and missing values (measurement gaps) were filled by linear interpolation. However, some measurement noise was

obvious, reflected, among others, in small shifts between recorded signals. Such measurement noise can be attributed to different recording sensitivities and might also be induced by influences of wind or heavy rain (e.g., Peters et al. 2014). Therefore, in this study, daily moving averages have been calculated as a simple (and conservative) smoothing routine for filtering the noisy data. This simple routine was used because the focus of this study is rather on longer term developments (daily to weekly changes, evaluating isotope measurements done on a weekly basis). In addition, ET estimation was simplified as follows (e.g., Gebler et al. 2015): any weight loss can either be due to Q or ET. Therefore, if weight loss Δm minus Q is positive it indicates ET, if negative it indicates "input" (and thus no ET):

$$ET_{actual,weight} = \begin{cases} \Delta m - Q & \text{if } \Delta m > Q \\ 0 & \text{if } \Delta m \leq Q \end{cases} \quad \text{Equation (3)}$$

The latter approach (Equation 3) implies that no ET is taking place during precipitation. $ET_{actual,weight}$ was considered as ET_i for the input function IF2.

2.4.2. HAUDE APPROACH

The Haude approach (Haude 1954 and 1955, Olbrisch 1975, Hölting and Coldewey 2019) enables estimation of potential evaporation ET_{pot} [mm/d = L/d] at a low data need:

$$ET_{pot}^{Haude} = f_{Haude} \cdot P_{14} \left(1 - \frac{F_{14}}{100}\right) \quad \text{Equation (4)}$$

where F_{14} [%] is the relative air humidity and P_{14} [hPa] the saturation vapor pressure measured at 2 p.m., respectively. The latter can be estimated from air temperature T_{air} [°C] by the following empirical equation (e.g., Hölting and Coldewey 2019):

$$P_{14} = 4.58 \cdot 10^{\frac{7.45 \cdot T_{air}}{235 + T_{air}}} \quad \text{Equation (5)}$$

Empirical monthly Haude coefficients f_{Haude} [mm / (hPa d)] are available for different types of vegetation covers (Table 3). In this study, f_{Haude} for maize was considered during the maize growth season (1 May to 1 October) and f_{Haude} for grass during the remaining period.

Table 3. Monthly Haude coefficients f_{Haude} [mm / (hPa d)] in Germany.

Plant	Jan	Feb	Mar	Apr	May	Jun	Jul	Aug	Sep	Oct	Nov	Dec
Maize*	0.15	0.15	0.18	0.18	0.18	0.26	0.26	0.26	0.24	0.21	0.14	0.14
Grass**	0.26	0.26	0.33	0.39	0.39	0.37	0.35	0.33	0.31	0.26	0.26	0.26

*for maize cultivation (Haude 1955), **for grass (Löpmeier 1994)

Actual evapotranspiration ET_{act} (considered as ET_i for input function IF3) was obtained as

$$ET_{act} = K_C \cdot ET_{pot}^{Haude}, \quad \text{Equation (6)}$$

where K_C [-] is the crop coefficient taking into account specific aspects related to crop cultivation that may influence evapotranspiration. Those include the crop canopy and aerodynamic resistance, as well as frequency and depth of wetting (Allen et al. 1998). Three different stages are reported, including $K_{C,ini}$ = 0.3 related to the initial crop growth stage (typical value for cereals), $K_{C,mid}$ = 1.2 for the mid-season stage of maize (corn) and $K_{C,end}$ = 0.35 for the end of the late-season stage and maize harvest after complete field drying of the grain (Allen et al. 1998). These reported values refer to non-stressed, well-managed crops in sub-humid climates (minimum relative air humidity above 45%). For Ly1, a reduced $K_{C,mid}$ of 0.732 was found to describe observations best, corresponding to a reduced growth of maize observed for this lysimeter, compared to Ly2. The length of the different periods was fitted based upon field observations of maize growth stages. $K_{C,ini}$ was also considered for the time outside the vegetation period, as similarly done by Legind et al. (2012) for background ET.

2.4.3. PENMAN-MONTEITH APPROACH

Using the Penman-Monteith approach, potential evapotranspiration ET_{pot} [mm/d = L/d] can be estimated as follows (Allen et al. 1998):

$$ET_{pot}^{PM} = \frac{1}{\lambda \rho_w} \cdot \frac{\Delta(R_n - G) + \rho_a c_p (e_s - e_a)/r_a}{\Delta + \gamma \cdot (1 + r_s/r_a)} \cdot 1000 \frac{L}{m^3} \cdot 86400 \frac{s}{d} \qquad \text{Equation (7)}$$

where λ is the latent heat flux (2.45×10^6 J/kg), ρ_w is the density of water (1000 kg/m^3), ρ_a is the density of air (1 kg/m^3), e_s is the saturation vapor pressure [kPa] and can be estimated from air temperature T_a [°C] as $e_s = 0.611 \times \exp [17.27\ T_a / (T_a + 237.3)]$, e_a is the actual vapor pressure [kPa] and can be estimated from e_s and relative air humidity RH [-] as $e_a = e_s \times RH/100$, Δ is the slope of the vapor pressure curve [kPa/°C] and can be estimated from e_a as $\Delta = 17.27 \times 237.3 \times e_a / (T_a+237.3)^2$, G is the soil heat flux [J/(m^{2}s)] (assumed zero), R_n is the net solar radiation [J/(m^{2}s)], c_p is the specific heat of air (1013 J/kg/°C), r_a is the aerodynamic resistance [s/m] and can be estimated from wind speed W [m/s] as $r_a = 208/W$, r_s is the surface bulk resistance [s/m] and can be estimated from stomatal resistance r_l [s/m] and leaf area index LAI [m^2 leaf per m^2 area] as $r_s = r_l / (0.5 \times LAI)$, γ is the psychrometic constant (0.066 kPa/°C).

The surface bulk resistance r_s depends on vegetation and is also influenced by CO_2 concentration, water salinity and acidity, as well as patterns of precipitation or irrigation (Takakura et al. 1975, Turan et al. 2009, Beardsell and Cohen 1975). Specific values for maize were used for its growth season (May to October); otherwise, values for short grass were considered for ET calculation. For short grass, a r_s of 70 s/m was used (Allen et al. 1998), and for maize, the best estimate of 131 s/m was found (with r_l = 294 s/m taken from Farahani (1995), and LAI = 4.5 m^2/m^2 taken from Wilson (2007)).

Net solar radiation R_n [J/(m^{2}s)] was obtained as $R_n = (R_{s,in} + R_{l,in}) - (R_{s,out} + R_{l,out})$ (Monteith and Szeicz 1961), where $R_{s,in}$ and $R_{l,in}$ is incoming short- and long-wave radiation, and $R_{s,out}$ and $R_{l,out}$ is outgoing short- and long-wave radiation. Observations of $R_{s,in}$ were taken from the meteorological station at Hohenpeissenberg (DWD) as daily averages (see chapter 2., Materials and Methods), and $R_{s,out}$ was estimated by

multiplying $R_{s,in}$ with the albedo or canopy reflection coefficient α [-] (according to Allen et al.1998). For α, average observed values for maize (0.175) and grass (0.23) were used (Allen et al. 1998), depending on the growth season (presence of maize). Long-wave radiation data ($R_{l,in}$ and $R_{l,out}$) were taken from satellite observations for the wider region (details see chapter 2., Materials and Methods) as monthly averages. Since data were only available for the time before 2015, for January to April 2016, average values were used, respectively, from observations between 2012-2015.

Actual evapotranspiration ET_{act} was obtained from $ET_{pot,PM}$ and K_C analogously to above (Equation 6). This was used as ET_i for input function IF4 and as $ET_{i,PM}$ in Equation 16 for IF5.

2.4.4. SIMULATION OF MAIZE TRANSPIRATION

For many annual plants including crops, logistic growth has been observed with an exponential growth phase at the beginning, which slows down until growth stops at ripening (e.g., Richards 1959, Trapp 2007). Transpiration is closely related to plant growth and can be obtained from changing plant mass dM/dt (e.g., Rein et al. 2011):

$$\frac{dM}{dt} = k \cdot M\left(1 - \frac{M}{M_{max}}\right) \qquad \text{Equation (8)}$$

where k [d^{-1}] is the rate constant for exponential growth and M_{max} [kg] is the maximum plant mass. Plant mass as a function of time can be calculated by integrating the growth function. With the initial plant mass M_0 it follows:

$$M(t) = \frac{M_{max}}{1 + (M_{max}/M_0 - 1) \cdot e^{-k\,t}} \qquad \text{Equation (9)}$$

Transpiration Q [L/d] of plants is closely related to growth via the transpiration coefficient T_C [L/kg], and can be calculated as:

$$Q = T_C \cdot \frac{dM}{dt} = T_C \cdot k \cdot M \left(1 - \frac{M}{M_{max}}\right) \qquad \text{Equation (10)}$$

where Q is the water flux through the roots and out of the stem, related via T_C to the change of total plant mass. Typical values of the transpiration coefficient T_C for crop plants in humid areas range from 200 to 900 L transpired water per kg produced biomass (dry weight) (Larcher 1995). A typical (average) value of 500 L is often used (e.g., Trapp 2007, Legind et al. 2012) and was also considered in this study. Transpiration Q was modeled for maize plants (denoted Q_{Maize}) using Equation 10. For initial plant mass M_0, a value of 0.031 kg (fresh weight) was considered, corresponding to the approximate mass of seeds (based upon Legind et al. 2012). The growth rate constant k and the maximum plant mass M_{max} were fitted for both considered lysimeters. The latter corresponds to harvested mass, where a range between 2.3 and 5.3 kg per m^2 is reported for the studied site.

2.5. DETERMINATION OF SOIL HYDRAULIC PARAMETERS

It was not possible to take soil samples from the studied lysimeters, because the soil cores had to be kept undisturbed for ongoing investigations at the lysimeters. Unfortunately, the original sites from where the soil cores were taken were not accessible, anymore, due to the construction of buildings and infrastructure. However, soil samples could be taken about 1 km West of the original excavation site for the soil core of Ly1 (near Garching, Germany), for which, based upon information from pedological and geological maps, similar soil types and textures can be assumed. At the site near Garching, soil samples (three replicates) were taken at a fresh hillside cutting from three different depths, i.e., 0-0.1 m, 0.1-0.2 m and 1.0-1.2 m below surface (see Table 5). For these samples, water retention curves and unsaturated hydraulic conductivity were measured using the ku-pF apparatus DT 04-01 (Umwelt-Geräte-Technik GmbH UGT, Germany). Measurements yielded the following soil hydraulic parameters (SHP): residual and saturated soil water content (θ_r and θ_s), the water retention curve shape parameters α and n (van Genuchten-Mualem model), as well as

the saturated hydraulic conductivity K_s (see Table 2). For Ly2, soil sampling at a representative site was not possible due to restricted accessibility.

2.6. MATHEMATICAL MODELING

2.6.1. LUMPED-PARAMETER MODELING

In order to interpret the observed stable water isotope ratios, lumped-parameter models (LPM) were used to implement different assumptions. Such modeling describes the relationship between tracer input and tracer output concentration as a function of time by considering a specific transit-time distribution function for tracer particles within the hydraulic system. This function has to be chosen depending on relevant transport processes and the expected flow conditions. For a conservative tracer behavior (no decay, no reaction or sorption) and quasi-steady-state flow, the following convolution integral can be applied for tracer transport simulation (e.g., Maloszewski and Zuber 1982, Maloszewski et al. 2006, Stumpp et al. 2009a):

$$C_{out}(t) = \int_0^t C_{in}(t-\tau)\, g(\tau)\, d\tau \qquad \text{Equation (11)}$$

where C_{out} is the calculated tracer output concentration (here simulated stable water isotopes, i.e., delta-values [‰], in lysimeter seepage water) and C_{in} is the tracer input concentration (delta-values of infiltrating water) as a function of time (the input function). g(τ) is a continuous transit-time distribution function (weighting function or system response function) and τ corresponds to all transit times within the system. For tracer transport through the subsurface matrix, the following analytical solution of the advection-dispersion equation was used for g(τ) (considering a Dirac pulse for tracer input into inflowing water; Lenda and Zuber 1970, Kreft and Zuber 1978):

$$g_M(\tau) = \frac{1}{\tau\sqrt{4\pi P_D\, \tau/T}} exp\left[-\frac{(1-\tau/T)^2}{4P_D\, \tau/T}\right] \qquad \text{Equation (12)}$$

where T is the mean transit time (or mean travel time) of water [d] and P_D [-] is the dispersion parameter defined as $P_D = D_L / (v \cdot x) = \alpha_L / x = 1 / Pe$, (e.g., Leibundgut et al. 2009), with longitudinal dispersion coefficient D_L [m^2/d], mean water flow velocity v [m/s], flow length x [m] (x=lysimeter length= 2 m), longitudinal dispersivity α_L [m] and Peclet number Pe [-]. The average flow velocity in the subsurface matrix can be calculated as $v_{av} = x / T$, and the lysimeter discharge rate is obtained by $q = Q / A$, with lysimeter outflow rate Q and lysimeter surface area A. The average pore water content θ_{av} is given by dividing the average discharge rate by the average flow velocity. θ_{av} refers to the average portion of soil water taking part in flow through the soil matrix and thus can be seen as an estimate of the effective porosity.

To consider tracer transport through both (i) the subsurface matrix and (ii) along preferential flow paths, the model was extended (based on Maloszewski and Zuber 1982, Stumpp et al. 2007):

$$C_{out}(t) = (1 - p_{PF}) \int_0^t C_{in}(t-\tau)\, g_M(\tau)\, d\tau + p_{PF} \int_0^t C_{in}(t-\tau)\, g_{PF}(\tau)\, d\tau \qquad \text{Equation (13)}$$

where p_{PF} [-] is the portion of preferential flow on tracer transport, with

$$g_{PF}(\tau) = \delta(\tau - T_{PF}) \qquad \text{Equation (14)}$$

In Equation 14, preferential flow is described by a piston flow model, where δ is the Dirac delta function and T_{PF} is the mean transit time of water within preferential flow paths. This is a simplified assumption taking into account advective transport, only. In this study, T_{PF} was set to one day, corresponding to the chosen temporal resolution (also reflected in dτ). Information on preferential flow is restricted, however, by the temporal resolution of measurements. Thus, given weekly measurements of stable

water isotopes, observed transport with the preferential flow might be one week or less. Since measurement frequency sometimes differed from one week (as described in 2.2 Field measurements, sampling and monitored parameters), modeling was done on a 1-day basis. A more detailed investigation of preferential flow would require a higher resolution of measurements, which, however, was not the goal of this study.

Inherent to the LPM methodology, the soil core within the lysimeter is considered as a "black box" and thus homogeneous, so that one set of parameters is obtained for the entire subsurface. Models were set up with MATLAB R2018a (using the conv function) and within a Microsoft Excel TM spreadsheet (numerical approximation of the convolution integral).

As explained before, the tracer input function (IF) describes the isotope content in the recharging water as a function of time and thus the tracer input into the unsaturated zone (corresponding to in Equation 13). Since it was not directly measured, it had to be estimated. Our first assumption (IF0) considers the isotopic composition (delta-values) of precipitation as the input function $C_{in}(t-\tau)$ (no modification). For IF1 to 5, weighting is done to determine $C_{in}(t-\tau)$ as described in Equation 15. Delta-values measured in precipitation δ_i [‰] are weighted by the recharge at the same event i, which referred to the average recharge within the weighting period and to the average isotopic composition of lysimeter outflow within the total observation period $\overline{\delta_{out}}$ (based on Grabczak et al. 1984 and Maloszewski et al. 1992, similarly applied by and Stumpp et al. 2009a and b):

$$C_{in}(t_i - \tau) = \frac{N \cdot \alpha_i \cdot P_i}{\sum_{i=1}^{N} P_{eff,i}} \left(\delta_i - \overline{\delta_{out}}\right) + \overline{\delta_{out}} \qquad \text{Equation (15)}$$

Where $P_{eff,i}$ is recharge (infiltration) or effective precipitation ($\alpha_i \cdot P_i$), with precipitation rate P_i [L/d] and recharge factor α_i [-]. N [-] is the number of events during the weighting period. Weighting has been done considering periods of 1, 3 and 6 months in order to reflect the changing conditions of isotope input due to variable flow (infiltration). Six-month periods extended from May to October, i.e., corresponding to maize cultivation, and from November to April (grass cover). They were further subdivided into three-month periods. In this way, possible seasonal effects and the

influence of vegetation periods were studied. The period of one month was chosen to consider short-term processes influencing infiltration, such as varying rainfall intensities or plant growth conditions.

For IF1, as an upper estimate, $\alpha_i = 1$ is assumed: all precipitation water is infiltrating and evapotranspiration is neglected ($P_{eff,i} = P_i$). For input functions IF2 to 5, actual evapotranspiration (ET) was considered in the water balance as $P_{eff,i} = P_i - ET_i$ (infiltration or recharge = precipitation – evapotranspiration), and this was used for Equation 15 and the three weighting periods mentioned above (1, 3 and 6 months). For IF2, actual evapotranspiration was determined from the water balance, i.e., measured precipitation, lysimeter outflow and lysimeter weight. Furthermore, potential evapotranspiration was calculated by using the Haude and Penman-Monteith approach. This was done specifically for maize and grass covers, where the latter was used for periods outside maize growth (details see chapter 2.4.4., Determination of ET with simulation of maize transpiration). Actual evapotranspiration considers soil wetting conditions and crop cultivation via the crop coefficient K_C. This coefficient is dependent on the crop growth stage and was considered as a fitting parameter. Reported best estimate values (Allen et al. 1998; Piccinni et al. 2009) were used as a first guess for the initial, mid-season and late growth stage ($K_{C,ini}$ of 0.3, $K_{C,mid}$ of 1.2 and $K_{C,end}$ of 0.35, respectively). Actual evapotranspiration ET_i was determined, accordingly, for IF3 (Haude-based) and IF4 (Penman-Monteith-based).

Finally, IF5 considers plant uptake processes more specifically. During the maize growth period, transpiration induced by the maize plants significantly contributes to evapotranspiration. Therefore, we have simulated maize transpiration, explicitly, i.e., we have calculated it from changing plant mass according to Rein et al. (2011). In this scenario, we assume that simulated maize transpiration Q_{Maize} [L/d] as a function of time can be used to approximate the time course of actual evapotranspiration ET_i, in case maize transpiration is the dominating process:

$$ET_i = \begin{cases} ET_{i,PM} & \text{if } ET_{i,PM} \geq Q \\ Q_{Maize} & \text{if } ET_{i,PM} < Q \end{cases} \qquad \text{Equation (16)}$$

In Equation 16, $ET_{i,PM}$ is actual evapotranspiration based upon the Penman-Monteith approach, which can be seen as a background (for periods outside maize growth). In

the following, this scenario is named “transpiration plus background ET”. All above mentioned LPM is called “traditional” LPM in the following text.

2.6.1.1. Extended lumped-parameter model

In the next step, we have extended the LPM approach and subdivided the whole simulation time into several sub-periods. We have applied a summer-winter scheme, with summer from April to September, where maize is grown, and winter from October to March. This scheme was used for setting up six sub-periods for the observation time at the lysimeters, i.e., July 2013 to April 2016 (the final sub-period extended from October 2015 to April 2016), and for additional pre-phases. For each lysimeter, it was required to consider a pre-phase prior to the observations period, in order to ensure a complete tracer (stable water isotope) breakthrough. These pre-phases were determined iteratively over mass balances and encompassed one year for Ly1 and five years for Ly2. Eight sub-periods were considered, in total, for Ly1 (for July 2012 to April 2016) and nine for Ly2 (additional initial sub-period P1 for July 2008 to June 2012). Thus, eight parameter sets of T, P_D and p_{PF} were fitted for Ly1 and nine for Ly2, one for each sub-period.

2.6.2. NUMERICAL MODELING

The numerical modelling was carried out by Anne Imig.

2.6.2.1. Unsaturated flow

Water flow in the unsaturated zone of the studied lysimeter soil cores was simulated numerically with the software package HYDRUS-1D, which solves the Richards equation (Šimůnek et al. 2008 and 2016). The van Genuchten-Mualem approach was applied for the soil hydraulic functions θ(h) and K(h) (van Genuchten 1980 and Mualem 1976, respectively):

$$\theta(h) = \begin{cases} \theta_r + \dfrac{\theta_s - \theta_r}{[1 + |\alpha h|^n]^m} & if\ h < 0 \\ \theta_s & if\ h \geq 0 \end{cases}$$ Equation (17)

$$K(h) = K_s S_e^l \left[1 - \left(1 - S_e^{1/m}\right)^m\right]^2$$ Equation (18)

where θ(h) and K(h) are water content [L^3/L^3] and hydraulic conductivity [L/T] as a function of hydraulic pressure head h [L]; θ_r and θ_s are the residual and saturated water content, respectively [L^3/L^3], and K_s is the saturated hydraulic conductivity [L/T]. α [L^{-1}], n [-] and m [-] are empirical water retention curve shape parameters, where m = 1 – 1/n (n > 1). α is often related to the inverse air-entry suction, whereas n to the pore-size distribution. The effective saturation S_e [-] is given as $S_e = (\theta(h) - \theta_r) / (\theta_s - \theta_r)$. The pore connectivity factor l [-] represents the tortuosity of transport paths within the system. In order to decrease the number of fitting parameters, in this study, it was set to 0.5, as, e.g., proposed by Mualem (1976), who found this as an average value based on data for 45 mineral soils of different textures (clays, loams and sands) (as similarly done in, e.g., Sprenger et al. 2015 and 2017).

2.6.2.2. Stable water isotope transport in the unsaturated zone

Solute transport can be described by the advection-dispersion equation, which can be set up for the unsaturated zone as follows (e.g., Fetter 1993):

$$\frac{\partial(\theta C)}{\partial t} = \frac{\partial}{\partial z}\left(\theta D \frac{\partial C}{\partial z}\right) - \frac{\partial(qC)}{\partial z}$$ Equation (19)

where C is the tracer concentration [M/L^3], D is the dispersion coefficient [L^2/T], and q is the volumetric fluid flux [L/T]. In this study, for the transport of stable water isotopes, longitudinal dispersion is considered so that D is defined as $D_L = \alpha_L \cdot v$, where α_L is the longitudinal dispersivity [L] and v [L/T] is flow velocity. The dispersion

parameter P_D [-] is given as $P_D = \alpha_L / x$, where x is the flow length [L] (in our case x = 2 m, corresponding to lysimeter length).

For stable water isotope transport modeling with HYDRUS-1D, a modified approach developed by Stumpp et al. (2012b) was used. In the standard version of HYDRUS-1D, evaporation leads to an accumulation of solutes at the upper boundary. The modified code (Stumpp et al. 2012b) contains changes for the upper boundary so that evaporation has no effect on the solute concentration (isotope content). Thus, any isotopic fractionation due to evapotranspiration is neglected. This is expected to be a valid assumption if the observed regression line of stable isotopes of soil water is very close to the local meteoric water line (LMWL) of precipitation (Stumpp and Hendry 2012a). As it can be seen in Figure S7 in Appendix, such similarity is observed at our study site.

2.6.2.3. Consideration of preferential flow paths and the influence of immobile water

In addition, we also have considered preferential flow paths for numerical modeling in order to account for the presence of a second permeability system. This was done outside of HYDRUS-1D (within a model code set up within Python) since, currently, no model version is available that is adjusted for simulating the transport stable water isotopes in a dual permeability domain. As a simplified assumption, similar to lumped-parameter modeling (see above), piston flow (advective transport) was assumed for the preferential flow paths. A portion p_{PF} of precipitation directly enters preferential flow paths, and the remaining portion ($1-p_{PF}$) of precipitation reaches the surface of the subsurface matrix. Mean transit times of preferential flow T_{PF} between 1 and 7 days were compared for modeling, which would correspond to rapid flow within average sampling frequency. The model setup is illustrated in Figure S12 in Appendix. We have considered that for a T_{PF} of 1 day, 5% of precipitation (for the example of $p_{PF} = 0.05$) is transported along preferential flow paths of the lysimeter soil core: at lysimeter outflow, simulated preferential flow corresponds to 5% of precipitation shifted by one day. For higher T_{PF}, moving averages of daily precipitation rates were calculated: as an example, for T_{PF} = 7 days, we assume that precipitation water takes one week for passing the preferential flow paths and reaching lysimeter outflow. Precipitation water present within the preferential flow paths is assumed to be fully mixed. Preferential

flow paths were considered for the transport of stable water isotopes, accordingly (see Figure S12 in Appendix).

Furthermore, we have extended the model approach by the possibility of an additional isotopic component that accounts for the mixing of mobile water with immobile water. As a simplified assumption, the addition of a constant positive delta-value, leading to an upshift of delta-values in seepage water, might represent the influence of immobile water that is isotopically enriched.

2.6.2.4. Numerical model setup

For numerical modeling, the soil cores of the two lysimeters (Ly1 and Ly2) were represented as 1D model domains, discretized in 201 nodes with an equal distance of 1 cm. Two cases were considered, (i) a homogeneous subsurface (one-layer case) and (ii) several layers based upon information available for the soil profiles (multi-layer case). In the multi-layer case, four layers were considered for Ly1 and five layers for Ly2, as indicated in Table 4.

Table 4. Information on soil layers and grain size distributions. Comp.: components, wt.: weight, a: average of two layers with very similar grain size distribution.

Lysimeter 1					Lysimeter 2						
Layer	Horizon	Depth [cm]	Comp. <2 mm (%)	Comp. >2 mm (%)	Layer	Horizon	Depth [cm]	Gravel (wt. %)	Sand (wt. %)	Silt (wt. %)	Clay (wt. %)
1 a	Ah	0-30	50	50	1	Ap	0-40	4	23	49	23
2	Ah	30-40	67	33	2	Bv	40-90	2	20	35	43
3	C	40-50	34	66	3	BvCv	90-130	<1	5	55	39
4 a	C	50-200	20	80	4	Cv	130-180	2	25	45	27
-	-	-	-	-	5	C	180-200	3	21	55	20

Soil hydraulic parameters SHP for Ly1 were determined in the laboratory from soil samples taken at a site close to the location of the soil core of Ly1 (see Table 5). Average SHP-values from the three sampling depths were considered for the one-layer case. For the multi-layer-case of Ly1, individual SHP-values for layers 1, 2 and 4, as well as SHP-values from Rosetta for layer 3 were applied. As an initial guess, SHP-values for Ly2 were obtained from the Rosetta database, presented in HYDRUS-1D. These suggested SHP-values are based on the information on grain size distributions of soil.

Table 5. Soil hydraulic parameters were determined for soil samples taken close to the location of the soil core within Ly1. θ_r and θ_s: residual and saturated soil water content; α, n: shape parameters; K_S: saturated hydraulic conductivity.

Sampling depth [cm]	θ_r [cm^3/cm^3]	θ_s [cm^3/cm^3]	α [1/cm]	n [-]	K_s [cm/d]
0-10	0.023	0.193	0.094	1.499	1685
10-20	0.023	0.257	0.163	1.37	24970
100-120	0.01	0.2	0.069	1.377	38880
Average	0.019	0.22	0.109	1.408	20995

For the diffusion coefficient in free water, a value of 10^{-9} m^2/s was used (Stumpp et al. 2012; Stumpp and Hendry 2012a). For water flow, the upper boundary was set up as an atmospheric boundary condition with surface layer, and seepage face (h=0) was set for the lower boundary (lysimeter outflow). At the upper flow boundary, we specified measured precipitation and actual evapotranspiration (ET). The latter has been determined from the water balance at the lysimeters, as described in detail in chapter 2.4.1., Determination of ET with evaluation of the water balance. By default, HYDRUS-1D expects entered evapotranspiration to be potential ET and thus modifies it for estimating actual ET. For preventing such modification, h_{CritA} (the minimum allowed pressure head) was set to a value of -15,000,000 cm as also applied by Groh et al. (2018). Concerning solute transport boundary conditions, as a time-variable solute flux boundary was considered at the top and a zero-concentration gradient at the bottom.
Since positive values are required for transport modeling with HYDRUS-1D, a constant offset (23 ‰) was added to the (negative) delta-value input and subtracted again from the modeling results (as recommended by Stumpp et al. 2012b and Sprenger et al. 2016).
As an initial condition for the modeling pre-phase, a pressure head of -340 cm was set for the whole soil column, corresponding to a water content of field capacity. With respect to boundary conditions, a modeling pre-phase of 2.5 years was considered for Ly1 (January 2011 to June 2013) and 5.5 years for Ly2 (January 2008 to June 2013) prior to the observation period for allowing the pore volume to exchange at least one time. Stable water isotope input for the modeling pre-phase was obtained from the meteorological station near Passau-Fürstenzell (as no measurements were available at the lysimeter site; see Figures S5 and S6 in Appendix). This stable water isotope data shows a similar LMWL for the Wielenbach site and Passau-Fürstenzell (see Figure S7 in Appendix). Initial stable water isotope content was set to an arbitrary value of 2 ‰ at all depths.

Furthermore, we have used the model-independent parameter estimation utility PEST, which is developed by Doherty (2020), and have inversely calibrated the soil-hydraulic and transport parameters. As objective functions, measured delta values in lysimeter outflow, measured discharge rates and water content changes (estimated from recorded lysimeter weight) were used (for details on measurement frequency, see chapter 2.2., Field measurements, sampling and monitored parameters and stable water isotope analysis). Details on parameter bounds for the fitting procedure are provided in Table S3 in Appendix.

2.6.2.5. Estimation of median transit times

Virtual tracer breakthrough curves were simulated with HYDRUS-1D for both lysimeters to derive median transit times (MTT). Those were then compared to mean transit times (T) found by lumped-parameter modeling, to evaluate both approaches. As suggested by Sprenger et al. (2016), ideal virtual tracers were injected every day (constant amounts) at the top of the unsaturated zone, and cumulative tracer breakthrough curves were calculated based on modeled concentration. For each of those curves, the time when median concentration occurred was considered the individual median transit time.

2.6.3. STATISTICAL EVALUATION OF MODEL CURVE FITS

Least-square fitting of predictions to observations was done by manual expert adjustment of model parameters in an iterative procedure. This was based upon statistical evaluation of curve fits using the root mean square error (RMSE), mean error (ME) and coefficient of determination (R^2) (Stumpp et al. 2009a). Statistical data on the curve fits are provided in the Appendix for all simulations.

For lumped-parameter modeling, values for T, P_D and p_{PF} were fitted by comparing observed and simulated time-dependent $\delta^{18}O$ in seepage water. In an iterative procedure, first, a set of T, P_D and p_{PF} was fitted for the whole modeling period. Then, parameters sets were fitted for yearly and finally for the seasonal (winter/summer) periods.

For numerical modeling, the soil-hydraulic and transport parameters were inversely calibrated. Details on parameter bounds for the fitting procedure are provided in Table S3 in Appendix. Transport of both $\delta^{18}O$ and $\delta^{2}H$ was simulated, yielding very similar fitting parameters. In the following, results for $\delta^{18}O$ are presented in detail.

3. Results and Discussion

3.1. Stable water isotope analyses

Stable water isotope characteristics in precipitation showed, as expected, seasonal trends as well as pronounced fluctuations at shorter (weekly to monthly) periods. Results for $\delta^{18}O$ observed in precipitation are presented in Figure S3a, ranging between -22.2 and -2.3 ‰ for the study period (July 2013 to April 2016). The amplitude between the minimum and maximum $\delta^{2}H$ values varied between -11.2 and -164.2 ‰. The seasonal trend reveals lower ^{2}H and ^{18}O contents during winter (more negative delta values) and higher contents during summer (less negative delta values). This typical development was also observed by Stumpp et al. (2014) based on long-term measurements (~30 years) of precipitation in the Munich area.

The observed seasonal fluctuations of isotopic signals are strongly damped in lysimeter seepage water, with $\delta^{18}O$ ranging from -13.8 to -7.0 ‰ for Ly1 and -12.4 to -6.7 ‰ for Ly2, and moreover, seasonal fluctuations were shifted compared to those of precipitation (Figure S3). Such general patterns are mainly induced by transport processes, i.e., advection and dispersion of stable water isotopes within the subsurface (Stichler and Herrmann 1983). However, precipitation water translocated rapidly along preferential flow paths can also contribute to isotopic signals observed in the lysimeter outflow. Comparing both lysimeters, delta values in the outflow of Ly2 filled with silt (Q2) were less negative ($\delta^{18}O$ of -9.4 in average) than those in the outflow of Ly1 filled with sandy gravel (Q1) (with $\delta^{18}O$ of -10.3 in average). This could be due to the slower infiltration of precipitation in the silt soil, so that water resides longer in upper soil and may be affected more strongly by evaporation (thus getting enriched in the heavier isotopes). Moreover, the discharge is generally higher in Ly1, and winter precipitation mainly contributes to the recharge. Since winter precipitation is characterized by more negative delta values compared to summer precipitation, this can be a possible explanation for the observed differences (more negative delta values in the outflow of Ly1, compared to Ly2). Another possible contribution might be related to the higher soil water storage in Ly2. If some of the stored winter precipitation is accessed by plants later during the growing seasons, this could possibly lead to a higher loss of (more negative) winter water in Ly2. Fluctuations were slightly more damped

in Q2 than in Q1, with a total amplitude (range maximum – range minimum) of 6.8 ‰ for Q1 and 5.7 ‰ for Q2. This may reflect higher dispersion and may be influenced by a more intense mixing with immobile water stored from previous rain events (Viville et al. 2006).

The slope and the deuterium-excess of the observed local meteoric water line (LMWL) stemming from the precipitation sampling point at the Wielenbach site were similar to the global meteoric water line (GMWL), as shown in Figure S4a for the total observation period and specifically for summer (April to September) and winter (October to March). This is similar to the findings of Stumpp et al. (2014) for the Munich area, for observations close to our field site. Deviations from the GMWL were more pronounced for lysimeter seepage water, where lines fitted to the isotopic composition of lysimeter outflow showed slightly lower slopes and higher intercepts (Figure S4b and c). Higher intercepts can be influenced by higher evaporation, so that leachate water would be more isotopically enriched in summer (e.g., Barnes and Turner 1998).

For the modeling of tracer (stable water isotope) transport through the unsaturated zone, we considered one additional year of input prior to the beginning of measurements (April 2013) as a pre-phase. Since isotopic data were not available for the Wielenbach site for this time period, we considered δ^2H and $\delta^{18}O$ measured in precipitation at the meteorological station Passau-Fürstenzell (DWD, Helmholtz-Zentrum München, Germany; Stumpp et al. 2014). These data were obtained from the International Atomic Energy Agency (IAEA) via their Global Network of Isotopes in Precipitation (GNIP), online platform WISER, as monthly averages. Figure S5 and S6 show the temporal development of $\delta^{18}O$, revealing similar patterns and a similar range of values compared to precipitation at the Wielenbach site. LMWLs of precipitation in Wielenbach and in Passau-Fürstenzell are similar to each other (see Figure S7).

3.2. WATER BALANCE AND DYNAMICS IN THE LYSIMETERS

Precipitations (P), lysimeter outflow (Q) and lysimeter weight (m) were monitored at the study site. The temporal development of cumulative amounts is shown in Figure S1 of the Appendix. Within the whole study period (~3 years), precipitation sums up to 2341 L and outflow to 1473 L for Lysimeter 1 (Ly1) and 1138 L for Lysimeter 2 (Ly2). Ly1 showed higher water outflow than Ly2 (63% versus 49% of precipitation), which

can be explained by a higher hydraulic conductivity and lower field capacity of the silty gravels (Ly1) compared to the clayey sandy silts (Ly2). The remaining parts, i.e., 37 and 51% of precipitation (868 and 1203 L), can be attributed to evapotranspiration (ET) and changes in soil water storage (ΔS), since surface water runoff can be assumed negligible (horizontal extension of lysimeter surface). Since soil water storage is expected to equilibrate for longer time periods (Stumpp et al. 2009c), the amounts of 868 and 1203 L might give an estimate of ET sums. ET determined from the water balance (including lysimeter weight changes) amounts to similar amounts of 858 L for Ly1 and 1267 L for Ly2. Figures 1 and 2 show ET as a function of time, indicating seasonal variations with lower values during winter and higher values during summer. Uncertainties are associated, among others, with changes in soil water storage (soil water content or suction heads could not be monitored within the soil columns) and measurement noise. Daily moving averages were calculated to eliminate measurement noise: This simple and conservative approach was chosen, because the focus of this study is on daily to weekly changes, rather than on a finer temporal resolution (See chapter 2.4.1., Determination of ET with the evaluation of water balance). ET is higher in Ly2 than in Ly1, which can be explained by a higher water availability due to a finer soil texture, and it corresponds to an observed higher growth of maize.

3.3. COMPARISON OF EVAPOTRANSPIRATION OBTAINED BY DIFFERENT APPROACHES

Evapotranspiration calculated with the Haude approach yielded considerable underestimation except for the winter months, which can be attributed to Haude coefficients that may not be representative of the site (results not shown). Penman-Monteith-based actual ET fits reasonably well to "measured" ET (obtained from the water balance); however, summer peaks seem to be shifted (appearing some weeks earlier), in particular for 2014 in both lysimeters (Figure 1 and 2). Application of the Penman-Monteith approach first yielded potential ET, which was calculated from meteorological parameters and plant-related properties being the same for both lysimeters. To determine actual ET, the reported best estimate values of K_C (see chapter 2., Material and Methods) yielded good results for Ly2. For Ly1, the best fit to measured ET was obtained with a lower K_C-value for the mid-season growth stage ($K_{C,mid}$ = 0.732).

This corresponds to an observed lower growth of maize, compared to Ly2. In addition, the duration of the three growth phases was adjusted based on field observations of maize growth. For the time outside the maize cultivation period, a K_C of 0.3 was considered relating to background ET, as, e.g., recommended by Legind et al. (2012).

By combining estimated actual ET (Penman-Monteith) for the background with calculated transpiration Q_{Maize} for the maize growing period (Equation 16), the fit to measured ET could be improved (Figures 1 and 2). This includes a better correspondence to the occurrence of maximum ET.

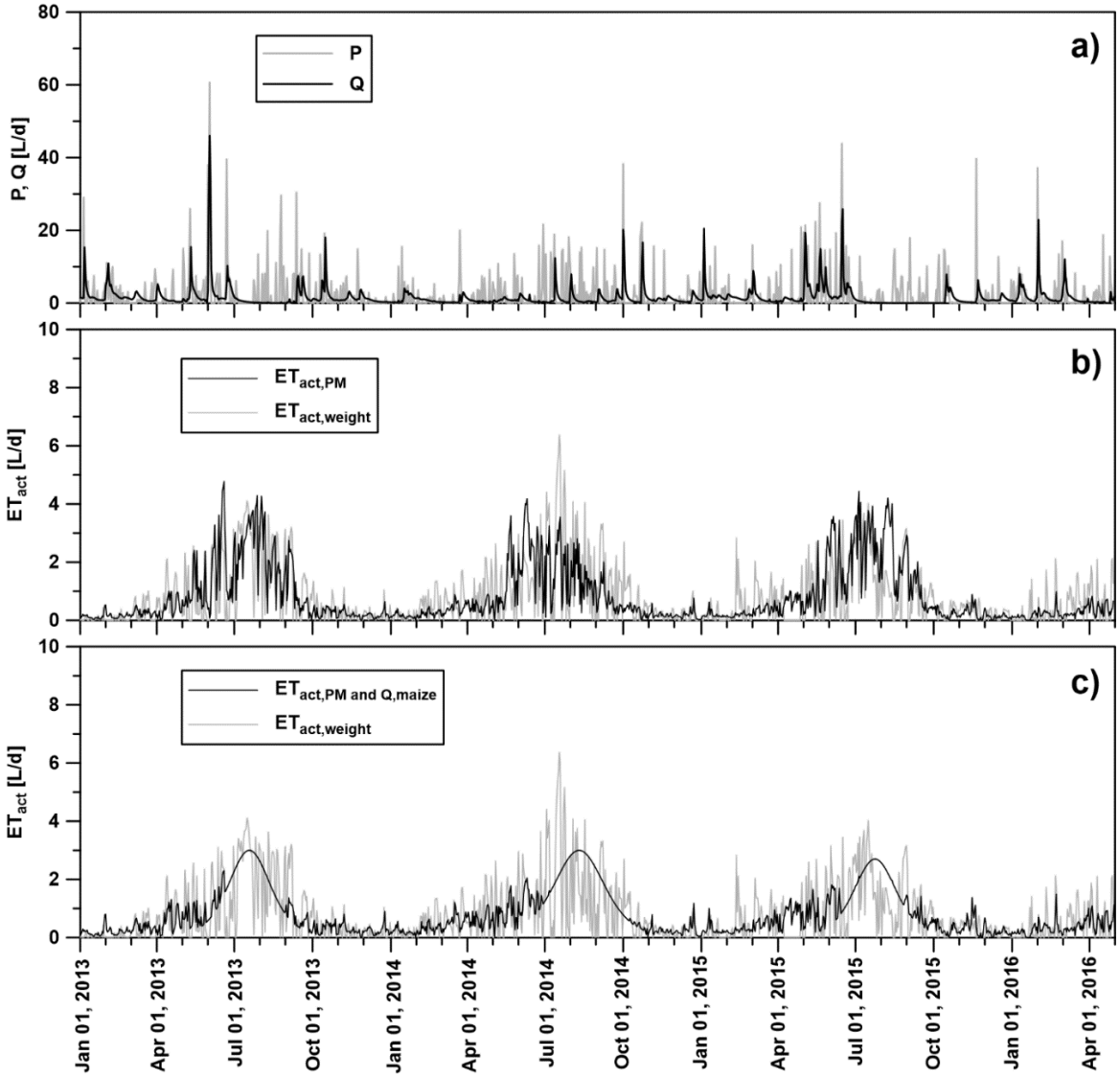

Figure 1. Precipitation, Outflow (seepage water) and Evapotranspiration at the site of Ly1.

Figure 1a) shows the monitored precipitation P and outflow Q over three years at the site of Ly1. Figure 1 b) and c) illustrate the actual evapotranspiration determined from the water balance ($ET_{act,weight}$), from the Penman-Monteith approach ($ET_{act,PM}$) and from

Penman-Monteith plus estimated transpiration for the maize plants ($ET_{act,PM\ and\ Q,maize}$) as a function of time.

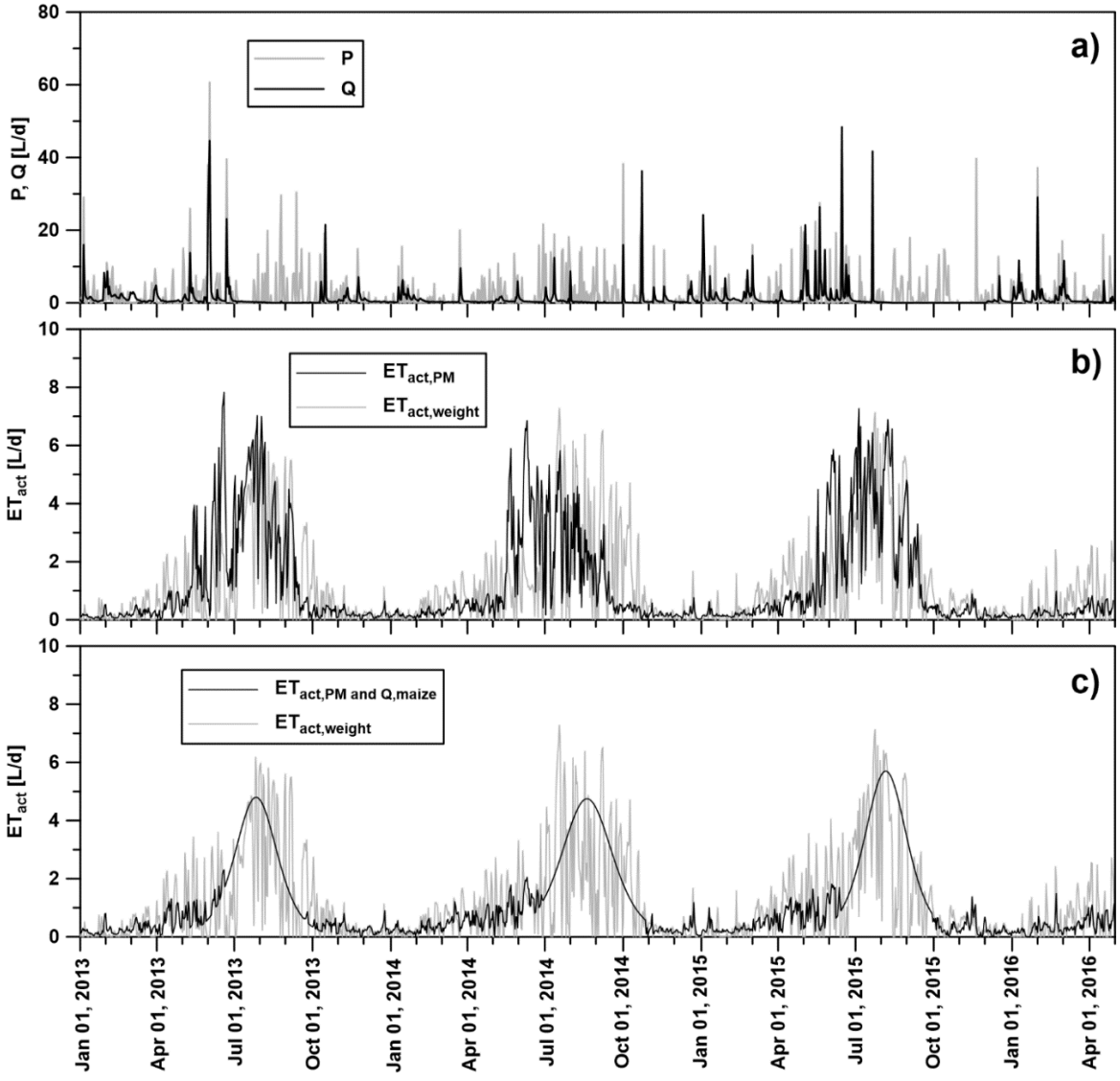

Figure 2. Precipitation, Outflow (seepage water) and Evapotranspiration at the site of Ly2.

Figure 2a) presents the monitored precipitation P and outflow Q over three years at the site of Ly2. Figure 2 b) and c) illustrate the actual evapotranspiration determined from the water balance ($ET_{act,weight}$), from the Penman-Monteith approach ($ET_{act,PM}$) and from Penman-Monteith plus estimated transpiration for the maize plants ($ET_{act,PM\ and\ Q,maize}$) as a function of time.

3.4. LUMPED-PARAMETER MODELING

3.4.1. "TRADITIONAL" LUMPED PARAMETER MODEL

3.4.1.1. Lysimeter 1

For Ly1, best model curve fits were obtained with a mean transit time of water (T) of 129 d and a dispersion parameter (P_D) of 0.12. Model results varied for the different chosen input functions and flow assumptions. Figures 3, S8 and S9 show measured versus modeled $\delta^{18}O$ in the seepage water of Ly1 as a function of time. If the isotopic composition of precipitation is considered as an input function (IF0, no modification) and transport through the soil matrix, only, is modeled, observations are described reasonably well (black lines in Figures 3, S8 and S9). The observed seasonal periodicity is met in general by the simulation; however, there are considerable underestimations of $\delta^{18}O$ values at some parts. These include the beginning, the minimum around April 2014 and before/after the third maximum (autumn 2015 and early 2016). Overestimation is less frequent, and can, e.g., be seen between July and October 2014 and in April/May 2016. Statistical evaluation for all simulation curve fits is provided in Table S1 and S2 in Appendix.

Applying input function IF1, i.e., weighting delta-values of precipitation over periods of 1, 3 and 6 months by accounting for precipitation amounts (see chapter 2., Material and Methods), modeling is improved partially. This can, in particular, be seen for the second maximum (July 2014 to May 2015) and April/May 2016 (Figure S8a, Table S1). Next, measured (water balance-based) evapotranspiration was considered to improve the input function (IF2, Figure 1 and S8b). This led to a further improvement of the curve fit for the second maximum (coefficient of determination of 0.88, root mean square error of 0.54 for the time between July 2014 and May 2015). For the whole period, this, however, resulted in a slightly lower coefficient of determination and slightly increased errors for the whole period (Table S1). This can be related to more pronounced underestimations, in particular, within the first year of simulation. Furthermore, we evaluated the appropriateness of estimated evapotranspiration (IF4 and IF5), which could be done with less effort, compared to measured ET. IF4 considers ET estimated from the Penman-Monteith approach, while IF5 considers background ET (Penman-Monteith) plus simulated maize transpiration. The resulting model curves were

similar; however, the use of IF5 yielded $\delta^{18}O$, which was closer to results obtained by using measured ET. Comparing the different weighting periods, durations of 3 months (and in addition, for IF1, 6 months) yielded the best estimates for $\delta^{18}O$ (see Table S1 in Appendix for the statistical evaluation of curve fits).

The consideration of preferential flow paths, together with soil matrix flow, could describe flow processes more adequately (Figure 3c and S9, Table S1). Preferential flow can explain short-term $\delta^{18}O$ fluctuations well, which occurred between measurements in a weekly to monthly frequency and ranged up to 1.5 ‰. Contributions of preferential flow p_{PF} were found to be 13% as the best estimate (IF0), and 8 to 10% for the modified input functions (IF1-5).

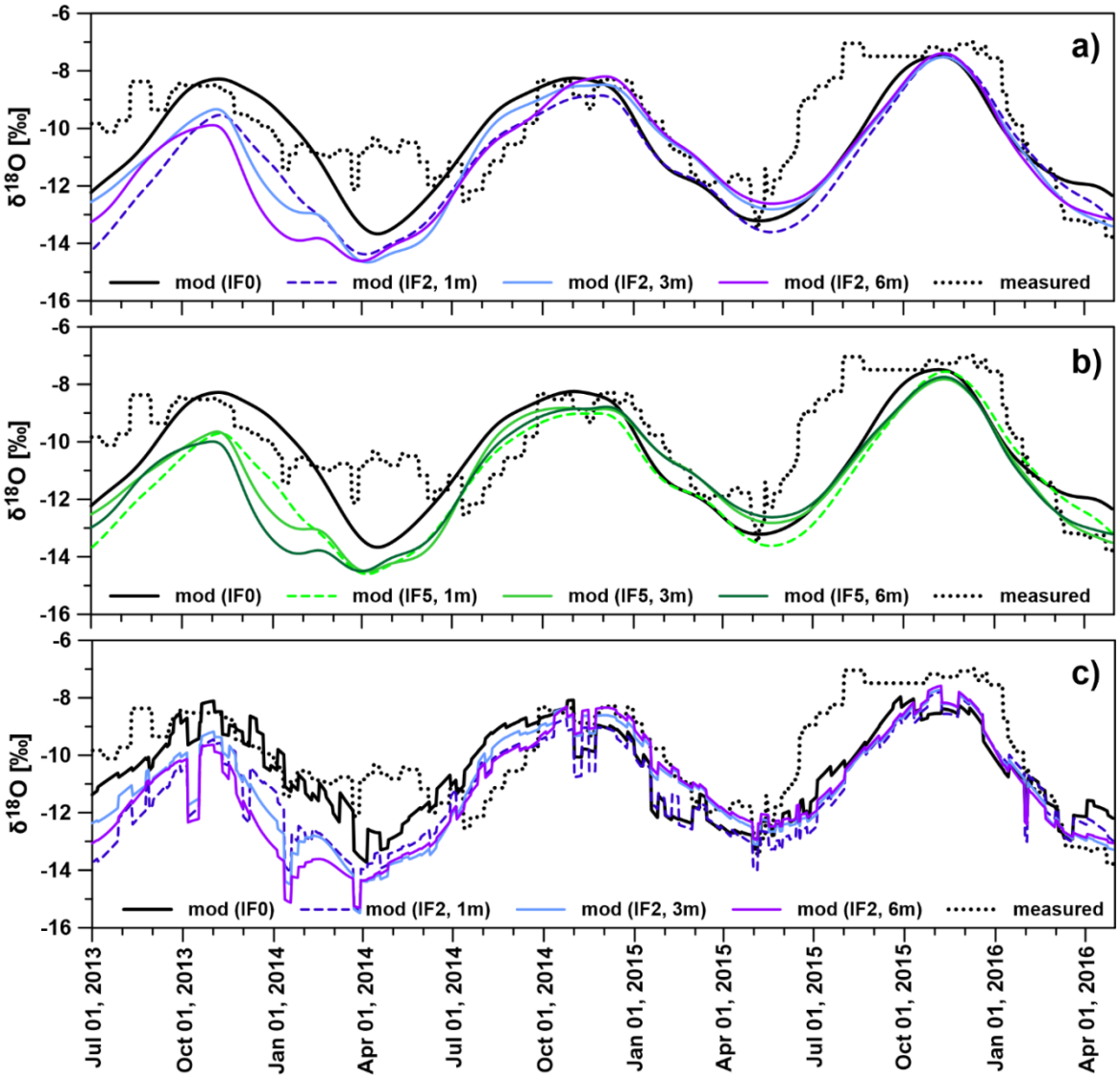

Figure 3. Measured vs. modeled (mod) $\delta^{18}O$ in the seepage water of Ly1.

Figure 3 presents measured vs. modeled (mod) $\delta^{18}O$ in the seepage water of Ly1 as a function of time; Part a) illustrates modeled isotope transport through the soil matrix with input function IF0 (isotopic composition of precipitation as input) and IF2 (considering measured evapotranspiration ET and weighting periods of 1, 3 and 6 months); Part b) shows modeled isotope transport through the soil matrix with IF0 and IF5 (considering ET estimated by Penman-Monteith plus modeled maize transpiration); Part c) presents the modeled isotope transport through the soil matrix plus along preferential flow paths with IF0 and IF2.

3.4.1.2. Lysimeter 2

For Ly2, the values of T = 362 d and P_D = 0.7 were found as the best estimate. Compared to Ly1, the observed curve characteristic was more difficult to describe with a constant T, which, together with more pronounced short-term fluctuations (up to 3 ‰), led to generally worse curve fits (also see Table S1 and S2 in Appendix). Considering isotope transport through the soil matrix flow, only, best curve fits were obtained with IF0 as well as with modified input functions and 3 or 6 months for the weighting periods. The assumption of preferential flow again led to a further improvement of simulation results, with contributions p_{PF} of 11% as the best estimate (range 9-11% for the different input functions). Results for Ly2 are presented in Figure 4 (selected curves), S10 and S11.

We have applied lumped-parameter modeling, which implements steady-state flow in order to describe stable water isotope transport. This process, however, occurs under transient flow conditions. Such variable flow conditions were addressed by adjusting the input function, where weighting periods of 3 and 6 months revealed to be most promising. I.e., isotope contents were weighted by actual recharge amounts referred to as average recharge within 3-month and 6-month periods, corresponding to season-related and vegetation-related variations and resulting changes in recharge. These modifications of the input function were successful for the modeling of $\delta^{18}O$ transport, yielding reasonable curve fits. The consideration of evapotranspiration for estimating recharge could partially improve the model results. For the whole observation period, however, a recharge factor α of 1 was most successful for both lysimeters, i.e., assuming that all precipitation water is infiltrating. This is an unexpected finding, which may

indicate that dividing the whole observation period into sub-periods with (quasi-) constant conditions (and specific T and P_D) could represent fluctuating flow more exactly. Indeed e.g., for Ly1, best fits were obtained for the central part (around the second maximum), but some deviations were obvious at an earlier and later time. Deviations within the first months could also be influenced by the use of the additional precipitation-$\delta^{18}O$ data, which was needed as input prior to the beginning of measurements at the lysimeter site (as described before in 2.6.2.4 Numerical model setup). These data were derived from another site (Passau-Fürstenzell) and isotope characteristics might have differed to some degree from those at the lysimeter site.

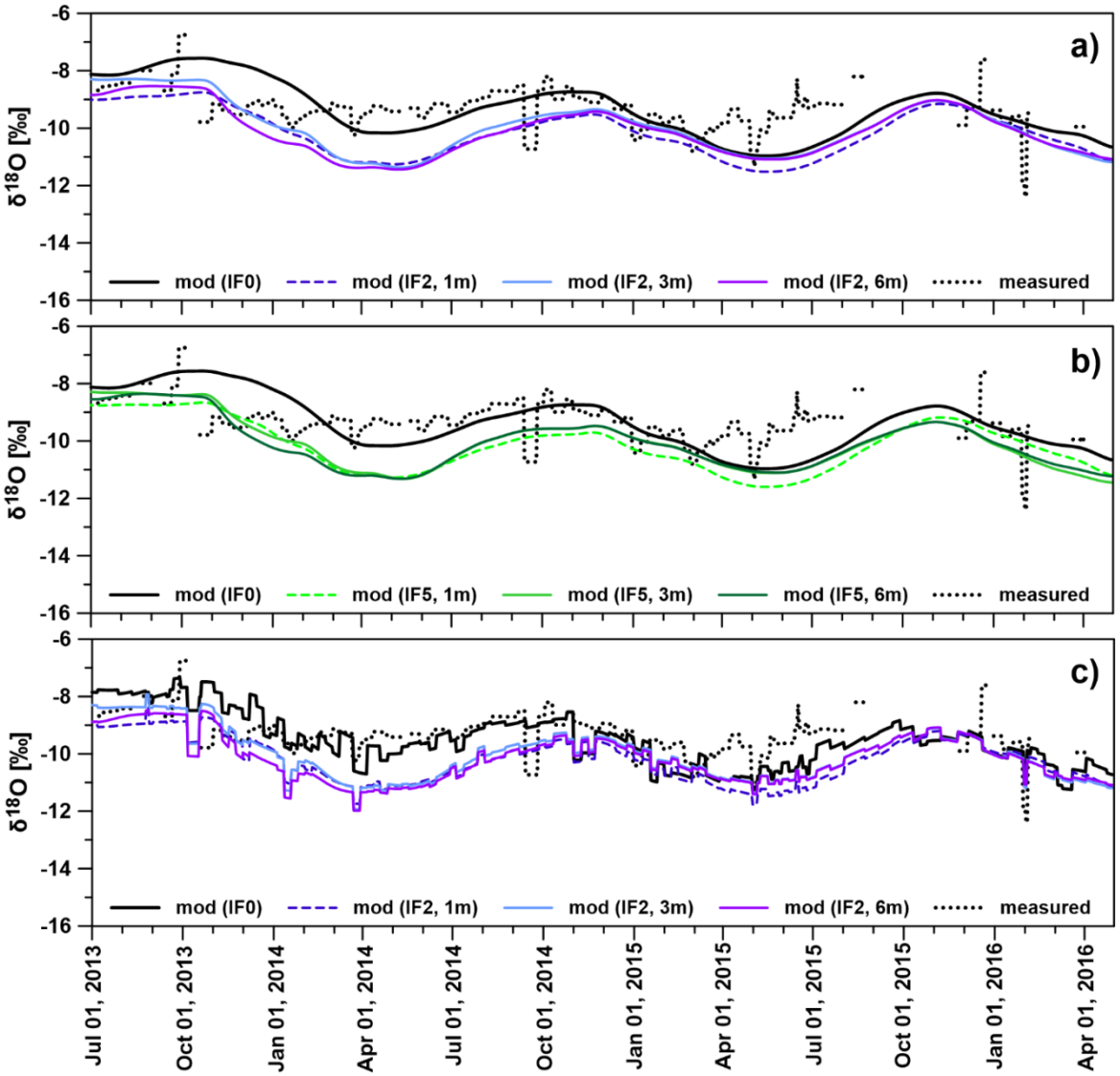

Figure 4. Measured vs. modeled (mod) $\delta^{18}O$ in the seepage water of Ly2.

Figure 4 shows the measured vs. modeled (mod) $\delta^{18}O$ in the seepage water of Ly2 as a function of time. Parts a) to c) are explained in detail in the above text (see Figure 3 explanation).

3.4.2. Extended lumped parameter model

3.4.2.1. Lysimeter 1

Figure 5 shows measured versus modeled $\delta^{18}O$ as a function of time in the seepage water of Ly1. In Figure 5a, modeling results from the "traditional" LPM (one period, dashed line) are compared to our extended approach (subdivided into eight sub-periods in order to mimic variable flow) for IF0, i.e., for using $\delta^{18}O$ of precipitation as input (without modification). The consideration of variable flow conditions could substantially improve the model fit (R^2 of 0.86 versus 0.48, RMSE of 0.86 ‰ versus 1.51 ‰, ME of -0.40 ‰ versus -0.61 ‰). Underestimations were reduced significantly, which in particular accounts for the first year and for the final part of the curve (third peak starting in June 2015).

Modification of the input function led to further improvements, as shown in Figure 5b and Table 6. The modified input function considers weighted input and thus reflects seasonal changes on a three- and six-month basis as well as shorter (one-month) fluctuations of infiltration. IF2 with 6-month weighting showed the highest R^2 (0.89). The consideration of preferential flow paths could further improve simulations (Figure 5c and Table 6). Rapid transport of recharging $\delta^{18}O$ along preferential flow paths can explain the observed short-term fluctuations of $\delta^{18}O$ in seepage water. Fitted mean transit times T varies significantly between the sub-periods, ranging from 88 to 178 days (Table 6). Also, fitted P_D reveals strong variation between 0.05 and 0.14, with 0.10 to 0.11 for the averages. Similar values were found for constant flow, with T of 129 days P_D of 0.12. As a best estimate, the portion of preferential flow paths p_{PF} varied between 6 and 15% from sub-period to sub-period (8-13% in averages, Table 6). The obtained p_{PF} -values are somewhat lower than those obtained from "traditional" LPM with constant flow assumption (p_{PF} of 13%).

Table 6 presents parameter values fitted (T, P_D and p_{PF}) for the eight sub-periods in extended lumped-parameter modeling for Ly1 with different input functions (IF) and statistical parameters for curve fit evaluation (R^2, RMSE, ME).

Table 6. Ly1: Parameter values fitted from lumped-parameter modeling with different input functions (IF) and statistics.

Par.	S12	W12/ 13	S13	W13/ 14	S14	W14/ 15	S15	W15/ 16	Av.	R^2 [-]	RMSE [‰]	ME [‰]
Input function IF0												
T [d]	121	118	135	145	98	119	165	138	131			
P_D [-]	0.14	0.14	0.08	0.14	0.10	0.09	0.05	0.05	0.10	0.86	0.81	-0.43
p_{PF} [%]	14	9	14	14	13	10	15	12	13			
Input function IF2, 1m												
T [d]	121	88	117	139	112	121	176	135	126			
P_D [-]	0.13	0.13	0.10	0.14	0.14	0.11	0.07	0.05	0.11	0.87	1.08	-0.79
p_{PF} [-]	7	6	12	9	10	8	12	8	9			
Input function IF2, 3m												
T [d]	100	95	115	149	122	119	177	138	127			
P_D [-]	0.13	0.08	0.10	0.16	0.13	0.09	0.07	0.05	0.10	0.87	1.06	-0.63
p_{PF} [%]	7	6	8	6	12	6	12	7	8			
Input function IF2, 6m												
T [d]	100	91	111	152	122	119	178	138	126			
P_D [-]	0.13	0.08	0.10	0.14	0.14	0.09	0.07	0.05	0.10	0.89	1.03	-0.67
p_{PF} [%]	8	7	12	6	10	6	12	7	9			

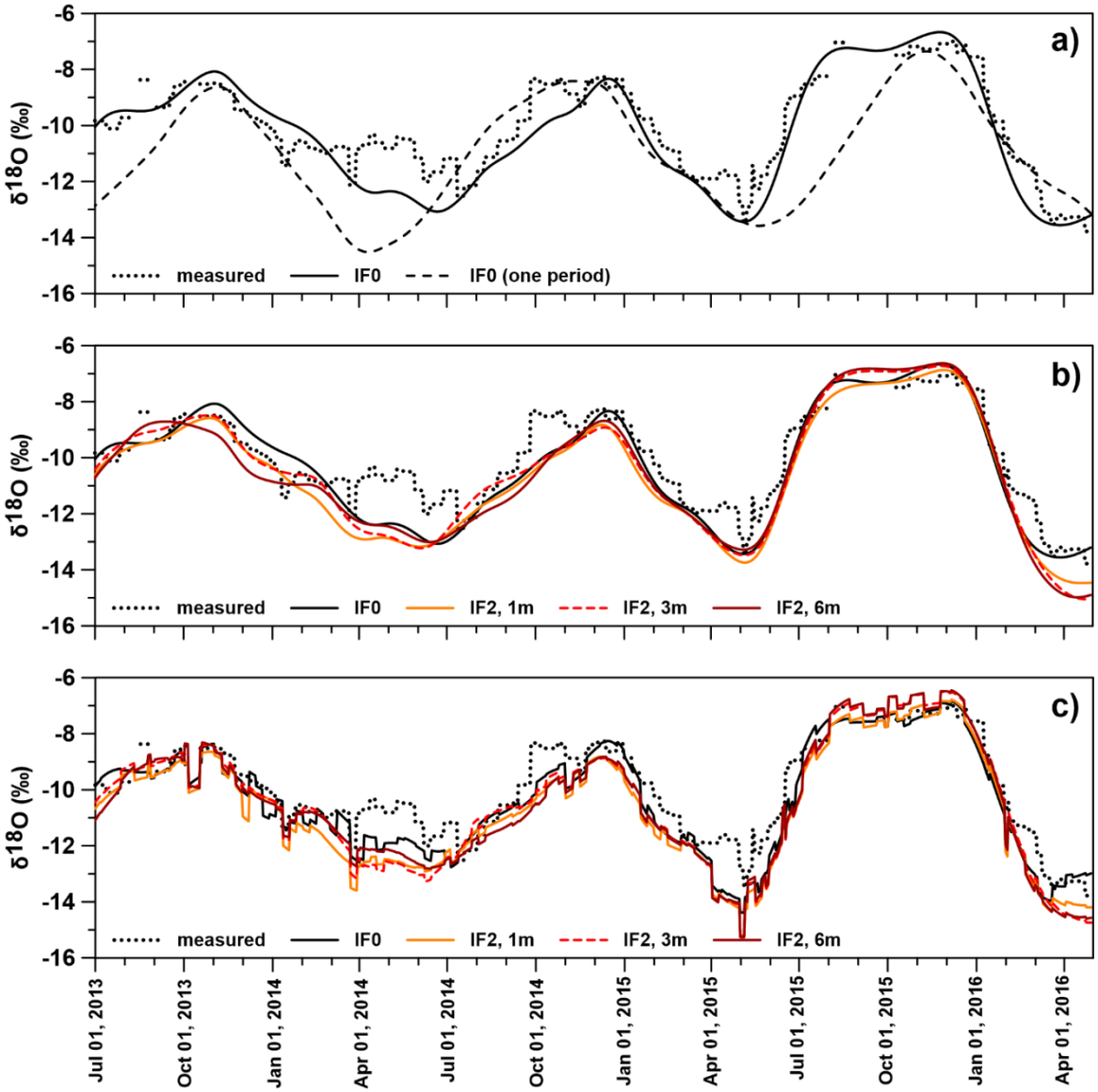

Figure 5. Measured and modeled (extended LPM) $\delta^{18}O$ in the seepage water of Ly1.

Figure 5 shows the measured and modeled (extended LPM) $\delta^{18}O$ in the seepage water of Ly1 as a function of time; Part a) presents the modeled isotope transport through the soil matrix with input function IF0 ($\delta^{18}O$ of precipitation as input), considering variable flow (extended LPM, eight sub-periods, solid line) and constant flow ("traditional" LPM, one period, dashed line); Part b) illustrates the modeled isotope transport through the soil matrix with IF2 and weighted input within 1, 3 and 6 months (1m, 3m, 6m), considering variable flow; Part c) shows transport through the matrix plus along preferential flow paths (PF).

3.4.2.2. Lysimeter 2

Figure 6 presents measured versus modeled $\delta^{18}O$ as a function of time in the seepage water of Ly2. In line with our previous findings in "traditional" LPM, observations in Ly 2 were more difficult to explain by LPM modeling as compared to Ly 1. Similar to Ly1, the consideration of varying flow (here nine sub-periods, each with constant conditions) improved lumped-parameter modeling, significantly. As can be seen in Figure 6a, this approach is able to represent observations better than the LPM approach considering constant flow, i.e., one period (solid line versus dashed line; R^2 of 0.31 versus 0.19, RMSE of 0.67 ‰ versus 0.92 ‰, ME of 0.10 ‰ versus -0.05 ‰). Underestimations are reduced for many parts of the curve, especially for the first year and the third peak (May to November 2015).

As a major change to our previous LPM ("traditional" LPM), we have considered a longer modeling pre-phase of 5 years (instead of 1 year) for LPM modeling of Ly2. This was done both for constant flow (dashed curve in Figure 6a) and varying flow (other model curves in Figure 6). This longer pre-phase revealed to be more adequate given the finer-grained structure and higher mean residence time of water within Ly2: as can be seen from the simulated curves of relative recovery (RR) shown in Figure S13a in Appendix, about 98 % of tracer breakthrough is reached after 5 years, versus only ~70 % after 1 year. These curves were obtained from applying the analytical solution of Lenda and Zuber (1970) for constant initial tracer concentration:

$$RR(t) = \frac{1}{2}\left[erfc\left(\frac{1 - t/T}{\sqrt{4P_D\, t/T}}\right) + exp\left(\frac{1}{P_D}\right) erfc\left(\frac{1 + t/T}{\sqrt{4P_D\, t/T}}\right)\right] \qquad \text{Equation (20)}$$

with T = 362 d and P_D = 0.7 as for Ly2 in our previous chapter (chapter 3.4.1., "traditional" LPM). For Ly1, using a pre-phase of 1 year (as in our previous study) revealed that 99 % of tracer breakthrough after one year is reached; the curve is not shown. However, only considering a second component was able to explain observations, well: a constant value of $\delta^{18}O$ = 1 ‰ was added to the model curves in order to obtain an upshift and thus correct for underestimation (see Figure S13). This second component, contributing to advective/dispersive isotope transport from the lysimeter top, might result from the re-mobilization of immobile water within the soil

column of Ly2, as further discussed in chapter 3.6., Evaluation of findings and Comparison of lumped-parameter and numerical modeling.

LPM modeling with varying flow led to a mean transit time T between 300 and 445 d (354-361 d in average) and a P_D of 0.3 to 0.9 (0.6-0.7 in average) for the different input functions. Average P_D is thus very close to the value obtained from applying the one-period LPM (0.7). The consideration of preferential flow could improve model curve fits (R^2 0.38-0.40 versus R^2 up to 0.34 with matrix flow, only) with portions of preferential flow p_{PF} between 3 and 12 % (7-9 % in average) as best estimate (see Table 7). Average values are lower than the p_{PF} of 11% derived using the one-period LPM.

Similar to Ly1, the consideration of weighted IF2 could slightly improve model curve fits (Figure 6).

Table 7 presents parameter values fitted (T, P_D and p_{PF}) for the nine sub-periods in extended lumped-parameter modeling for Ly2 with different input functions (IF) and statistical parameters for curve fit evaluation (R^2, RMSE, ME).

Table 7. Ly2: Parameter values fitted from lumped-parameter modeling with different input functions (IF) and statistics.

Par.	P1	S12	W12/ 13	S13	W13/ 14	S14	W14/ 15	S15	W15/ 16	Av.	R^2 [-]	RMSE [‰]	ME [‰]
Input function IF0													
T [d]	350	370	300	360	430	320	380	300	375	354			
P_D [-]	0.7	0.7	0.8	0.5	0.8	0.5	0.9	0.4	0.8	0.7	0.39	0.73	-0.09
p_{PF}	7												
[%]		8	7	6	10	9	8	12	12	9			
Input function IF2, 1m													
T [d]	350	350	300	350	445	310	370	330	375	354			
P_D [-]	0.7	0.7	0.8	0.7	0.8	0.5	0.7	0.4	0.6	0.7	0.38	0.68	-0.30
p_{PF}	7												
[%]		8	8	4	11	10	8	12	11	9			
Input function IF2, 3m													
T [d]	350	350	300	390	445	310	370	330	385	360			
P_D [-]	0.7	0.7	0.8	0.7	0.7	0.4	0.7	0.3	0.5	0.6	0.40	0.60	-0.11
p_{PF}	7												
[%]		8	8	3	9	11	8	7	11	8			
Input function IF2, 6m													
T [d]	350	350	305	365	445	330	390	310	390	361			
P_D [-]	0.7	0.7	0.8	0.6	0.7	0.5	0.9	0.4	0.7	0.7	0.40	0.64	-0.23
p_{PF}	7												
[%]		9	8	3	9	6	5	7	6	7			

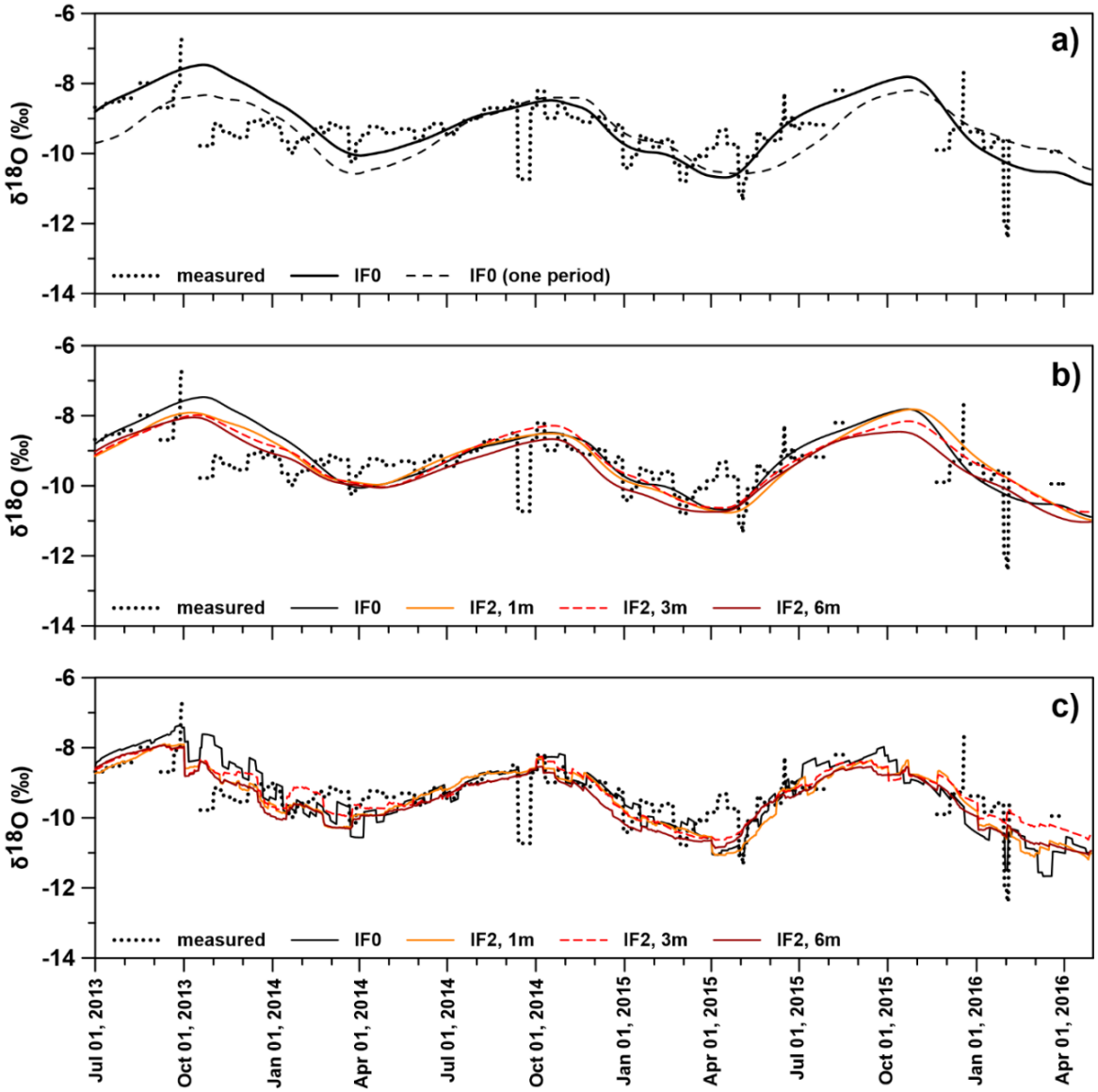

Figure 6. Measured and modeled (extended LPM) $\delta^{18}O$ in the seepage water of Ly2.

Figure 6 presents the measured and modeled (extended LPM) $\delta^{18}O$ in the seepage water of Ly2 as a function of time. More detail about parts a) to c) are well explained in Figure 5 explanation.

3.5. NUMERICAL MODELING OF UNSATURATED FLOW AND STABLE WATER ISOTOPE TRANSPORT

The results of numerical modelling were obtained by Anne Imig.

3.5.1. LYSIMETER 1

Figure 7a shows observed versus numerically simulated $\delta^{18}O$ in the seepage water of Ly1. Here, the soil column is considered as a homogeneous case (one layer case). As it can be seen there, the numerically modeled curves describe the observed behavior of $\delta^{18}O$ well, reproducing seasonal periodicity. As found above for lumped-parameter modeling, the consideration of stable water isotope transport along preferential flow paths resulted in slightly better overall curve fits (R^2 of 0.8 versus 0.83). Portions of preferential flow p_{PF} of 8-11% led to similarly good model curve fits, with mean residence times of water within preferential paths (T_{PF}) between 6-7 days. This rather wide range of p_{PF} and T_{PF} points towards a low sensitivity of preferential flow characteristics. This could possibly be explained by the coarse texture of the soil within Ly1, which is characterized by sandy gravels. Wider pores may act similar to preferential flow paths (enabling rapid transport of some portions of the infiltrating water).

Soil hydraulic parameters (SHP) and P_D-value fitted for Ly1 are summarized in Table 8, and simulated soil water retention curves are shown in Figure S14. Fitted values of saturated water content θ_s and dispersion parameter P_D (Table 8) correspond to typical ranges found for sandy gravels (Stumpp et al. 2009b; Sprenger et al. 2015). For saturated hydraulic conductivity K_S, fitted values correspond to findings from Stumpp et al. (2009c) and Freeze and Cherry (1979).

Figure S15 illustrates the observed versus simulated discharge rates Q for the multi-layer case. Obtained model curves for the multi-layer scenario were very similar to the homogeneous case (results not shown).

Figure 7 presents the measured and numerically modeled (HYDRUS-1D) $\delta^{18}O$ in the seepage water of Ly1 (a) and Ly2 (b), transported through the subsurface matrix and along preferential flow paths (PF).

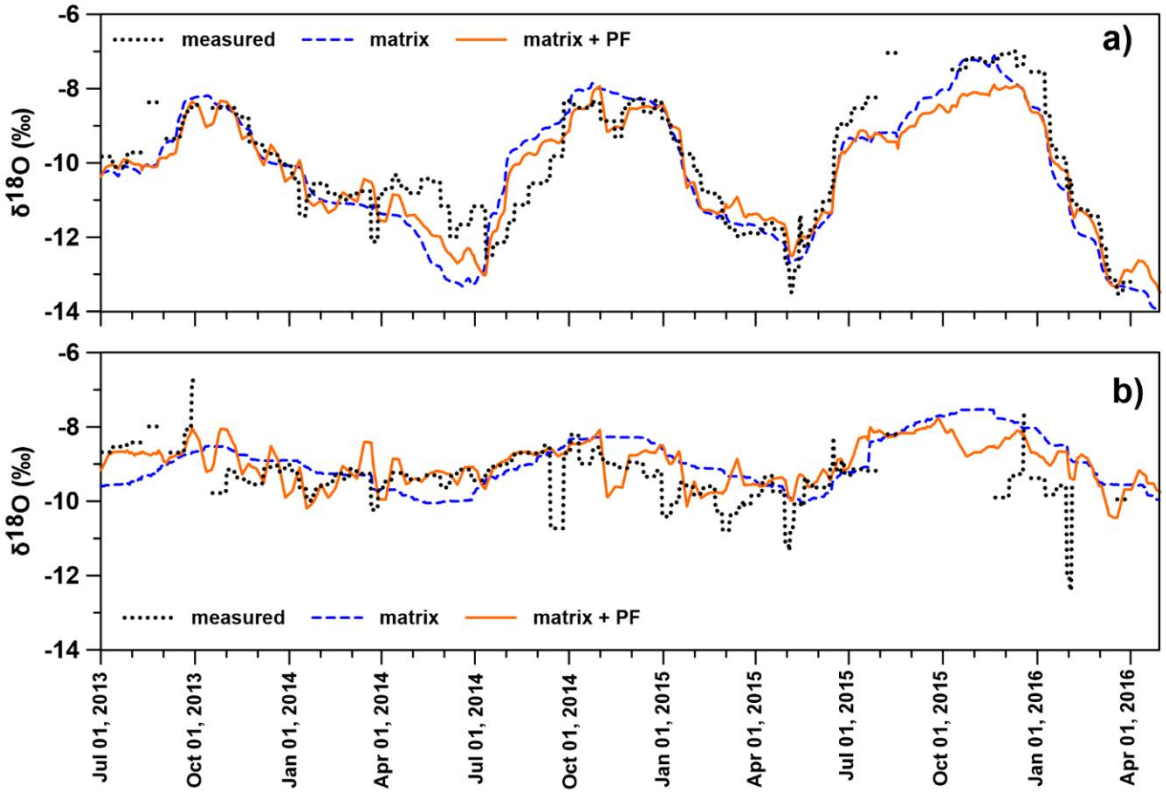

Figure 7. Measured and numerically modeled $\delta^{18}O$ in the seepage water of Ly1 and Ly2.

Table 8 shows parameter sets fitted for Ly1 by inverse numerical flow and isotope transport modeling, as well as statistical evaluation of resulting curve fits (modeled versus measured $\delta^{18}O$ in lysimeter outflow). θ_r and θ_s: residual and saturated soil water content; α, n: shape parameters; K_S: saturated hydraulic conductivity; l: tortuosity parameter; P_D: dispersion parameter; p_{PF}: portion of preferential flow; T_{PF}: mean transit time for preferential flow.

Table 8. Parameter sets fitted for Ly1 by inverse numerical flow and isotope transport modeling, as well as statistics.

Depth [cm]	θ_r [cm^3/cm^3]	θ_s [cm^3/cm^3]	α [1/cm]	n [-]	K_S [cm/d]	l [-]	P_D [-]	p_{PF} [%]	T_{PF} [d]	R^2 [-]	RMSE [‰]	ME [‰]
Ly1												
0-200	0.007	0.275	0.35	1.41	6040.20	0.5	0.07	8-11	6-7	0.85	0.67	-0.14

3.5.2. LYSIMETER 2

Results of numerical modeling for Ly2 are shown in Figure 7b. It is assumed here that the soil column is homogeneous (one-layer case). The modeled curves were shifted up by a constant value (0.8 ‰). This upshift corresponds to a second component that contributes to delta values in seepage water. From Figure 7b, it can be seen that the seasonal periodicity seems not fully matched by the simulation. The consideration of preferential flow (Figure 7b) could substantially improve simulation and reduce under- and overestimations. Moreover, short-term fluctuations were described better (see Table 9 for statistical evaluation of curve fits with the preferential flow). The fitted saturated water content θ_s of 0.29 appears to be at the lower end of more frequently reported ranges around 0.3-0.5. This could possibly be explained by the relatively high contents of sand (see Table 4) together with a poor sorting of grain sizes (Vrugt et al.2001; Durner et al. 2008; Graham et al. 2018; Thoma et al. 2014). Fitted saturated hydraulic conductivity K_s (146.34 cm/d, Table 9) is within typical observations for sandy silt soils (e.g., Freeze and Cherry, 1979; Jiang et al. 2010). Observed versus simulated discharge rates Q for multi-layer cases are shown in Figure S15. The obtained model curve for the multi-layer scenario was very similar to the homogeneous case (results not shown).

Table 9 shows parameter sets fitted for Ly2 by inverse numerical flow and isotope transport modeling, as well as statistical evaluation of resulting curve fits (modeled versus measured $\delta^{18}O$ in lysimeter outflow). θ_r and θ_s: residual and saturated soil water content; α, n: shape parameters; K_S: saturated hydraulic conductivity; l: tortuosity parameter; P_D: dispersion parameter; p_{PF}: portion of preferential flow; T_{PF}: mean transit time for preferential flow.

Table 9. Parameter sets fitted for Ly2 by inverse numerical flow and isotope transport modeling, as well as statistics.

Depth [cm]	θ_r [cm^3/cm^3]	θ_s [cm^3/cm^3]	α [1/cm]	n [-]	K_S [cm/d]	l [-]	P_D [-]	p_{PF} [%]	T_{PF} [d]	R^2 [-]	RMSE [‰]	ME [‰]
Ly2												
0-200	0.026	0.29	0.005	1.23	146.34	0.5	0.85	12-13	5-7	0.20	0.83	-0.52

3.6. EVALUATION OF FINDINGS AND COMPARISON OF LUMPED-PARAMETER AND NUMERICAL MODELING

3.6.1. EVALUATION OF FINDINGS FROM THE "TRADITIONAL" LUMPED PARAMETER MODEL

The estimated mean transit time T and dispersion parameter P_D were higher for the clayey sandy silt in Ly2 (T of 362 d, P_D of 0.7) than for the sandy gravel in Ly1 (T of 129 d, P_D of 0.12). The higher mean transit time in Ly2 corresponds to a higher average soil water content θ_{av} (0.199 versus 0.092 for Ly1) and a lower average flow velocity v_{av} (0.55 cm/d versus 1.55 cm/d in Ly1). The average discharge rate q was 0.142 cm/d for Ly1 and 0.110 cm/d for Ly2. The higher average soil water content in Ly2 corresponds to a higher mobile (effective) water volume (398 L in Ly2 versus 184 L in Ly1). Small pores are expected to dominate in the silt soil, which may lead to slower water movement (higher transit time) as compared to the gravel soil. The mean transit time T of 129 d, corresponding to 18.4 weeks, is within a wide range of values reported for similar soils in free drainage lysimeters and exposed to similar climatic conditions. E.g., for fluvioglacial gravels, T-values between 7 and 18 weeks (varying from year to year) were found for conditions without plant coverage (Stumpp et al. 2007). The lysimeter had the same length as in the present work but a lower surface area of 0.125 m^2. In another study, T-values of 39-45 weeks were found for sandy gravels vegetated with different crops (Stumpp et al. 2009c; same lysimeter dimensions as in the present work). The higher T-values in the latter study, compared to Ly1, where accompanied by higher effective water volumes of 230-266 L. This could possibly be explained by a different texture, where Ly1 shows much higher gravel (lower silt) contents in the A-horizon. Average water contents were around 0.10 and 0.12 in the two lysimeters mentioned above (Stumpp et al. 2009c and 2007, respectively).

The mean transit time (362 days) and average flow velocity (0.55 cm/d) for Ly2 are within reported ranges for similar soils. E.g., Stumpp et al. (2012) found mean transit times of 212-272 days for five lysimeters of 150 cm in length, corresponding to flow velocities of 0.55-0.71 cm/d. The lysimeters were filled with a Dystric Cambisol. Gravel and sand contents were higher, while silt and clay contents were somewhat lower compared to Ly2. The lysimeters were embedded in an agricultural field and vegetated with maize, winter rye and grass. Soil water contents measured in the lysimeters

ranged between 0.14 and 0.26, while for Ly2, it was 0.199 in average. For the Attert catchment located in Luxembourg, Sprenger et al. (2016) modeled median travel times (TT) for the unsaturated zone, considering soil moisture time series and the depth profiles of stable water isotopes measured in soil water. Present soil types involve Cambisols, Arenosols and Stagnosols, covered by forest and grassland. For the Cambisols and Arenosols, allowing freely draining conditions, TT-values of 238-918 (average 548) days and 287-651 (average 497) days, respectively, were found at a depth of 200 cm. Soil textures varied between loam, silty loam and clayey loam for the Cambisol (16 sites) and between sandy loam, sandy clay and loam for the Arenosols (12 sites).

The dispersion parameter was around 6 times higher for Ly2 than for Ly1 (0.7 versus 0.12, respectively). A higher P_D value is associated with higher heterogeneity of the system, so that in such a case, the distribution of travel times is wider and more asymmetrical (Maloszewski and Zuber 1996). This can be seen for Ly2, where the higher P_D might be induced by the presence of finer grain sizes and also by hydraulic processes, as further discussed below. The obtained P_D values correspond to dispersivities α_L of 0.24 m for Ly1 and 1.4 m for Ly2, and they are comparatively high. Referring to the studies mentioned above, α_L estimated for Ly1 is similar to maximum values found for fluvioglacial gravels (Stumpp et al. 2007) but higher than those determined for sandy gravels (Stumpp et al. 2009c). This might be explained by a higher heterogeneity in Ly1, compared to the mentioned studies. The dispersivity found for Ly2 exceeds the values found by Sprenger et al. (2016) for Cambisols and Arenosols (ranging up to 27.3 cm); however, it is close to findings from column experiments with loam under transient flow conditions, showing α_L around 123 cm (Vanderborght et al. 2000). Parker and Albrecht (1987) found a dispersivity of 1.49 m for a loam core, however, under ponding conditions and thus for a different flow system. Dispersion can be influenced significantly by hydraulic processes. An increasing flow rate can lead to an increase in dispersivity due to the activation of large inter-aggregate pores, and this has been observed, in particular, in fine-textured soils. Moreover, larger dispersivities were identified for saturated than for unsaturated flow conditions (Vanderborght and Vereecken 2007). As an additional possible process, a tracer transported in mobile water can exchange with quasi-immobile water and thus may get diluted (Maloszewski et al. 2006). Depending on the distribution of immobile

water in the subsurface, this can vary spatially and temporally. Such influences can be considered by defining an apparent dispersion parameter; however, it is difficult to obtain the required information on the presence of immobile water in the subsurface (e.g., Maloszewski et al. 2006). A possible hint can be an effective water volume (effective water content) that is significantly lower than expected for the considered soils and flow conditions. This is not obvious for the considered lysimeters, although the average water content estimated for Ly1 is within a rather low range, compared to other studies.

The contribution of preferential flow paths was estimated to be slightly higher for the gravel than for the silt soil (13% in Ly1 versus 11% in Ly2 as best estimates). This can be explained by higher portions of macropores in the gravel soil, possibly due to connected pore networks with wider pores, influenced by the texture involving gravel components (e.g., Rücknagel et al. 2013). The contribution of preferential flow (PF) can vary pronouncedly depending on the soil texture, macropore and vegetation types, rainfall intensity, soil hydraulic parameters and hydraulic conditions. The initiation of PF is reported to strongly depend on the hydraulic boundary and initial conditions (Ghodrati et al. 1999; Langner et al. 1999; Lennartz and Kamra 1998; Seyfried and Rao 1987). In studies with seven lysimeters, the saturated hydraulic conductivity crucially influenced the contribution of direct flow. This was observed for different soil textures and flow rates (Stumpp et al. 2007). The authors found PF contributions for quartz sand of 17-21% (moderate grain size) and 20-27% (coarser grain size). For fluvioglacial gravels, PF contributions were 25-30%. In a lysimeter with sandy soil vegetated with different crops, Stumpp and Maloszewski (2010) found PF contributions of 1-6% of the precipitation amount (2-10% of the discharge), varying seasonally and depending on vegetation. PF contribution was lowest for maize plantation (1.1% of precipitation). Everts and Kanwar (1990) report PF contributions <2% of total drain outflow for a loam soil (clayey silty sand), estimated from a tracer experiment at an irrigated field with corn crop cultivation. In field experiments on pesticides and tracer transport in loamy sand soil, Ghodrati and Jury (1992) revealed widespread PF leading to accelerated chemical movement. 9.4-18.8% of the applied chemical mass was recovered in soil depths between 30 and 150 cm, mainly attributed to transport along PF. Stone and Wilson (2006) investigated PF in a field with rotating

corn and soybean cultivation, where the subsurface predominantly consisted of silt loams and silty clay loams. PF contributed between 11 and 51% to total storm drain flow within a subsurface tile drain, depending on rainfall intensity. PF contributions estimated for Ly1 and Ly2 in the present study (13 and 11% as the best estimate, respectively) are within reported ranges, as reflected in the previously mentioned studies.

3.6.2. EVALUATION OF FINDINGS FROM THE EXTENDED LUMPED PARAMETER APPROACH

Application of the extended LPM approach revealed pronounced seasonal variations (winter-summer) and annual differences of model parameters.

The temporal variation of parameters found from applying the extended LPM for Ly1 (d-f) and Ly2 (j-l) are presented in Figure 8, where straight lines indicate best model fit, dotted lines alternative model fit (see Table 6 and 7). Parameters are compared to 6-month-averages of precipitation (P), lysimeter discharge rate (Q) and lysimeter weight (m); in this figure, panels a-c are identical and panels g-i are identical).

Figure 8 shows fitted parameters as a function of time (winter-summer), obtained by using different input functions (data from Tables 6 and7). Parameter fluctuation is compared to 6-month-averaged precipitation, lysimeter discharge rate and lysimeter weight (see Figure S2). As can be seen in Figures 8d and e, for Ly1, neither T nor P_D variation revealed a clear pattern with respect to the season. As described before, the fitted parameters for this study are within a typical range that can be found for similar soils.

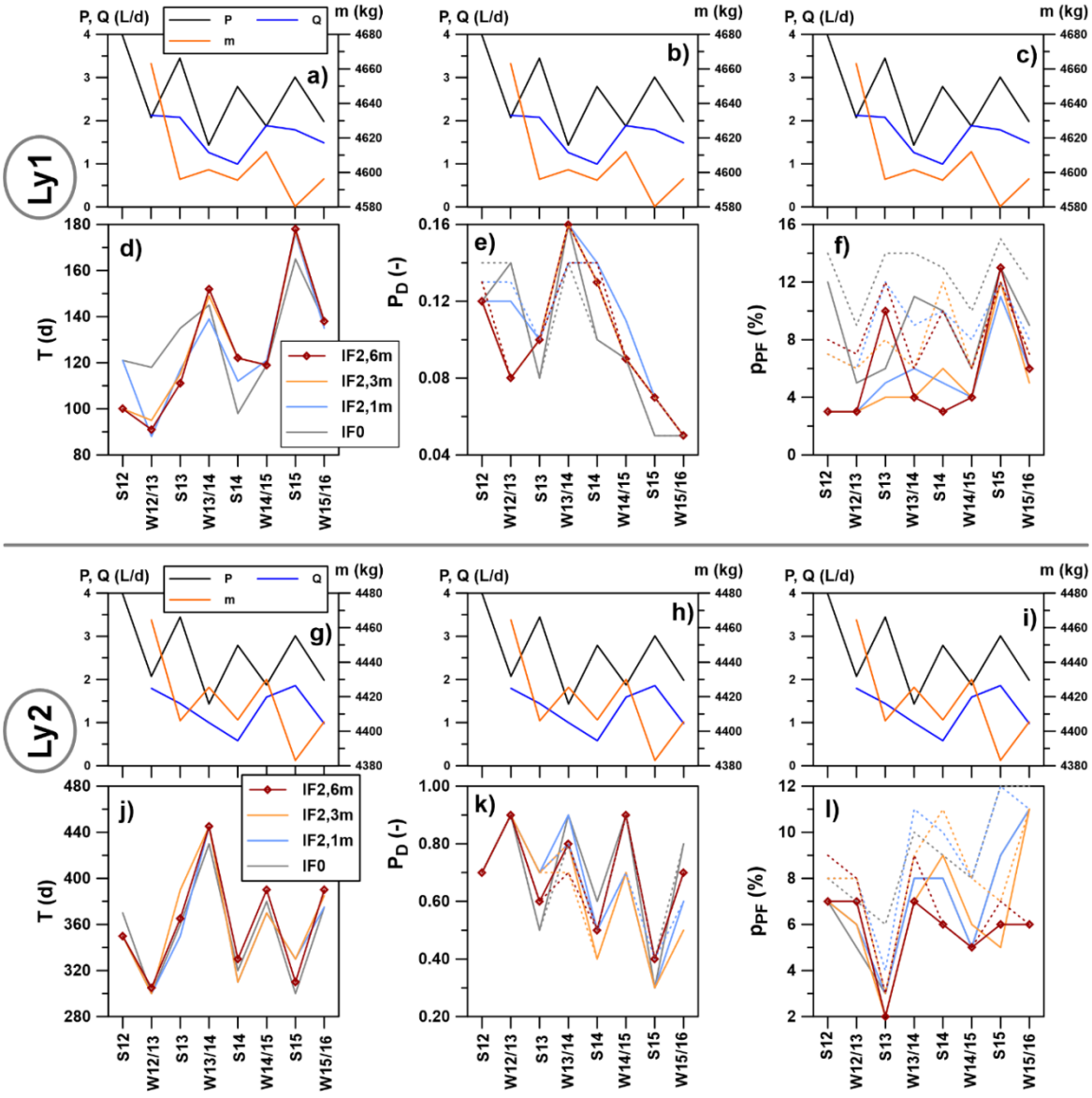

Figure 8. Temporal variation of parameters found from applying the extended LPM.

Stumpp et al. (2009b) found seasonal variations of T and P_D between 26-59 weeks and 0.09-014, respectively, where a clear trend of summer-winter oscillation seems not obvious. Parameter variations from year to year, found in the present study, are within a similar range as observed by Stumpp et al. (2009b) and also by Maloszwski et al. (2006) for different soils.

For many soils, as found for Ly1 (with some exceptions), contributions of preferential flow tend to be higher in summer (e.g., Täumer et al. 2006 and Demand et al. 2019). This can be explained by low water contents that prevail during extended dry periods, combined with precipitation events that provide high precipitation amounts (Demand et al. 2019). Accordingly, p_{PF} tends to be increased when the precipitation rate is high (Figure 8f versus 8c). Such a dependency was also found by Stumpp et al. (2007). In

contrast, no clear season-dependency of p_{PF} can be seen for Ly2. Such a difference between the lysimeters could possibly be explained by a different activation of preferential flow paths. Due to the higher water content in Ly2 and slow movement of water in the clayey sandy silt, seasonal variation of p_{PF} was not observed in Ly2.
Gazis and Feng (2004) studied the isotopic composition of precipitation and soil water in sandy loam soils. Their observations suggest that the mixing of percolating water with immobile water takes a strong influence, which can lead to higher $\delta^{18}O$ values compared to modeled values (due to the prevalence of isotopically heavy summer water), as observed in our study for Ly2. This finding supports our assumption of a "constant upshift" of modeled isotope values in the seepage water of Ly2, for mimicking the contributions of immobile water. In contrast, based on the soil structure and the absence of more immobile water within Ly1, such a mixing between mobile and quasi-immobile water might have had a lower influence for the seepage of Ly1 (no upshift was required there). This might be due to the finer pore structure and thus as a higher effective soil water volume in Ly2 (398 L in Ly2 versus 184 L in Ly1, for more detail, see chapter 2.4.1., Determination of ET with evaluation of the water balance). Consideration of the constant isotopic upshift within the LPM did not impact the values of T, P_D, and p_{PF}.

3.6.3. Comparison of lumped parameter modeling and numerical modeling

For Ly1, the results of lumped-parameter and numerical modeling are similar (Figure 5 vs. 7a): both describe observations, well. Seasonal periodicity of stable water contents in seepage water is met well by both approaches. For Ly2, observations are more difficult to describe by the two model approaches (Figures 6 and 7b). Seasonal periodicity is generally met by LPM application; however, deviations are obvious for numerical modeling, as reflected by considerably lower R^2 for the latter (0.2 vs. up to 0.4 for LPM, Table 9 and 7). Numerically modeled peaks seem to appear ~2 months later for the first and second maximum (August-September 2013 and October 2014, respectively).
P_D-values found from numerical modeling differed from those found from the LPM application. For Ly1, P_D is lower, with 0.07 versus 0.10-0.11 from LPM modeling.

In contrast, for Ly2, P_D obtained from numerical modeling was slightly higher (0.85, Table 9) compared to LPM (averages 0.6-0.7, Table 7). Immobile water can have an influence on dispersion processes due to the mixing between mobile and immobile water phases (e.g., Maloszewski et al. 2006). From numerical modeling studies, Robin et al. (1983) found higher P_D-values when neglecting immobile water as a second porosity system, compared to its consideration. Similar observations are reported for comparative simulations done by Stumpp et al. (2009c) and Maraqa et al. (1997).

Concerning preferential flow, for Ly1, p_{PF} found from numerical modeling (5-7%, Table 9) is slightly lower than from LPM application (average 8-13%, Table 6). For Ly2, p_{PF} found from numerical modeling (12-13%, Table 9) exceeds the LPM best fit (7-9%, Table 7).

Table 10 shows the median transit time (MTT) obtained by numerical modeling of virtual tracers for Ly1 and Ly2 (averages for LPM sub-periods). This allows a comparison to mean transit times T determined from the LPM application (Tables 6 and 7). MTT and T are similar for Ly1, with a somewhat lower average for MTT (100 d for MTT vs. 126-131 d for LPM, for the different input functions). For Ly2, MTT is much lower than T, with 198 d in average vs. 354-361 d. Additional simulation studies with a higher saturated water content θ_s led to an increase in MTT, with averages of 274 d (θ_s = 0.4 cm^3/cm^3) and 342 d (θ_s = 0.5 cm^3/cm^3) (Table 10). Such higher values of θ_s (instead of the fitted values around 0.29 cm^3/cm^3) are also more often reported for silty soils, as discussed above.

Table 10 presents the Median transit time (MTT) obtained by numerical modeling of virtual tracers for Ly1 and Ly2.

Table 10. Median transit time (MTT) was obtained by numerical modeling of virtual tracers for Ly1 and Ly2.

Sub-period	S12	W12/13	S13	W13/14	S14	W14/15	S15	W15/16	Av.
Lysimeter 1									
MTT [d]	76	96	91	163	97	103	93	97	100
Lysimeter 2									
MTT [d]	199	242	223	230	187	185	176	162	197
$MTT_{0.4}$ [d]	298	335	293	304	247	254	226	222	274
$MTT_{0.5}$ [d]	393	408	350	365	299	306	267	267	342

$MTT_{0.4}$ and $MTT_{0.5}$: assuming a higher saturated water content θ_s of 0.4 and 0.5 cm^3/cm^3, respectively.

3.7. COMPARISON OF MODEL CONCEPTS AND POTENTIAL IMPROVEMENTS

Due to a more complex process description (in particular of flow) in HYDRUS-1D compared to LPM, the variation of simulated delta-values in seepage water by adjusting SHP and α_L, is more restricted. Moreover, flow variation is described in a much higher temporal resolution by the numerical model (daily output) than by the extended LPM (half-year variations, due to the parameter changes in each sub-periods). As a consequence, the degree of freedom concerning T and P_D value-fits seems higher for the extended LPM approach than for the numerical model (with MTT instead of T).

In contrast to the HYDRUS-1D setup, the LPM takes an integral view within a "black box": T encompasses the mean transit time of soil water in total, i.e., percolating (mobile) water, as well as contributions of (remobilized) immobile water. Accordingly, MTT would only be a part of this T. This could explain the large difference between T and MTT for Ly2.

The possible overestimation of P_D in Ly2 might be related to shortcomings in our model setup. An extension of our numerical model to a dual-porosity approach could possibly reduce deviations, as well. It has the potential to describe immobile water and its influence on flow and stable water isotope transport mechanistically. However, measurements of soil water contents and/or hydraulic potential within the soil at different depths, are recommended (which were not available for the present study) for model calibration, in order to reduce uncertainties associated with such a (more complex) approach.

The numerical model approach could also be extended by considering the uptake of water by plant roots within the soil column. Although root water uptake is not expected to alter the isotopic composition, significantly (e.g., Zimmermann et al. 1967; Allison et al. 1984), it can have an effect on soil water contents during the vegetation period (e.g., Sprenger et al. 2016).

4. SUMMARY, CONCLUSION AND OUTLOOK

The combination of stable water isotope measurements with lumped-parameter modeling was applied successfully for a three-year study to characterize water flow in the unsaturated zone of two lysimeters filled with different soil textures and planted with the same vegetative cover (maize).

As a first approach, lumped-parameter modeling was applied with the aim of determining flow and transport parameters that are representative of the whole observation period ("traditional" lumped-parameter model, LPM). By that, the mean transit time of water T and the dispersion parameter P_D were determined for the sandy gravel (Ly1) and clayey sandy silt (Ly2) soil cores. The consideration of preferential flow (PF), in addition to soil matrix flow, improved the simulations substantially, and the portion of preferential flow p_{PF} was estimated for both soils.
Modifications of the input function, aimed at improving the estimate of stable water isotope infiltration into the unsaturated zone, succeeded to a different degree depending on the chosen assumptions. The consideration of weighting periods for the input function, in order to account for varying recharge, was most successful for 3- and 6-month periods, corresponding to changing vegetation phases and seasonal variations. In addition, the consideration of evapotranspiration within the input function resulted in more realistic estimates of the recharge. Indeed, this caused some improvements for parts of the observation period. Such temporal differences point towards the influence of changing flow conditions, whose consideration potentially may improve the modeling.

To consider variable flow and transport conditions, an extended LPM approach (as a second approach) was derived by subdividing the whole simulation time into hydraulically characteristic sub-periods. Each sub-period is characterized by constant coefficients, which can vary between sub-periods in order to mimic temporally variable flow conditions. A clear improvement was obtained in comparison to "traditional" lumped-parameter modeling that considered steady-state flow for the whole simulation period. Pronounced seasonal (summer-winter) and year-to-year variations were found for T, P_D and p_{PF}. In simplified assumptions, the model addresses preferential flow as a second permeability system and the influence of immobile water

on stable water isotopes (by a constant isotopic upshift), in addition to water flow and stable water isotope transport within the subsurface matrix.

Numerical modeling with HYDRUS-1D was performed considering matrix and preferential flow as well as the influence of immobile water, in analogy to the extended LPM. Findings obtained from applying the extended LPM approach were compared to results from numerical modeling. In general, model curves from both approaches do correspond well. To deepen this work, a more detailed calibration or a more complex dual-porosity numerical approach is suggested. It might bring some improvements in numerical modeling results.

Comparing the numerical modeling and LPM approach gives us a good hint for future work. Uncertainties for numerical modeling are associated, among others, with missing measurements within the soil columns, so model calibration had to be done solely with discharge rates, weight change of the lysimeters and stable water isotopes measured in seepage water. Furthermore, soil hydraulic parameters needed to be estimated (for Ly1, measurements were done for a similar soil). As an advantage of the extended LPM approach, uncertainties concerning flow characterization can be reduced by identifying ranges of plausible parameters as a result of temporally changing flow (and transport) conditions. The LPM approach represents a valuable tool for flow characterization, with the advantage of lower data requirements compared to numerical modeling. Moreover, LPM provides us the possibilities to consider different assumptions for stable water isotope transport. Since the numerical model is a mechanistic approach, it can be used to verify the LPM results. If the results achieved from LPM are similar to results obtained from the numerical model, it might be avoided that it is a mere fitting success only, for LPM.

For future modeling, the LPM approach is recommended because it is a trustable approach that can provide precise results with relatively less effort, compared to numerical modeling. In LPM, a stepwise procedure is advised, finding (i) one set of parameters (T, P_D and p_{PF}) for the whole simulation time ("traditional" LPM approach) and (ii) temporally varying parameters, corresponding to hydraulically relevant fluctuation patterns (extended LPM approach).

For future work, an investigation of root water uptake within the soil is highly recommended. This could be done in combination with measurements of water

content and/or hydraulic potential at different depths of the soil column, in addition to the monitoring of discharge rates and stable water isotope contents at the seepage water (lysimeter outflow). Such investigations will provide useful information and valuable datasets for further advancing the understanding of water flow and stable water isotope transport in the unsaturated zone.

REFERENCES

Abbasi, F., Jacques, D., Simunek, J., Feyen, J., and van M. T. Genuchten. 2003. Inverse estimation of soil hydraulic and solute transport parameters from transient field experiments: heterogeneous soil. Society, 46, no. 4: 1097–1111.

Abbott, M. D., Lini, A., and P. R. Bierman. 2000. $\delta^{18}O$, δD and 3H measurements constrain groundwater recharge patterns in an upland fractured bedrock aquifer, Vermont, USA. Journal of Hydrology 228, no. 1-2: 101-112.

Adelana, S.M.A. 2005. Environmental Isotopes in Hydrogeology. Water Encyclopedia (eds J.H. Lehr and J. Keeley), doi: 10.1002/047147844X.gw211.

Allen, R.G., L.S. Pereira, D. Raes, and M. Smith. 1998. Crop Evapotranspiration, Guidelines for computing crop water requirements. FAO Irrigation and Drainage Paper 56, Rome, Italy.

Allison, G. B., Barnes, C., Hughes, C. M., and F. Leaney .1984. Effect of climate and vegetation on oxygen-18 and deuterium profiles in soils. In Isotope Hydrology 1983 (pp. 105–122), Vienna, IAEA.

Asadollahi, M., Stumpp, C., Rinaldo, A., and P. Benettin. 2020. Transport and water age dynamics in soils: A comparative study of spatially integrated and spatially explicit models. Water Resources Research, 56, no. 3: e2019WR025539.

Barnes, C. J., and G. B. Allison. 1983. The distribution of deuterium and ^{18}O in dry soils: 1. Theory. Journal of Hydrology 60, no. 1-4: 141-156.

Barnes, C.J., and J.V. Turner. 1998. Isotopic exchange in soil water. In: Kendall, C., McDonnell, J.J. Eds., Isotope Tracers in Catchment Hydrology. Elsevier Science, pp. 137–163.

Beardsell, M. F., and Cohen, D. 1975. Relationships between leaf water status, abscisic acid levels, and stomatal resistance in maize and sorghum. Plant Physiology 56, no. 2: 207–212.

Benettin, P., Queloz, P., Bensimon, M., McDonnell, J. J., and A. Rinaldo. 2019. Velocities, residence times, tracer breakthroughs in a vegetated lysimeter: A multitracer experiment. Water Resources Research, 55, no. 1: 21-33.

Beven, K., and P. Germann. 1982. Macropores and water flow in soils. Water resources research 18, no. 5: 1311-1325.

Blanchoud, H., Moreau-Guigon, E., Farrugia, F., Chevreuil, M., and J. M. Mouchel. 2007. Contribution by urban and agricultural pesticide uses to water contamination at the scale of the Marne watershed. Science of the Total Environment, 375, no. 1-3: 168-179.

Bottinga, Y. (1969). Calculated fractionation factors for carbon and hydrogen isotope exchange in the system calcite-carbon dioxide-graphite-methane-hydrogen-water vapor. Geochimica et Cosmochimica Acta, 33, no.1, 49-64.

Bradford, S. A., Simunek, J., Bettahar, M., Van Genuchten, M. T., and S.R. Yates. 2003. Modeling colloid attachment, straining, and exclusion in saturated porous media. Environmental Science & Technology, 37, no. 10: 2242–2250.

Clark, I. D., Fritz, P. 2013. Environmental isotopes in hydrogeology. CRC press, doi: 10.1201/9781482242911.

Cheviron, B., Coquet, Y., 2009. Sensitivity Analysis of Transient-MIM HYDRUS-1D: Case Study Related to Pesticide Fate in Soils. Vadose Zo. J. 8, 1064–1079.

Craig, H. 1961. Isotopic variations in meteoric waters. Science 133, no. 3465: 1702-1703.

Criss, R. E. (1991). Temperature dependence of isotopic fractionation factors. Stable Isotope Geochemistry: A Tribute to Samuel Epstein, 3, 11-16.

Dann, R., Close, M., Flintoft, M., Hector, R., Barlow, H., Thomas, S., and G. Francis. 2009. Characterization and estimation of hydraulic properties in an alluvial gravel vadose zone. Vadose Zone Journal, 8, no. 3: 651.

Demand, D., Blume, T., and M. Weiler. 2019. Spatio-temporal relevance and controls of preferential flow at the landscape scale. Hydrology and Earth System Sciences, 23, no. 11: 4869–4889.

Dinelli, G., Accinelli, C., Vicari, A., and P. Catizone. 2000. Comparison of the persistence of atrazine and metolachlor under field and laboratory conditions. Journal of Agricultural and Food Chemistry, 48, no. 7: 3037–3043.

Doherty, J., 2020. Model-Independent Parameter Estimation User Manual Part II: PEST Utility Support Software. Watermark Numerical Computing, Retrieved from https://www.nrc.gov/docs/ML0923/ML092360221.pdf.

Durner, W., Jansen, U., and S. C. Iden. 2008. Effective hydraulic properties of layered soils at the lysimeter scale determined by inverse modelling. European Journal of Soil Science, 59, no. 1: 114–124.

Earle, S. 2019. Physical Geology – 2nd Edition. Victoria, B.C.: BCcampus. Retrieved from https://opentextbc.ca/physicalgeology2ed/.

Einsiedl, F., Maloszewski, P., and W. Stichler. 2009. Multiple isotope approach to the determination of the natural attenuation potential of a high-alpine karst system. Journal of Hydrology, 365, no. 1-2: 113–121.

Everts, C. J., and R. S. Kanwar. 1990. Estimating preferential flow to a subsurface drain with tracers. Transactions of the ASAE, 33, no. 2: 451-0457.

Farahani, H. J., and Bausch, W. C. (1995). Performance of evapotranspiration models for maize—bare soil to closed canopy. Transactions of the ASAE, 38, no 4: 1049-1059.

Fetter, C. W. 2001. Applied Hydrogeology. Applied Hydrogeology.

Fetter, C. W. 1993. Contaminant hydrogeology. New York: Macmillan Publishing Company.

Fontes, J. C., Yousfi, M., and G. B. Allison. 1986. Estimation of long-term, diffuse groundwater discharge in the northern Sahara using stable isotope profiles in soil water. Journal of Hydrology 86, no. 3-4: 315-327.

Freeze, R. A., and Cherry, J. A. 1979. Groundwater. Englewood Cliffs: Prentice-Hall Inc.

Friedman, I. (1953). Deuterium content of natural waters and other substances. Geochimica et cosmochimica acta, 4(1-2), 89-103.

Gazis, C., and X. Feng. 2004. A stable isotope study of soil water: Evidence for mixing and preferential flow paths. Geoderma, 119, no. 1.2: 97–111.

Gebler, S., H.-J. Hendricks Franssen, T. Pütz, H. Post, M. Schmidt, and H. Vereecken. 2015. Actual evapotranspiration and precipitation measured by lysimeters: a comparison with eddy covariance and tipping bucket. Hydrology and Earth System Sciences 19: 2145–2161.

Ghodrati, M., and W. A. Jury. 1992. A field study of the effects of soil structure and irrigation method on preferential flow of pesticides in unsaturated soil. Journal of contaminant Hydrology 11, no. 1-2: 101-125.

Ghodrati, M., Chendorain, M., and Y. J. Chang. 1999. Characterization of macropore flow mechanisms in soil by means of a split macropore column. Soil Science Society of America Journal 63, no. 5: 1093-1101.

Grabczak, J., Rózański, K., Maloszewski, P., and A. Zuber. 1984. Estimation of the tritium input function with the aid of stable isotopes. Catena, 11, no. 2-3: 105–114.

Graham, S. L., Srinivasan, M. S., Faulkner, N., and S. Carrick. 2018. Soil hydraulic modeling outcomes with four parameterization methods: Comparing soil description and inverse estimation approaches. Vadose Zone Journal, 17, no. 1: 1-10.

Groh, J., Stumpp, C., Lücke, A., Pütz, T., Vanderborght, J., and H. Vereecken. 2018. Inverse estimation of soil hydraulic and transport parameters of layered soils from water stable isotope and lysimeter data. Vadose Zone Journal, 17, no. 1: 1–19.

Hale, V. C., McDonnell, J. J., Stewart, M. K., Solomon, D. K., Doolitte, J., Ice, G. G., and R. T. Pack. 2016. Effect of bedrock permeability on stream base flow mean transit time scaling relationships: 2. Process study of storage and release. Water Resources Research 52, no. 2: 1375-1397.

Haude, W. 1954. Zur praktischen Bestimmung der aktuellen und potentiellen Evaporation und Evapotranspiration. Mitteilungen Deutscher Wetterdienst 8.

Haude, W. 1955. Zur Bestimmung der Verdunstung auf möglichst einfache Weise. Mitteilungen Deutscher Wetterdienst 11.

Hirschi, M, D. Michel, I. Lehner, and S.I. Seneviratne. 2017. A site-level comparison of lysimeter and eddy covariance flux measurements of evapotranspiration. Hydrology and Earth System Sciences 21: 1809–1825.

Hölting, B., and W. G. Coldewey. 2019. Hydrological Cycle: Water Balance. In Hydrogeology, ed. B. Hölting, and W. G. Coldewey, 63–89. Berlin, Heidelberg, Germany, Springer.

Hrachowitz, M., Soulsby, C., Tetzlaff, D., Dawson, J. J. C., Dunn, S. M., and I. A. Malcolm. 2009. Using long-term data sets to understand transit times in contrasting headwater catchments. Journal of Hydrology, 367(3-4), 237-248.

Hsieh, P., Bahr, J., Doe, T., Flint, A., Gee, G., Gelhar, L., Solomon, K., van Genuchten, M. T., and S. Wheatcraft. 2001. Conceptual models of flow and transport in the fractured vadose zone. Washington, DC: The National Academies Press.

Isch, A., Montenach, D., Hammel, F., Ackerer, P., and Y.Coquet. 2019. A comparative study of water and bromide transport in a bare loam soil using lysimeters and field plots. Water 11, 1–25.

Jain, S. 2014. Fundamentals of physical geology. Springer India.

Jiang, S., Pang, L., Buchan, G.D., Šimůnek, J., Noonan, M.J., and M.E. Close. 2010. Modeling water flow and bacterial transport in undisturbed lysimeters under irrigations of dairy shed effluent and water using HYDRUS-1D. Water Research, 44, no. 4, 1050–1061.

Johnson, A. I. 1967. Specific yield – compilation of specific yields for various materials. US Geolological Survey Water-Supply Paper1662-D, 74 p.

Kendall, C., Caldwell, E. A. 1998b. Fundamentals of Isotope Geochemistry, In: C. Kendall and J.J. McDonnell (Eds.), Isotope Tracers in Catchment Hydrology. Elsevier Science: 51-86.

Kendall, C., Sklash, M.G. and Bullen, T.D. 1995. Isotope Tracers of Water and Solute Sources in Catchments, In: S.T. Trudgill (Ed.), Solute Modelling in Catchment Systems, John Wiley and Sons Ltd: 261-303.

Koeniger, P., Leibundgut, C., Link, T., and J. D. Marshall. 2010. Stable isotopes applied as water tracers in column and field studies. Organic Geochemistry 41, no. 1: 31-40.

Komor, S. C., and D. G. Emerson. 1994. Movements of water, solutes, and stable isotopes in the unsaturated zones of two sand plains in the upper Midwest. Water Resources Research 30, no. 2: 253-267.

Kreft, A., and A. Zuber. 1978. On the physical meaning of the dispersion equation and its solutions for different initial and boundary conditions. Chemical Engineering Science, 33, no. 11: 1471-1480.

Kundzewicz, Z. W., and P. Döll. 2009. Will groundwater ease freshwater stress under climate change? Hydrological Sciences Journal, 54, no. 4: 665-675.

Langner, H. W., Gaber, H. M., Wraith, J. M., Huwe, B., and W. P. Inskeep. 1999. Preferential flow through intact soil cores effects of matric head. Soil Science Society of America Journal 63, no. 6: 1591-1598.

Larcher, W. 1995. Physiological plant ecology, 3rd ed., Springer, Berlin, Germany.

Legind, C. N., Rein, A., Serre, J., Brochier, V., Haudin, C. S., Cambier, P., Houot, S., and S. Trapp. 2012. Simultaneous simulations of uptake in plants and leaching to groundwater of cadmium and lead for arable land amended with compost or farmyard manure. PloS one 7, no. 10: e47002.

Leibundgut, C., Maloszewski, P., and C. Külls. 2009. Environmental tracers. Tracers in Hydrology, John WileyandSons, Ltd., Chichester, UK, 13-56.

Lenda, A., and A. Zuber. 1970. Tracer dispersion in groundwater experiments. Isotope Hydrology 1970: 619-641.

Lennartz, B., and S. K. Kamra. 1998. Temporal variability of solute transport under vadose zone conditions. Hydrological processes 12, no. 12: 1939-1949.

Löpmeier, F.-J. 1994. Berechnung der Bodenfeuchte und Verdunstung mittels agrarmeteorologischer Modelle. Zeitschrift für Bewässerungswirtschaft 29: 157–167.

Luckner, L., Van Genuchten, M. T., Nielsen, D. R. 1989. A consistent set of parametric models for the two-phase flow of immiscible fluids in the subsurface. Water Resources Research 25, no. 10: 2187-2193.

Mali, N., Urbanc, J., and A. Leis. 2007. Tracing of water movement through the unsaturated zone of a coarse gravel aquifer by means of dye and deuterated water. Environmental geology 51, no. 8: 1401-1412.

Maloszewski, P., and A. Zuber. 1982. Determining the turnover time of groundwater systems with the aid of environmental tracers. 1. Models and their applicability. Journal of Hydrology, 57, no. 3-4: 207–231.

Maloszewski, P., and A. Zuber. 1996. Lumped parameter models for the interpretation of environmental tracer data No. IAEA-TECDOC-910.

Maloszewski, P., Maciejewski, S., Stumpp, C., Stichler, W., Trimborn, P., and D. Klotz .2006. Modelling of water flow through typical Bavarian soils: 2. Environmental deuterium transport. Hydrological Sciences Journal, 51, no. 2: 298–313.

Maloszewski, P., Rauert, W., Trimborn, P., Herrmann, A., and R. Rau. 1992. Isotope hydrological study of mean transit times in an alpine basin (Wimbachtal, Germany). Journal of Hydrology, 140, no. 1-4: 343-360.

Maloszewski, P., Stichler, W., Zuber, A., and D. Rank. 2002. Identifying the flow systems in a karstic-fissured-porous aquifer, the Schneealpe, Austria, by modelling of environmental ^{18}O and ^{3}H isotopes. Journal of Hydrology, 256, no. 1-2: 48–59.

Maraqa, M. A., Wallace, R. B., and T. C. Voice. 1997. Effects of degree of water saturation on dispersivity and immobile water in sandy soil columns. Journal of Contaminant Hydrology, 25, no. 3-4: 199–218.

McGuire, K. J., DeWalle, D. R., and W. J. Gburek. 2002. Evaluation of mean residence time in subsurface waters using oxygen-18 fluctuations during drought conditions in the mid-Appalachians. Journal of Hydrology 261, no. 1-4: 132-149.

Monteith, J. L., and Szeicz, G. 1961. The radiation balance of bare soil and vegetation. Quarterly Journal of the Royal Meteorological Society 87, no. 372: 159–170.

Mualem, Y. 1976. A new model for predicting the hydraulic conductivity of unsaturated porous media. Water Resources Research, 12, no. 3: 513-522.

Nimmo, J. R. 2006. Unsaturated zone flow processes. Encyclopedia of hydrological sciences.

O'driscoll, M. A., DeWalle, D. R., McGuire, K. J., and W. J. Gburek. 2005. Seasonal 18O variations and groundwater recharge for three landscape types in central Pennsylvania, USA. Journal of Hydrology 303, no. 1-4: 108-124.

Olbrisch, H. D. 1975. Beitrag zur Methodik der Datenanalyse bei Lysimeteruntersuchungen.

Parker, J. C., and K. A. Albrecht. 1987. Sample Volume Effects on Solute Transport Predictions. Water Resources Research 23, no. 12: 2293-2301.

Peters, A., T. Nehls, H. Schonsky, and G. Wessolek. 2014. Separating precipitation and evapotranspiration from noise – a new filter routine for high-resolution lysimeter data. Hydrology and Earth System Sciences 18: 1189–1198.

Piccinni, G., Ko, J., Marek, T., and T. Howell. 2009. Determination of growth-stage-specific crop coefficients KC of maize and sorghum. Agricultural water management 96, no. 12: 1698-1704.

Radolinski, J., Pangle, L., Klaus, J., and R.D. Stewart. 2021. Testing the 'two water worlds' hypothesis under variable preferential flow conditions. Hydrological Process 35, no. 6: 1–14.

Rein, A., C.N. Legind, and S. Trapp. 2011. New Concepts for Dynamic Plant Uptake Models. SAR and QSAR in Environmental Research 22, no. 1-2: 191–215.

Richards, F.L. 1959. A flexible growth function for empirical use. Journal of Experimental Botany 10: 290–300.

Robin, M. J., Laryea, K. B., and D. E. Elrick. 1983. Hydrodynamic dispersion during absorption of water by soil: 2. Immobile water model. Journal of Hydrology, 65, no. 4: 333–348.

Rozanski K., L. Araguás-Araguás, and R. Gonfiantini. 1993. Isotopic patterns in modern global precipitation. Geophysical Monograph Series. In Climate Change in Continental Isotopic Records, ed. P.K. Swart, K. C. Lohman, J. McKenzie, and S. Savin, Geophysical Monograph 78: 1–36, American Geophysical Union, Washington, DC.

Rücknagel, J., Götze, P., Hofmann, B., Christen, O., and K. Marschall. 2013. The influence of soil gravel content on compaction behaviour and pre-compression stress. Geoderma 209: 226-232.

Schwärzel, K., Šimůnek, J., Stoffregen, H., Wessolek, G., and M. Th. van Genuchten. 2006. Estimation of the unsaturated hydraulic conductivity of peat soils. Vadose Zone Journal, 5, no. 2: 628–640.

Seyfried, M. S., and P. S. C. Rao. 1987. Solute Transport in Undisturbed Columns of an Aggregated Tropical Soil: Preferential Flow Effects 1. Soil Science Society of America Journal 51, no. 6: 1434-1444.

Shajari, F., Einsiedl, F., and A. Rein. 2020. Characterizing water flow in vegetated lysimeters with stable water isotopes and modeling. Groundwater, 58, no. 5: 759–770.

Šimůnek, J., and M. T. van Genuchten. 2008. Modeling nonequilibrium flow and transport processes using HYDRUS. Vadose Zone Journal 7, no. 2: 782–797.

Šimůnek, J., Šejna, M., Saito, H., Sakai, M., and M. T. van Genuchten. 2009. The HYDRUS-1D software package for simulating the one-dimensional movement of water, heat, and multiple solutes in variably-saturated media. Version 4.08 January 2009. Riverside, California: Department of Environmental Sciences,

University of California Riverside. Retrieved from https://www.pc-progress.com/Downloads/Pgm_hydrus1D/ HYDRUS1D-4.08.pdf

Šimůnek, J., Van Genuchten, M. T., and M. Šejna. 2008. Development and applications of the HYDRUS and STANMOD software packages and related codes. Vadose Zone Journal, 7, no. 2: 587–600.

Šimůnek, J., Genuchten, M.T., Šejna, M., 2016. Recent Developments and Applications of the HYDRUS Computer Software Packages. Vadose Zone Journal, 15, no. 17, 1–25.

Sprenger, M., Seeger, S., Blume, T., and M. Weiler. 2016. Travel times in the vadose zone: Variability in space and time. Water Resources Research 52, no. 8: 5727-5754.

Sprenger, M., Tetzlaff, D., Buttle, J., Laudon, H., Leistert, H., Mitchell, C. P. J., Snelgrove, J., Weiler, M., and C. Soulsby. 2017. Measuring and modeling stable isotopes of mobile and bulk soil water. Vadose Zone Journal, 17, no. 1.

Sprenger, M., Volkmann, T. H., Blume, T., and M. Weiler. 2015. Estimating flow and transport parameters in the unsaturated zone with pore water stable isotopes. Hydrology and Earth System Sciences 19: 2617-2635.

Srivastava, P. K., Singh, P., Pandey, V., Gupta, M. 2021. Development of android application for visualisation of soil water demand. Agricultural Water Management: 375-389. Academic Press, doi: 10.1016/B978-0-12-812362-1.00018-7.

Stauffer, P. H., and Z. Lu. 2012. Quantifying transport uncertainty in unsaturated rock using Monte Carlo sampling of retention curves. Vadose Zone Journal 11, no. 4.

Stichler, W., and A. Herrmann. 1983. Application of environmental isotope techniques in water balance studies of small basins. In New Approaches in Water Balance Computations Proceedings of the Hamburg Workshop, IAHS, Hamburg, Germany, pp. 93-112.

Stockinger, M. P., Bogena, H. R., Lücke, A., Stumpp, C., and H. Vereecken. 2019. Time variability and uncertainty in the fraction of young water in a small headwater catchment. Hydrology and Earth System Sciences 23, no. 10: 4333-4347.

Stone, W. W., and J. T. Wilson. 2006. Preferential flow estimates to an agricultural tile drain with implications for glyphosate transport. Journal of Environmental Quality 35, no. 5: 1825-1835.

Stumpp C., J. Klaus, and W. Stichler. 2014. Analysis of long-term stable isotopic composition in German precipitation. Journal of Hydrology 517: 351–361.

Stumpp, C, Nützmann, G., Maciejewski, S., and P. Maloszewski. 2009c. A comparative modeling study of a dual tracer experiment in a large lysimeter under atmospheric conditions. Journal of Hydrology, 375, no. 3-4: 566–577.

Stumpp, C, Stichler, W., and P. Maloszewski. 2009b. Application of the environmental isotope $\delta^{18}O$ to study water flow in unsaturated soils planted with different crops: Case study of a weighable lysimeter from the research field in Neuherberg, Germany. Journal of Hydrology, 368, no. 1-4: 68–78.

Stumpp, C., and M. J. Hendry. 2012a. Spatial and temporal dynamics of water flow and solute transport in a heterogeneous glacial till: The application of high-resolution profiles of $\delta^{18}O$ and $\delta^{2}H$ in pore waters. Journal of Hydrology, 438-439, 203–214.

Stumpp, C., and P. Maloszewski. 2010. Quantification of preferential flow and flow heterogeneities in an unsaturated soil planted with different crops using the environmental isotope $\delta^{18}O$. Journal of Hydrology 394, no. 3-4: 407-415.

Stumpp, C., Klaus, J., and W. Stichler. 2014. Analysis of long-term stable isotopic composition in German precipitation. Journal of hydrology 517: 351-361.

Stumpp, C., Maloszewski, P., Stichler, W., and J. Fank. 2009a. Environmental isotope $\delta^{18}O$ and hydrological data to assess water flow in unsaturated soils planted with different crops: Case study lysimeter station “Wagna”Austria. Journal of hydrology 369, no. 1-2: 198-208.

Stumpp, C., Maloszewski, P., Stichler, W., and S. Maciejewski. 2007. Quantification of the heterogeneity of the unsaturated zone based on environmental deuterium observed in lysimeter experiments. Hydrological Sciences Journal, 52, no. 4: 748-762.

Stumpp, C., Nützmann, G., Maciejewski, S., and P. Maloszewski. 2009c. A comparative modeling study of a dual tracer experiment in a large lysimeter under atmospheric conditions. Journal of hydrology 375, no. 3-4: 566-577.

Stumpp, C., Stichler, W., and P. Maloszewski. 2009b. Application of the environmental isotope $\delta^{18}O$ to study water flow in unsaturated soils planted with different crops: Case study of a weighable lysimeter from the research field in Neuherberg, Germany. Journal of Hydrology 368, no. 1-4: 68-78.

Stumpp, C., Stichler, W., Kandolf, M., and J. Šimůnek. 2012b. Effects of land cover and fertilization method on water flow and solute transport in five lysimeters: A long-term study using stable water isotopes. Vadose Zone Journal, 11, no. 1: 1-14.

Takakura, T., J. Goudriaan, and W. Louwerse. 1975. A behaviour model to simulate stomatal resistance. Agricultural Meteorology 15, no. 3: 393–404.

Täumer, K., Stoffregen, H., and G. Wessolek. 2006. Seasonal dynamics of preferential flow in a water repellent soil. Vadose Zone Journal, 5, no. 1: 405–411.

Tetzlaff, D., Birkel, C., Dick, J., Geris, J., and C. Soulsby. 2014. Storage dynamics in hydropedological units control hillslope connectivity, runoff generation, and the evolution of catchment transit time distributions. Water Resources Research 50, 969- 985.

Thoma, M. J., Barrash, W., Cardiff, M., Bradford, J., and J. Mead. 2014. Estimating unsaturated hydraulic functions for coarse sediment from a field-scale infiltration experiment. Vadose Zone Journal, 13, no. 3: 1-17.

Tindall, J. A., Kunkel, J. R., and D. E. Anderson. 1999. Unsaturated zone hydrology for scientists and engineers (Vol. 4). Upper Saddle River, NJ: Prentice Hall.

Trapp, S. 2007. Fruit Tree model for uptake of organic compounds from soil and air. SAR and QSAR in Environmental Research 18: 367–387.

Turan, M. A., A. H. A. Elkarim, N. Taban, and S. Taban. 2009. Effect of salt stress on growth, stomatal resistance, proline and chlorophyll concentrations on maize plant. African Journal of Agricultural Research 4, no. 9: 893–897.

Urey, H. C. (1947). The thermodynamic properties of isotopic substances. Journal of the Chemical Society (Resumed), 562-581.

U.S. Department of Agriculture, Natural Resources Conservation Service 2012. National soil survey handbook, title 430-VI. http://www.nrcs.usda.gov/wps/portal/nrcs/detail/soils/ref/?cid=nrcs142p2_054242 (accessed 9/13/2012).

van Genuchten, M. T. 1980. A closed-form equation for predicting the hydraulic conductivity of unsaturated soils. Soil Science Society of America Journal, 44, no. 5: 892–898.

Van Ommen, H. C., Van Genuchten, M. T., Van der Molen, W. H., Dijksma, R., and J. Hulshof. 1989. Experimental and theoretical analysis of solute transport from a diffuse source of pollution. Journal of Hydrology 105, no. 3-4: 225-251.

Vanderborght, J., and H. Vereecken. 2007. Review of Dispersivities for Transport Modeling in Soils. Vadose Zone Journal 6, no. 1: 29-52. doi:10.2136/vzj2006.0096.

Vanderborght, J., Timmerman, A., and J. Feyen. 2000. Solute transport for steady-state and transient flow in soils with and without macropores. Soil Science Society of America Journal 64, no. 4: 1305-1317.

Varis, O. 2018. Population megatrends and water management. In A.K. Biswas, C. Tortajada, and P. Rohner (Eds.), Assessing global water megatrends (pp. 41-59). Singapore: Springer Nature.

Veröffentlichung des Instituts für Wasserforschung GmbH Dortmund und Hydrologische Abteilung Dortmunder Stadtwerke GmbH, 22.

Viville, D., Ladouche, B., and T. Bariac. 2006. Isotope hydrological study of mean transit time in the granitic Strengbach catchment Vosges massif, France: application of the FlowPC model with modified input function. Hydrological Processes: An International Journal 20, no. 8: 1737-1751.

Vrba, J., and A. Richts. 2015. The global map of groundwater vulnerability to floods and droughts, Explanatory notes. Paris, France: UNESCO, International Hydrological Programme.

Vrugt, J. A., Bouten, W., and A. H. Weerts. 2001. Information content of data for identifying soil hydraulic parameters from Outflow experiments. Soil Science Society of America Journal, 65, no. 1: 19–27.

Walker, C. D., and S. B. Richardson. 1991. The use of stable isotopes of water in characterising the source of water in vegetation. Chemical Geology 94, no. 2: 145-158.

Wilson, T. B., and Meyers, T. P. (2007). Determining vegetation indices from solar and photosynthetically active radiation fluxes. Agricultural and Forest Meteorology, 144(3-4), 160-179.

Winton, K., and J.B. Weber. 2018. A review of field lysimeter studies to describe the environmental fate of pesticides. Weed Technology, 10, no. 1: 202–209.

Woldeamlak, S. T., Batelaan, O. and F. De Smedt. 2007. Effects of climate change on the groundwater system in the Grote-Nete catchment, Belgium. Hydrogeology Journal, 15, no. 5: 891-901.

Zimmermann, U., Ehhalt D., and K. O. Muennich. 1967. Soil-water movement and evapotranspiration: Changes in the isotopic composition of the water. In Isotopes in hydrology 1967 (pp. 567–585), Vienna: IAEA.

APPENDIX: SUPPLEMENTARY TABLES AND FIGURES

Table S1. Statistical evaluation of model curve fits for $\delta^{18}O$ content in seepage water of Ly1 (shown in Figure S8 and S9). Mean error ME, root mean squared error RMSE and coefficient of determination R^2 for the different modeling scenarios.

Scenario	Isotope transport through soil matrix			Isotope transport through soil matrix plus along preferential flow paths		
	R^2 [-]	RMSE [‰]	ME [‰]	R^2 [-]	RMSE [‰]	ME [‰]
mod (IF0)	0.480	1.51	-0.61	0.535	1.36	-0.64
mod (IF1, 1m)	0.492	1.78	-1.05	0.541	1.65	-1.07
mod (IF1, 3m)	0.510	1.63	-0.82	0.526	1.54	-0.84
mod (IF1, 6m)	0.536	1.65	-0.96	0.542	1.61	-0.97
mod (IF2, 1m)	0.464	1.97	-1.35	0.503	1.88	-1.36
mod (IF2, 3m)	0.502	1.81	-1.14	0.511	1.76	-1.15
mod (IF2, 6m)	0.492	1.92	-1.26	0.486	1.89	-1.27
mod (IF4, 1m)	0.500	1.94	-1.39	0.538	1.87	-1.40
mod (IF4, 3m)	0.532	1.81	-1.26	0.538	1.78	-1.28
mod (IF4, 6m)	0.510	1.90	-1.32	0.502	1.89	-1.33
mod (IF5, 1m)	0.477	1.98	-1.39	0.511	1.90	-1.40
mod (IF5, 3m)	0.511	1.84	-1.26	0.515	1.82	-1.27
mod (IF5, 6m)	0.495	1.92	-1.34	0.490	1.91	-1.35

Table S2. Statistical evaluation of model curve fits for $\delta^{18}O$ content in seepage water of Ly2 (shown in Figure S10 and S11).

Scenario	Isotope transport through soil matrix			Isotope transport through soil matrix plus along preferential flow paths		
	R^2 [-]	RMSE [‰]	ME [‰]	R^2 [-]	RMSE [‰]	ME [‰]
mod (IF0)	0.189	0.92	-0.05	0.317	0.80	-0.18
mod (IF1, 1m)	0.168	1.05	-0.48	0.315	1.01	-0.59
mod (IF1, 3m)	0.168	0.91	-0.25	0.316	0.88	-0.36
mod (IF1, 6m)	0.183	0.93	-0.32	0.313	0.90	-0.43
mod (IF2, 1m)	0.159	1.23	-0.91	0.287	1.25	-1.00
mod (IF2, 3m)	0.183	1.10	-0.70	0.290	1.13	-0.80
mod (IF2, 6m)	0.168	1.20	-0.86	0.268	1.24	-0.95
mod (IF4, 1m)	0.164	1.25	-0.90	0.290	1.26	-1.00
mod (IF4, 3m)	0.181	1.10	-0.72	0.297	1.14	-0.83
mod (IF4, 6m)	0.146	1.21	-0.91	0.253	1.25	-0.99
mod (IF5, 1m)	0.174	1.26	-0.92	0.290	1.29	-1.03
mod (IF5, 3m)	0.211	1.11	-0.75	0.302	1.17	-0.86
mod (IF5, 6m)	0.216	1.13	-0.80	0.293	1.18	-0.89

Table S3. Parameter bounds selected for the application of the parameter optimization algorithm PEST; based on expected value ranges for the considered soils.

Parameter	Lysimeter 1		Lysimeter 2	
	Lower bound	Upper bound	Lower bound	Upper bound
θ_r [cm³/cm³]	0.001	0.1	0.01	0.2
θ_s [cm³/cm³]	0.1	0.4	0.1	0.5
α [1/cm]	0.005	0.5	0.005	0.6
n [-]	1.0	4.0	1.0	4.0
K_s [cm/d]	4,000	80,000	25	300
P_D [cm]	0	200	0	200
p_{pf} [%]	0	15	0	15
T_{pf} [d]	0	7	0	7

Main references for the considered bounds: Jiang et al. (2010), Stumpp et al. (2009), Sprenger et al. (2015), Thoma et al. (2014), Vanderborght et al. (2000), Abbasi et al. (2003), Cheviron and Coquet (2009)

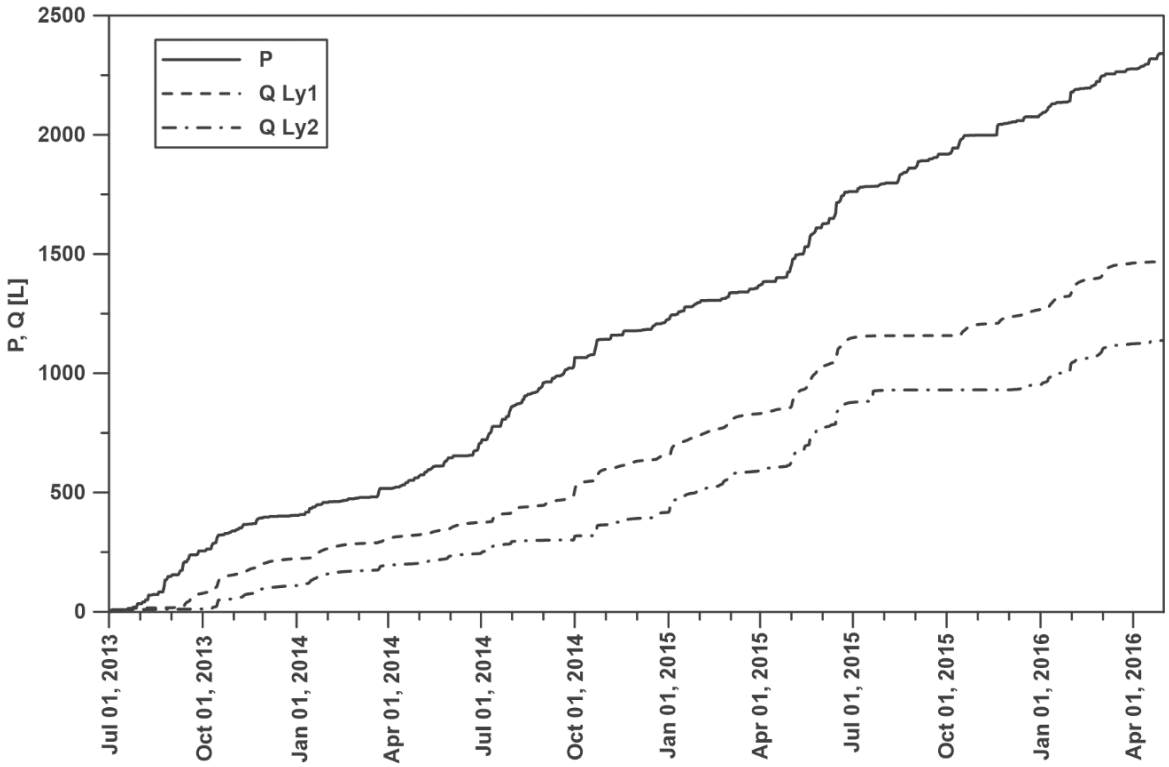

Figure S1. Cumulative amounts of precipitation (P) and outflow (Q) in Ly1 and Ly2 as a function of time.

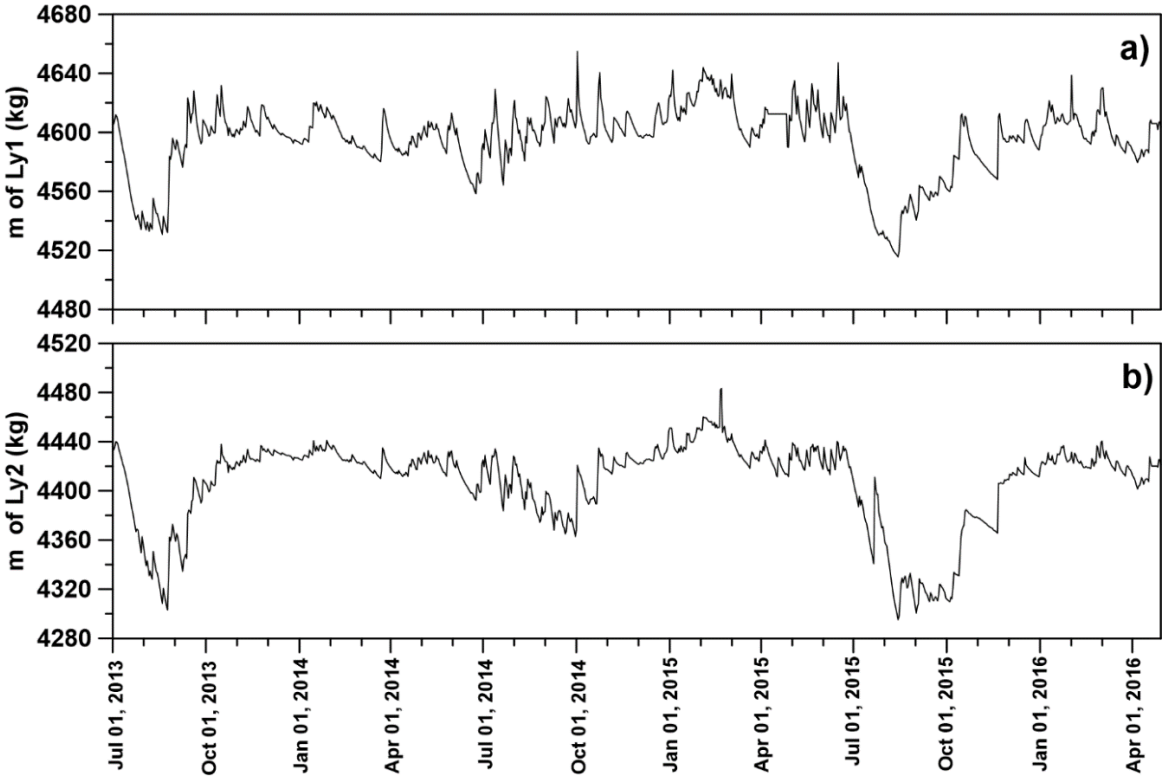

Figure S2. Measured lysimeter weight m of Ly1 (a) and Ly2 (b) as a function of time.

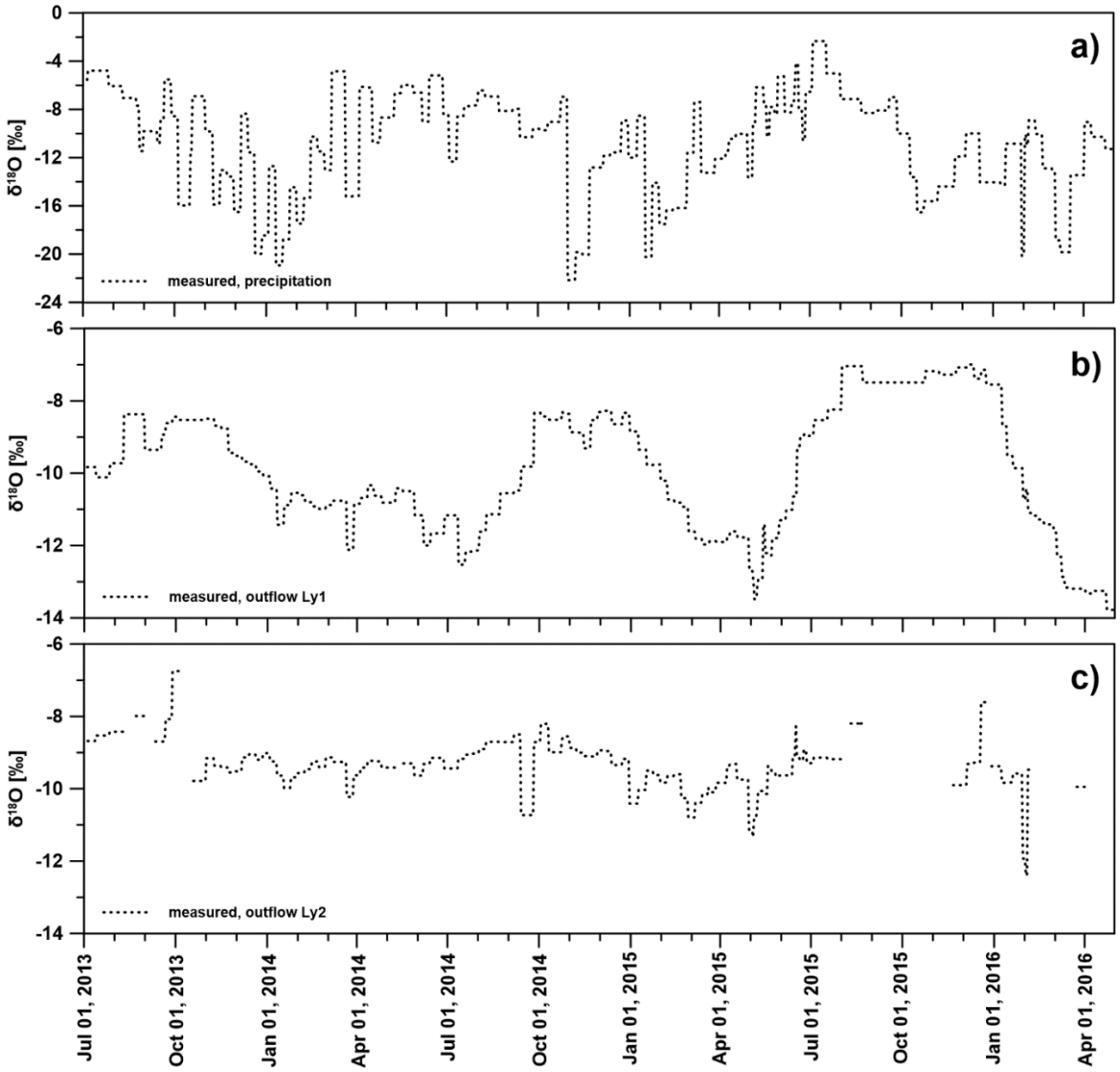

Figure S3. Measured $\delta^{18}O$ in precipitation (a), seepage water from Ly1 (b) and outflow from Ly2 (c).

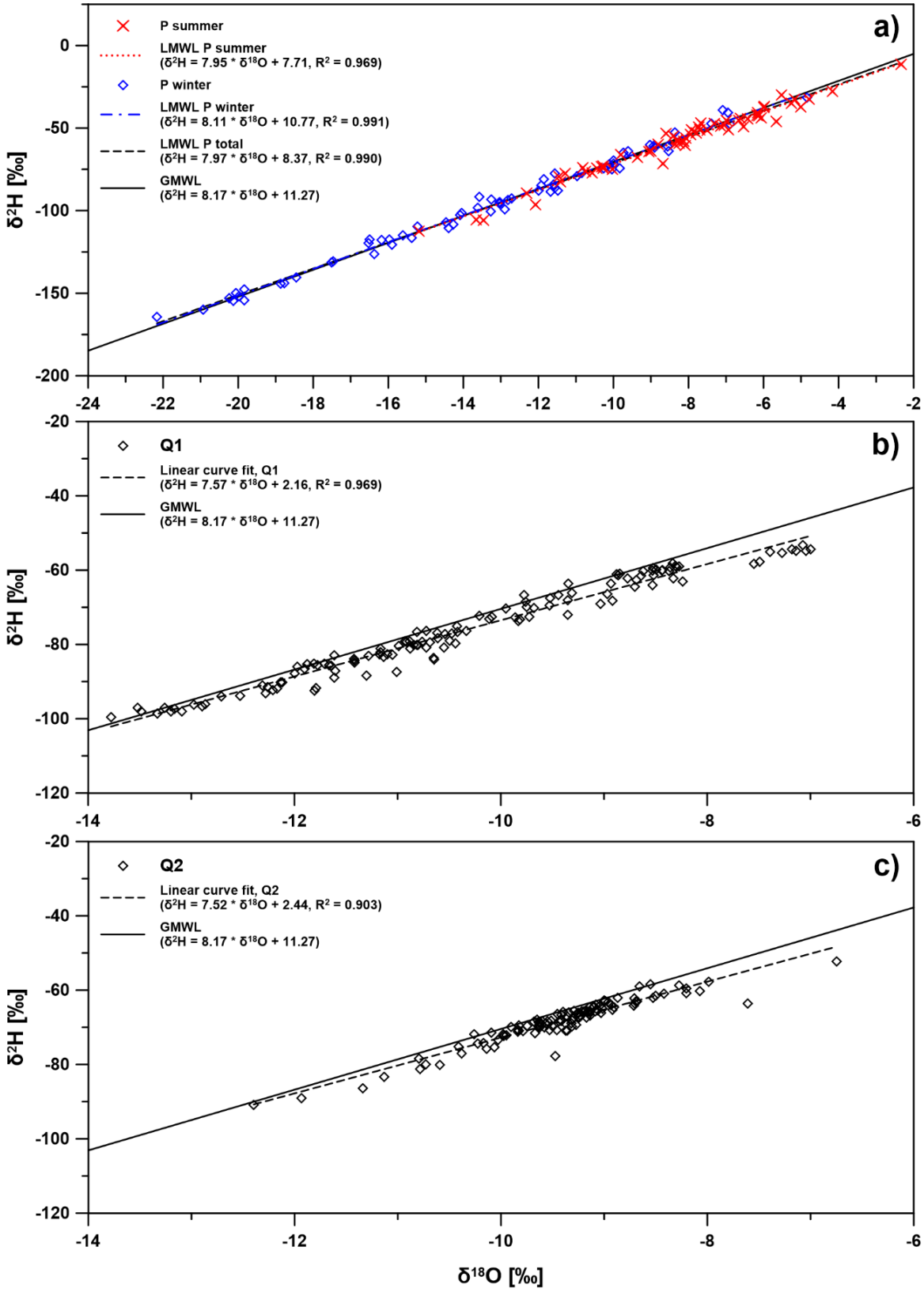

Figure S4. Global meteoric water line GMWL based upon Vienna Standard Mean Ocean Water V-SMOW (Rozanski et al. 1993), local meteoric water lines LMWL for precipitation P (a), lines fitted to the isotopic composition of lysimeter seepage water for Ly1 Q1 (b) and Ly2 Q2 (c). R^2: coefficient of determination.

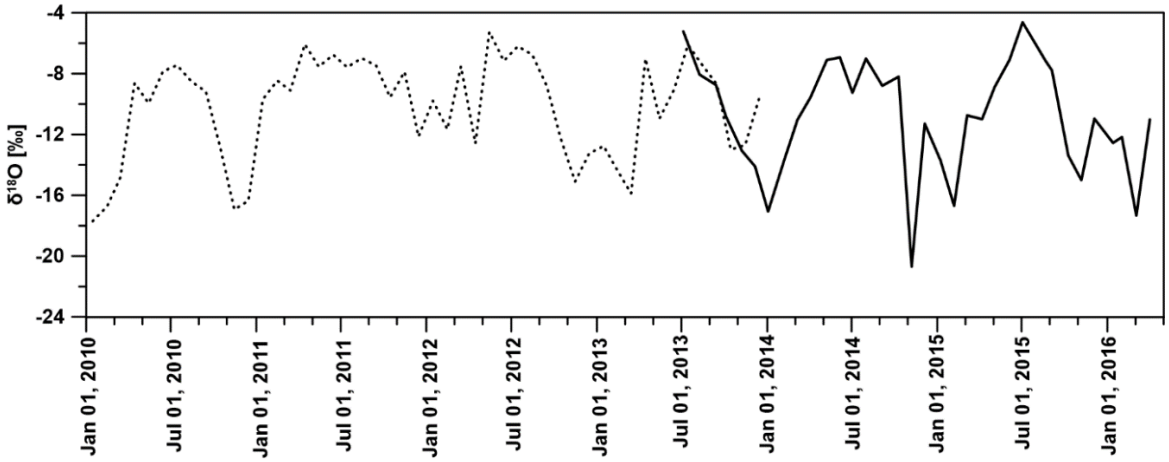

Figure S5. Monthly average of $\delta^{18}O$ in precipitation observed at the Wielenbach site (solid line) and measured the meteorological station Passau-Fürstenzell (Stumpp et al. 2014; dotted line).

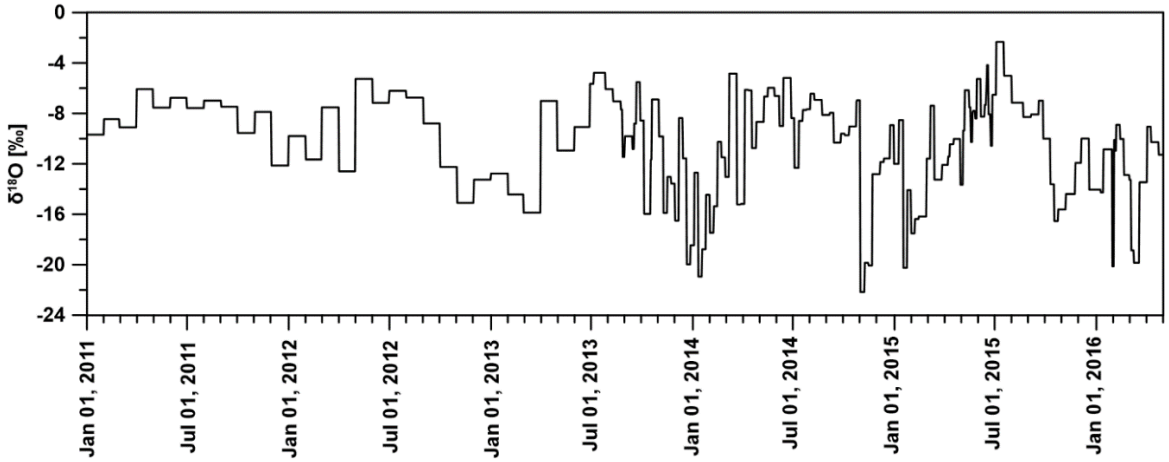

Figure S6. $\delta^{18}O$ as a function of time, measured in precipitation (before 2013: weather station Passau-Fürstenzell, Germany; 2013-2016: lysimeter study site).

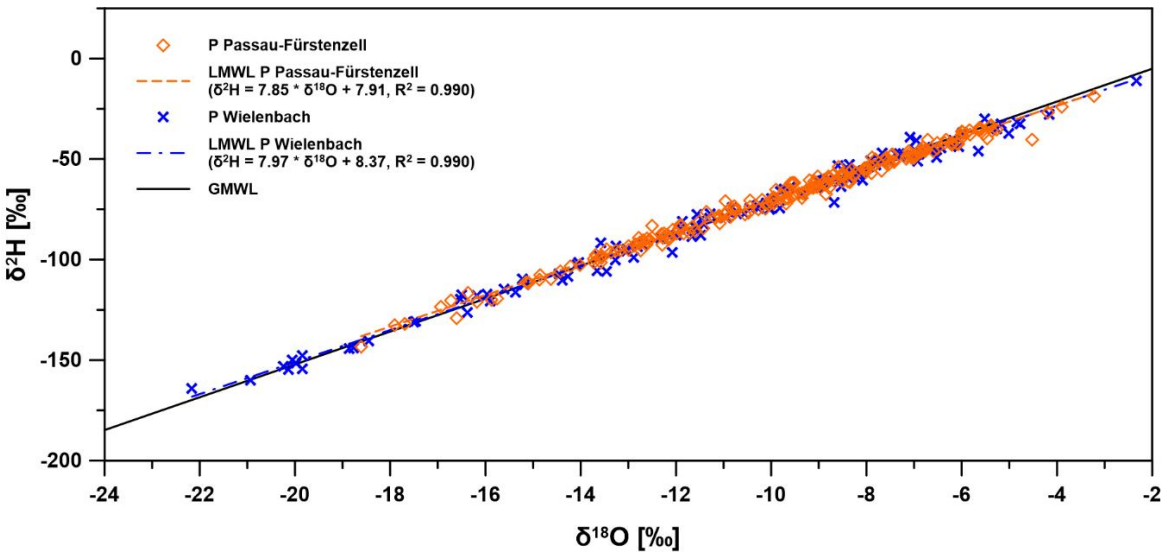

Figure S7. Global meteoric water line (GMWL) based upon V-SMOW (Rozanski et al. 1993) and local meteoric water lines (LMWL) for precipitation sampled at the Wielenbach site and the meteorological station Passau-Fürstenzell, 1997-2013 (Stumpp et al. 2014).

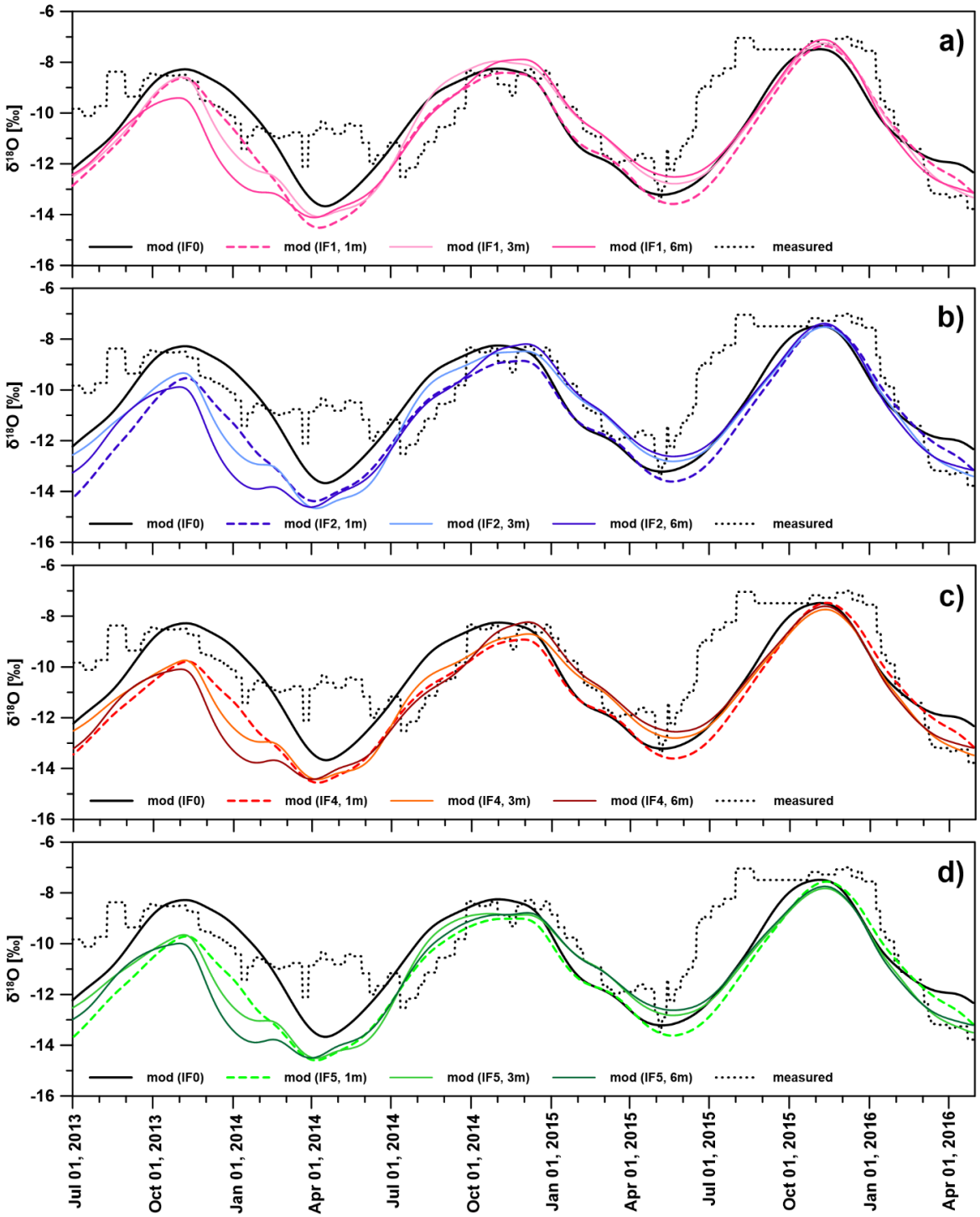

Figure S8. Measured and modeled $\delta^{18}O$ in the seepage water of Ly1 as a function of time. Isotope transport through the soil matrix is modeled (mod), with input function IF0 (isotopic composition of precipitation as input) and a) IF1 (weighting, only; weighting period 1, 3 and 6 months), b) IF2 (considering measured evapotranspiration ET), c) IF4 (considering ET estimated by Penman-Monteith), d) IF5 (considering ET estimated by Penman-Monteith plus modeled maize transpiration).

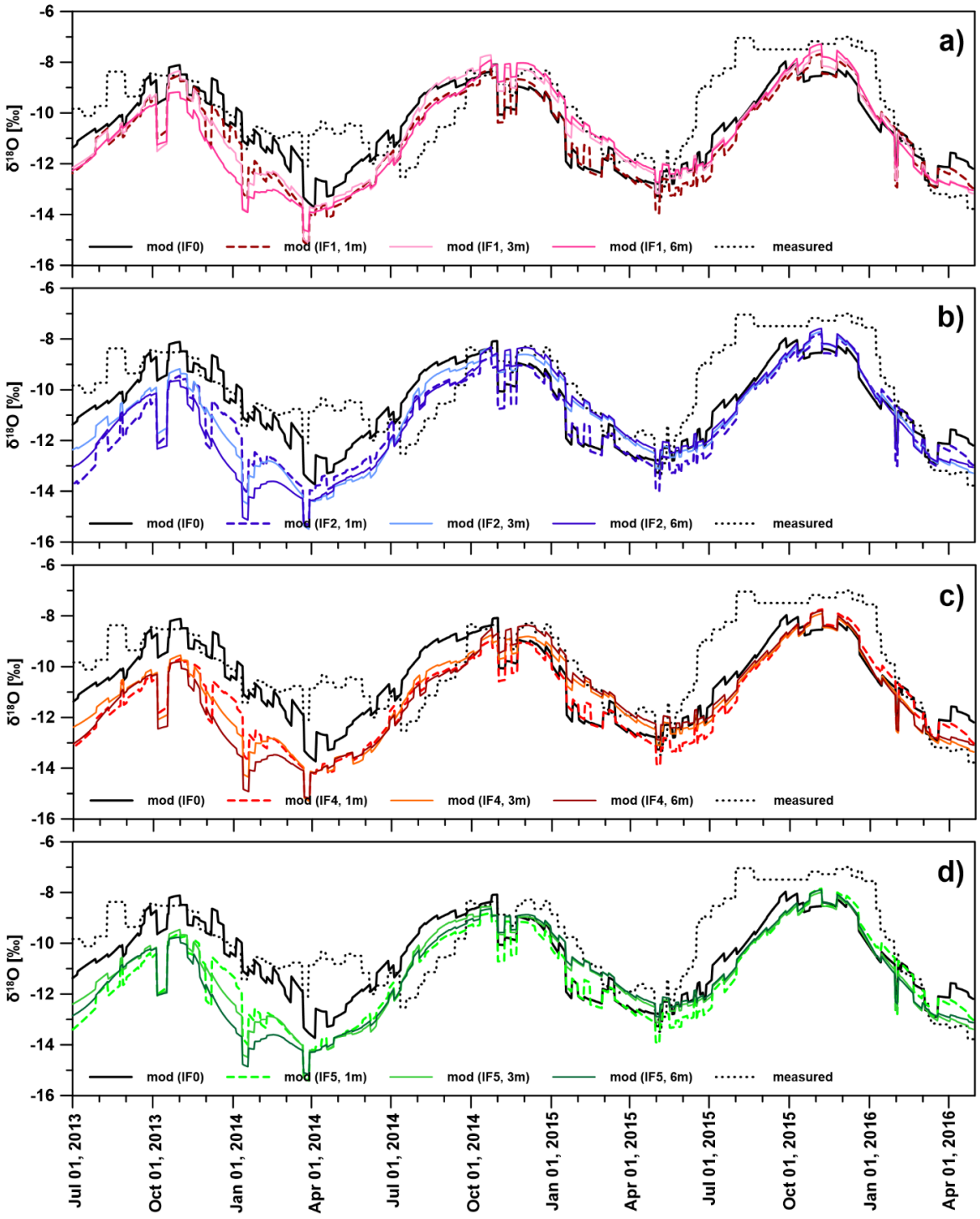

Figure S9. Measured and modeled $\delta^{18}O$ in the seepage water of Ly1 as a function of time. Isotope transport through the soil matrix and along preferential flow paths is modeled (mod), with input function IF0 (isotopic composition of precipitation as input) and a) IF1 (weighting, only; weighting period 1, 3 and 6 months), b) IF2 (considering measured evapotranspiration ET), c) IF4 (considering ET estimated by Penman-Monteith), d) IF5 (considering ET estimated by Penman-Monteith plus modeled maize transpiration).

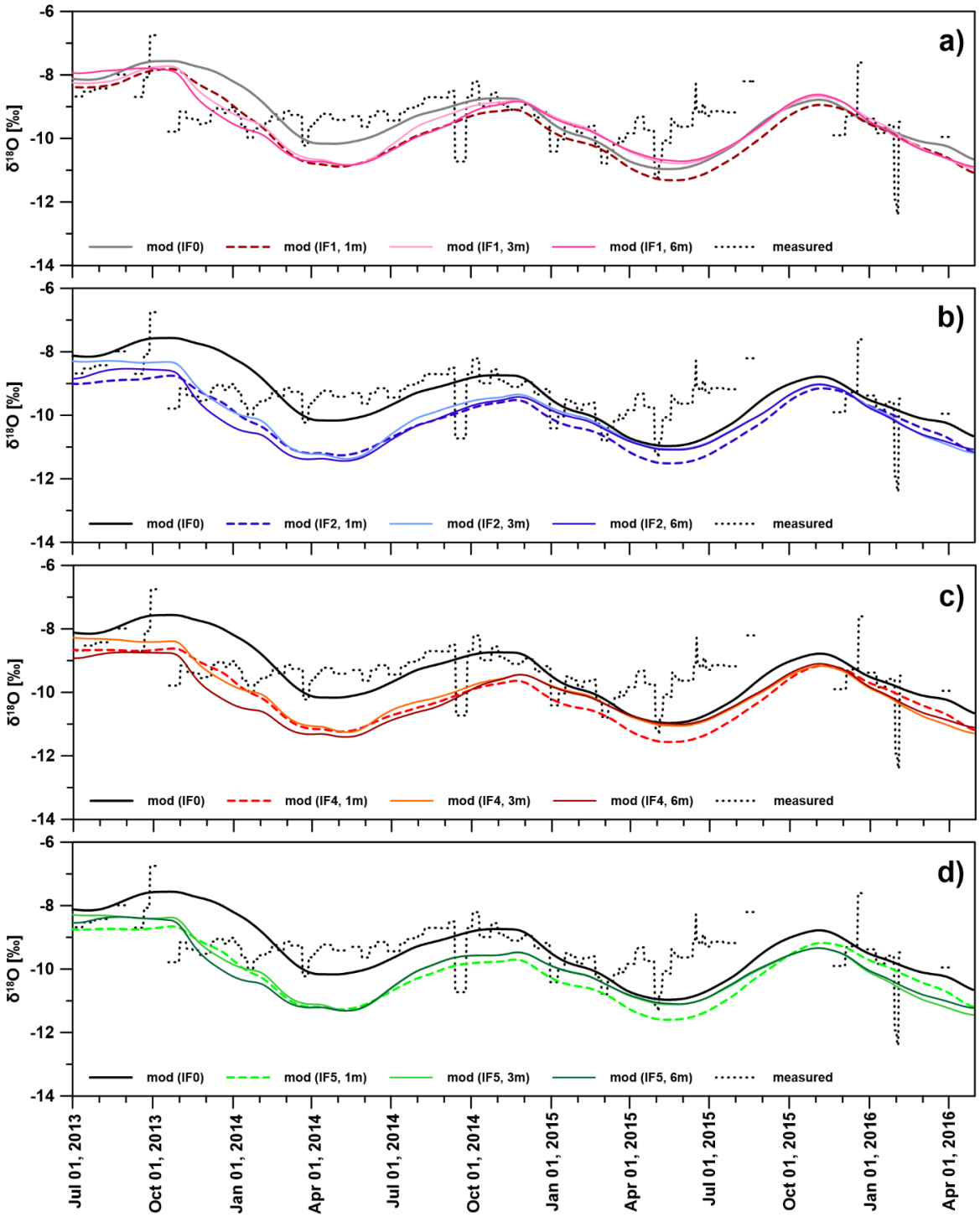

Figure S10. Measured and modeled $\delta^{18}O$ in the seepage water of Ly2 as a function of time. Isotope transport through the soil matrix is modeled (mod), with input function IF0 (isotopic composition of precipitation as input) and a) IF1 (weighting, only; weighting period 1, 3 and 6 months), b) IF2 (considering measured evapotranspiration ET), c) IF4 (considering ET estimated by Penman-Monteith), d) IF5 (considering ET estimated by Penman-Monteith plus modeled maize transpiration).

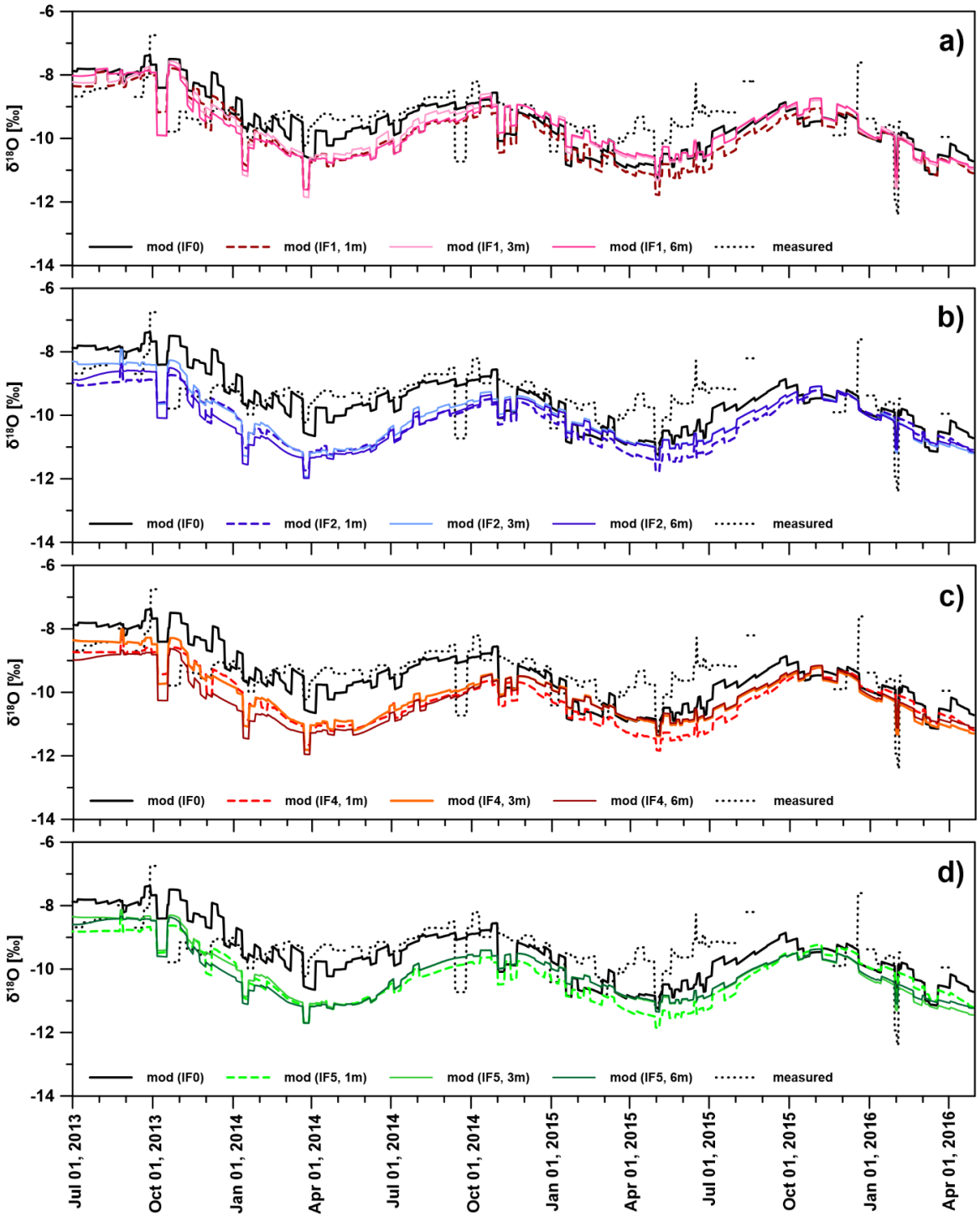

Figure S11. Measured and modeled $\delta^{18}O$ in the seepage water of Ly2 as a function of time. Isotope transport through the soil matrix and along preferential flow paths is modeled (mod), with input function IF0 (isotopic composition of precipitation as input) and a) IF1 (weighting, only; weighting period 1, 3 and 6 months), b) IF2 (considering measured evapotranspiration ET), c) IF4 (considering ET estimated by Penman-Monteith), d) IF5 (considering ET estimated by Penman-Monteith plus modeled maize transpiration).

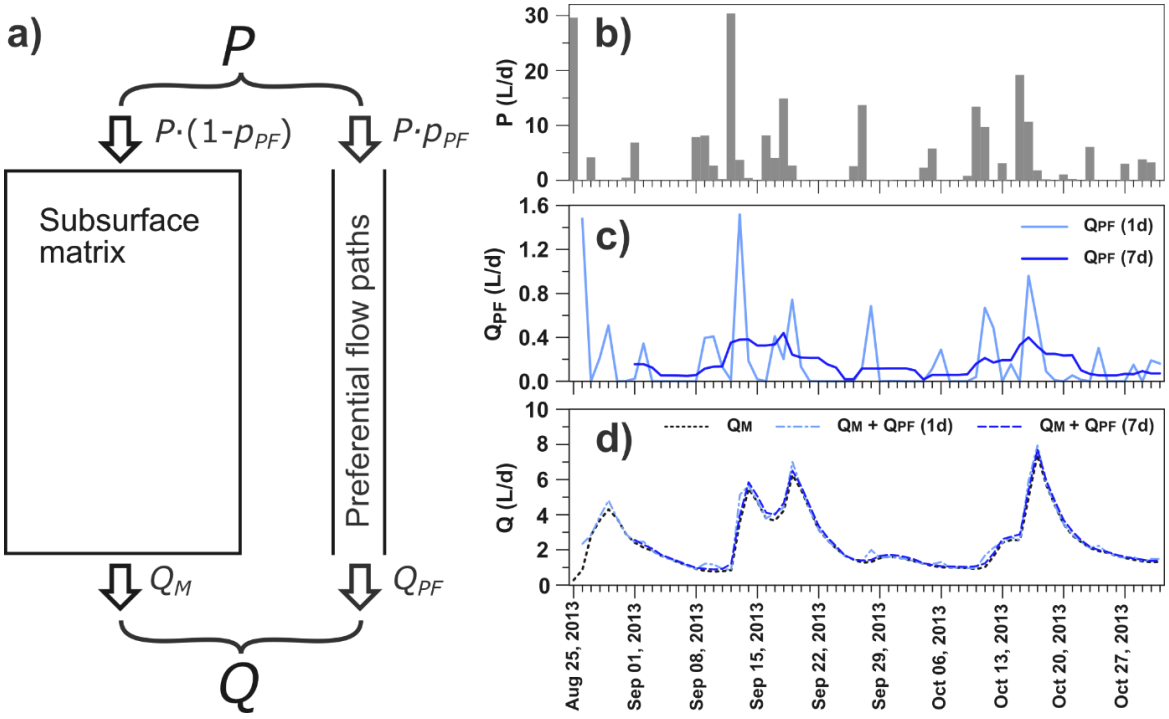

Figure S12. a): Concept for simulating water flow in the unsaturated zone (numerical modeling). b-d): Example with 5% preferential flow for the time between August and October 2013. b): Observed precipitation (P) as a function of time. c): Simulated lysimeter outflow resulting from water flow along preferential flow paths (Q_{PF}), assuming a mean transit time of water within preferential flow paths (T_{PF}) of 1 day (1d) and 7 days (7d). d): Simulated lysimeter outflow within the subsurface matrix (Q_M), without or with consideration of preferential flow. Q: total lysimeter outflow, p_{PF}: portion of preferential flow.

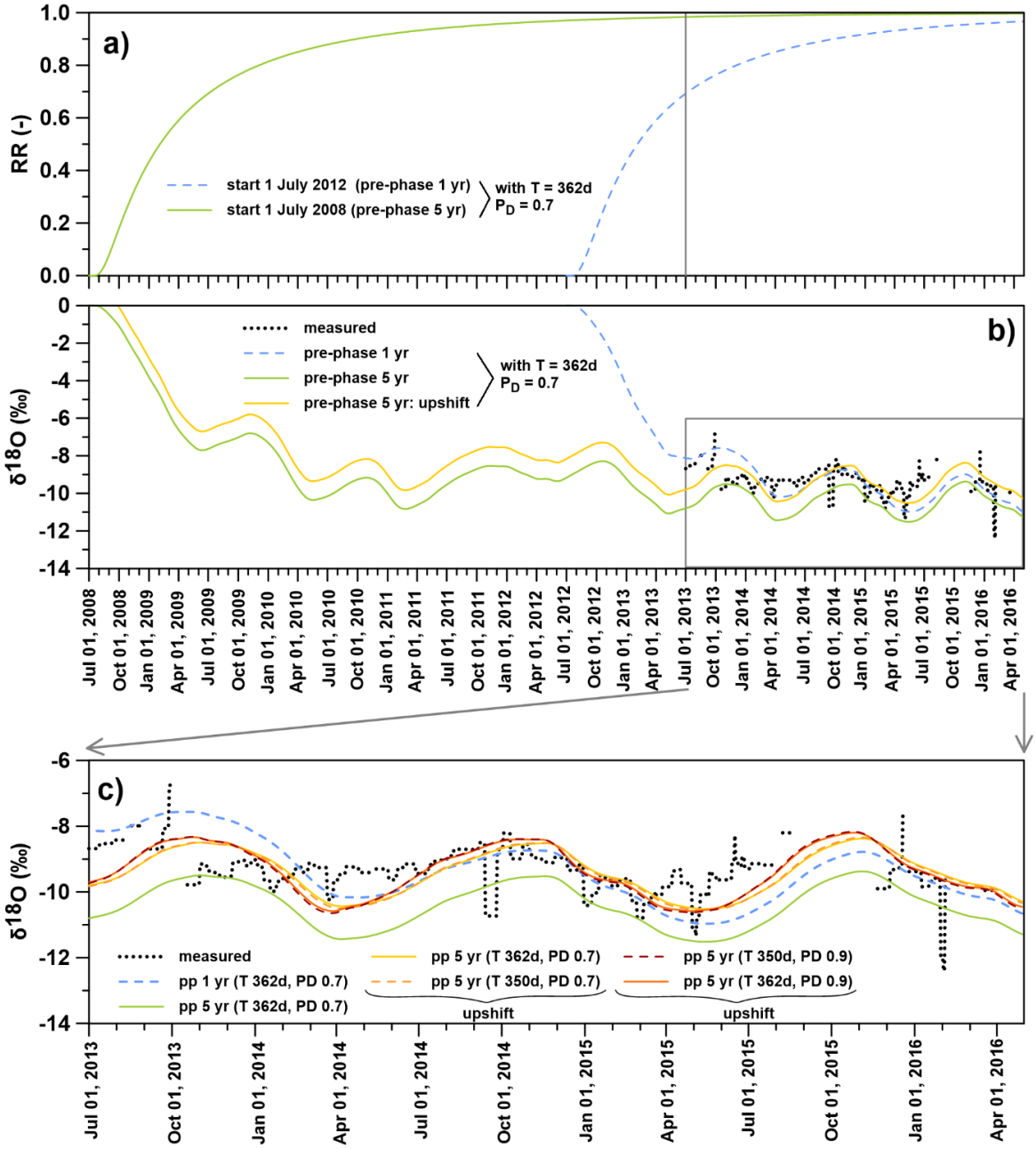

Figure S13. a) Simulated relative recovery (RR) as a function of time for constant input, with mean transit time T = 362 d and dispersion parameter PD = 0.7 (analytical solution of Lenda and Zuber 1970, Equation 20 in main manuscript). Input starts at 1 July 2008 (blue dashed curve) and 1 July 2012 (green curve), corresponding to a pre-phase of 5 years and 1 year, respectively. The vertical gray line indicates the start of lysimeter outflow measurements (end of modeling pre-phase). b) Simulated (LPM) versus measured $\delta^{18}O$ as a function of time. The orange curve considers a second component that adds to simulated $\delta^{18}O$, leading to constant upshift of 1 ‰. c) Zoom into the time frame of lysimeter outflow measurements (skipping the pre-phase). Consideration of the longer pre-phase (5 years, pp 5 yr) plus the second component ("upshift") could significantly improve curve fits.

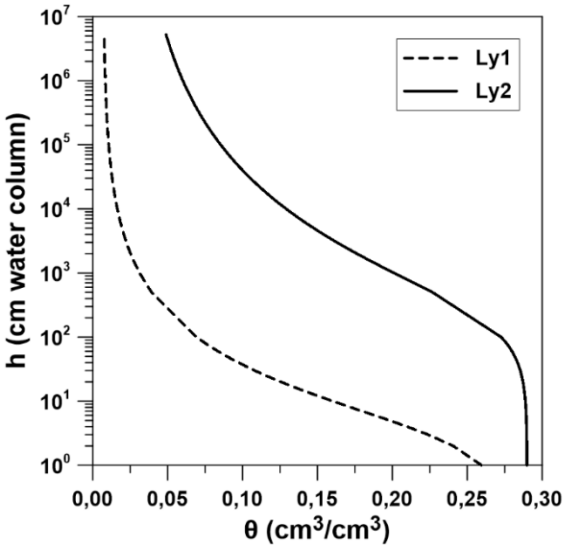

Figure S14. Water retention curves for Ly1 and Ly2 calculated based on fitted soil hydraulic parameters, SHP (see Table 8 and 9).

Due to the lack of in situ measurements in the studied lysimeters, we have analyzed these simulated soil water retention curves and compared our findings to those of similar studies. For example, Stauffer and Lu (2012) and Thoma et al. (2014) conclude that the shape of water retention curves can act as a suitable proxy to identify the physical correctness of a fitted set of SHP, which can reduce computational efforts. As expected for coarse soil textures, the water retention curve for Ly1 tends to be S-shaped, a behavior that is controlled by shape parameter n. It leads to a steep increase at a higher water content (air entry point), and then the curve is flattening, followed by a strong increase at lower water contents. Such a behavior is typical for the dewatering of considerably different pore sizes. Such differences have been observed for similar soils, e.g., by Stumpp et al. (2009c) and Sprenger et al. (2015). The soil water retention curve for Ly2 is steeper in comparison to Ly1 (lower n), as expected due to the finer soil texture.

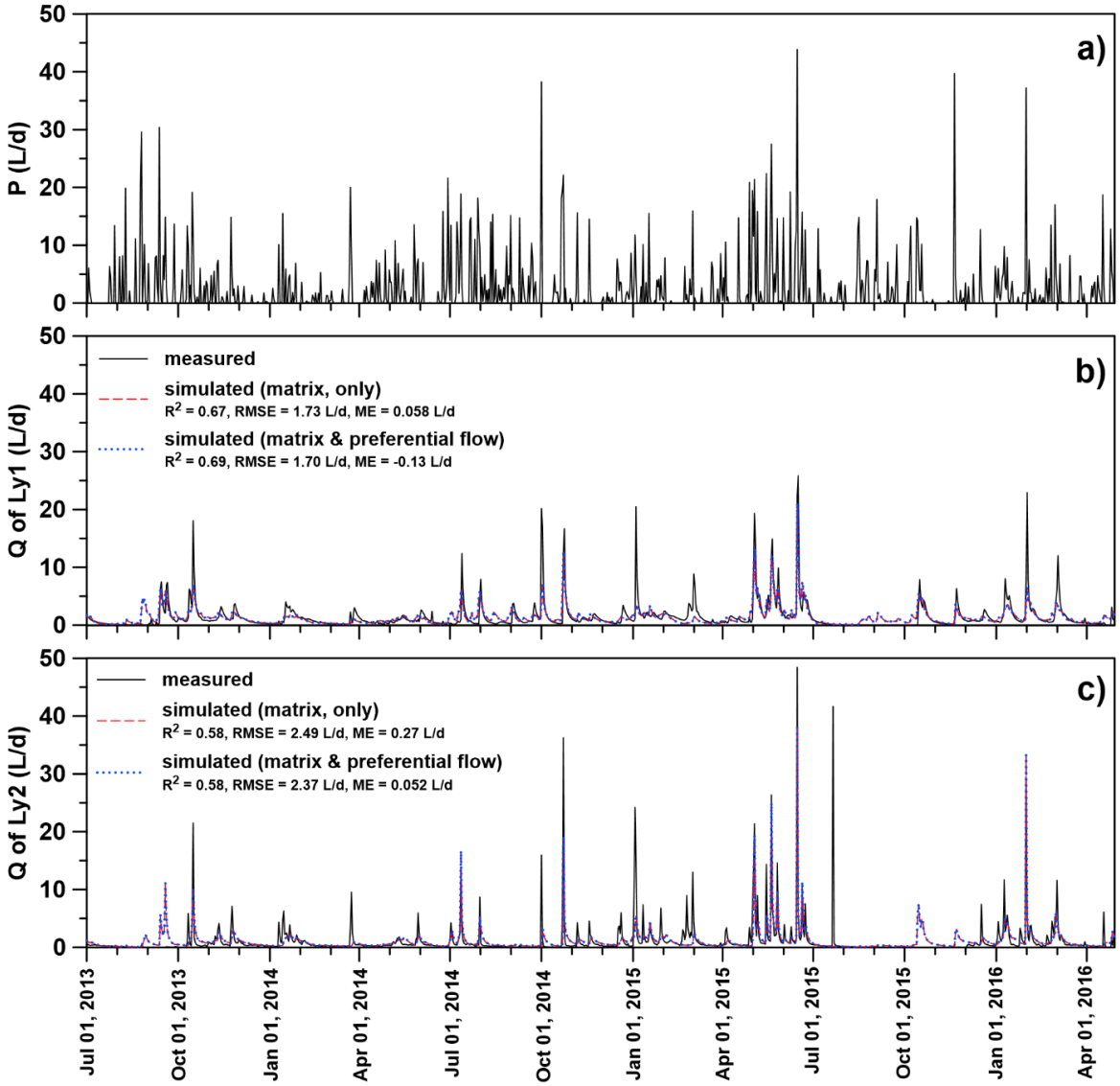

Figure S15. Precipitation P (a) and discharge rates Q at Ly1 (b) and Ly2 (c) as a function of time. Simulated (HYDRUS-1D) outflow rates (b and c) refer to multi-layer cases.